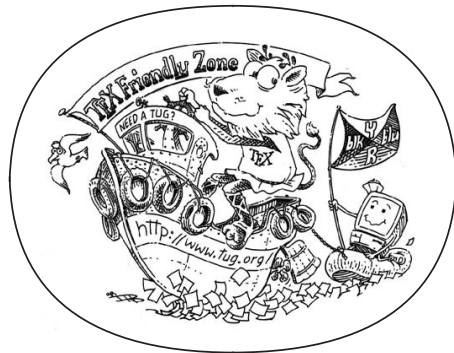


SPATIAL PATTERNS OF DROPLETS IN TURBULENT
CLOUDS

KATARZYNA KARPIŃSKA



Ph.D. thesis

Atmospheric Physics Department
Faculty of Physics
University of Warsaw

2018 – version 1.0

Katarzyna Karpińska: *Spatial patterns of droplets in turbulent clouds*, Ph.D. thesis, © 2018

SUPERVISOR:

prof. dr hab. Szymon Malinowski

LOCATION:

Warszawa

Ohana means family.
Family means nobody gets left behind, or forgotten.
— Lilo & Stitch

Dedicated to the loving memory of Rudolf Miede.

1939 – 2005

ABSTRACT

Short summary of the contents... a great guide by Kent Beck how to write good abstracts can be found here:

<https://plg.uwaterloo.ca/~migod/research/beck00PSLA.html>

PUBLICATIONS

Some ideas and figures have appeared previously in the following publications:

Put your publications from the thesis here. The packages `multibib` or `bibtopic` etc. can be used to handle multiple different bibliographies in your document.

*Curiosity killed the cat,
but satisfaction brought it back.*

— English proverb

ACKNOWLEDGEMENTS

Put your acknowledgements here.

Podziekowania itp.

Inne:

CONTENTS

0.1 Organization of the thesis - to be filled	1
I INTRODUCTION	4
1 INTRODUCTION	7
1.1 Research problem exploration - literature review	7
1.1.1 Turbulence	7
1.1.2 Single particle motion in the flow	14
1.1.3 Particle motion in turbulent environment	17
1.1.4 Vortex structures versus cloud droplet clustering	21
1.2 Research problem statement	22
2 METHODS	25
2.1 Vortex model	25
2.2 Dynamical systems formalism	28
2.3 Numerical simulations	32
2.3.1 Single particle trajectory	32
2.3.2 Multiple particles in vortex domain	33
2.4 Cloud voids observation	35
2.4.1 Atmospheric turbulence measurements	36
2.4.2 Lasersheet photography	36
2.5 Cloud-like conditions	38
II RESULTS	41
3 CHARACTERISTICS OF SINGLE PARTICLE MOTION IN A BURGERS VORTEX	43
3.1 Motion along the vortex axis	43
3.2 Motion in the plane perpendicular to vortex axis	49
3.2.1 Without gravity (vertical vortex)	49
3.2.2 With gravity (inclined vortex)	58
3.3 Time scales of single particle motion	63
4 CLOUD VOIDS - INTERPRETATION AND EXPLANATION	65
4.1 Cloud voids experiment description	65
4.2 Polydisperse particle motion analysis	65
4.3 Cloud voids creation mechanism	65
4.4 Cloud voids simulation	65
5 POLYDISPERSE PARTICLE MOTION - STATISTICAL ANALYSIS	67
5.1 Section Title	67
5.1.1 Subsection Title	67
5.1.2 Subsection Title	67
5.2 Section Title	67

III APPENDIX	69
BIBLIOGRAPHY	71

LIST OF FIGURES

Figure 1	Turbulent eddy size ranges and transfer of energy diagram (from Saeedipour et al. [102]).	10
Figure 2	Some example of 4/5 law.	11
Figure 3	Tu bedzie rysunek takich rurek itp. z wymienionych prac.	13
Figure 4	Moze tu jakiś wykres pomiarow epsilona z POSTu? Cos co bedzie jasne i czytelne bez wielkiego wyjariania	14
Figure 5	Straining of vorticity in Burgers vortex. δ is vortex core size (from Davidson [37]).	26
Figure 6	Burgers vortex dimensionless velocity components in cylindrical coordinates for arbitrary strain parameter $A = 0.001$. r_s is defined in the text.	27
Figure 7	Trajectories in linearized neighborhoods of several 2-dimensional equilibria: (a) saddle (hyperbolic), (b) stable node (attracting), (c) center (elliptic), (d) stable spiral (from Cvitanović et al. [35]).	30
Figure 8	Trajectories in linearized neighborhoods of 3-dimensional equilibria: (a) saddle, (b) saddle-focus.	31
Figure 9	Hopf bifurcation depicted in a plane. α is bifurcation parameter, its critical value is $\alpha_{cr} = 0$. The figure comes from [62].	31
Figure 10	A scheme of numerical simulation's vortex model domain. D is cylinder radius, Z is its half-length, δ is vortex core size, θ is gravity alignment angle, \bar{g} is gravity direction.	34
Figure 11	Upper part of the figure presents an image of UFS observatory on the slope of Zugspitze. Lower part shows the arrangement of instruments at the UFS roof.	35
Figure 12	Relative intensity of scattered light (on radial axis, in logarithmic scale) on scattering angle and sphere radius according to Mie scattering theory.	37
Figure 13	Equilibrium position z_b versus vortex core size δ and particle radius R . Plot variables' ranges correspond to cloud-like conditions.	44

Figure 14	Characteristic time of the motion along vortex axis τ_z relative error versus vortex core size δ and particle radius R . Color indicates dependence on R . Plot variables' ranges correspond to cloud-like conditions.	46
Figure 15	Logarithmic factor in τ_{ex} vs. ratio of initial position and equilibrium position a_2 . Line colors present cases of different ratios of vortex half-length and equilibrium position, a_1	48
Figure 16	Particle stable orbit radius r_{orb}^+ dependence on parameter St/A	50
Figure 17	Particle stable orbit radius r_{orb} dependence on particle radius R and vortex strain parameter A for cloud-like parameter ranges and vortex core size $\delta = 0.5$ cm. Black line represents stable orbit existence condition.	50
Figure 18	Particle stable orbit angular velocity ω_{orb} dependence on particle radius R and vortex core radius δ for cloud-like parameter ranges.	51
Figure 19	Particle docking in orbit for different parameters St and A , $\epsilon = 10^{-4}$. Line color corresponds to the value of parameter St/A . Panel a - radial coordinate, b - polar angle, c - radial velocity, d - angular velocity.	53
Figure 20	Same as in Fig. 19, but time is scaled by each particles docking time, c - radial velocity is scaled by the fluid velocity at the starting point $u_r(\epsilon)$, d - angular velocity is scaled by the particle orbit angular velocity ω_{orb}	54
Figure 21	Particle docking on axis for different parameters St and A , $\epsilon = 10^{-4}$. Line color corresponds to the value of parameter St/A . Panel a - radial coordinate, b - polar angle, c - radial velocity, d - angular velocity.	55
Figure 22	Same as in Fig. 21, but time is scaled by each particles docking time, c - radial velocity is scaled by the fluid velocity at the starting point $u_r(r_s)$, d - angular velocity is scaled by the fluid angular velocity $u_\varphi(\epsilon)/\epsilon$	56
Figure 23	Results of fitting the relation proposed in Eq. 62 to particle trajectories with the fitting parameter τ_{doc1} . For transparency Y axis shows fitting parameter times A	56

Figure 24	Docking time calculated numerically with respect to St and A for arbitrary variable ranges with $\epsilon = 10^{-5}$. Blank spaces represent lack of data, numerically too expensive.	57
Figure 25	The same as in Fig. 24, projection. Black line $St = St_{cr}(A)$ shows the stability boarder: particles to the left are attracted by periodic orbits, particles to the right by stable points on vortex axis.	57
Figure 26	Docking time calculated numerically with respect to St for a few chosen A values, $\epsilon = 10^{-5}$	58
Figure 27	Docking time calculated numerically with respect to A for a few chosen St values, for $A > St/16\pi^2$, $\epsilon = 10^{-5}$	59
Figure 28	Docking time calculated numerically with respect to A for a few chosen St values, for $A < St/16\pi^2$, $\epsilon = 10^{-5}$	59
Figure 29	Equilibrium curve plots for different A values. A_{cr} , r_s , r_i defined in the text body. Gray dashed line shows an equilibrium curve which is an asymptotic limit when $A \rightarrow 0+$	61
Figure 30	Plot of the function $\phi(r_0^+)$ determining equilibrium point stability (a) and its square radius $\sqrt{\phi(r_0^+)}$ (b) with respect to equilibrium point radial position.	62

LIST OF TABLES

Table 1	Existence of equilibrium points with respect to A and S_v parameters. A_{cr} , r_s^+ , r_{min}^+ , $S_{v min}$, $S_{v max}$ defined in the text body.	60
Table 2	Burgers vortex non-dimensional numbers . . .	60
Table 3	Stability conditions of particle equilibrium points present in the Burgers vortex with respect to vortex strain parameter A and dimensionless distance from the vortex axis r^+ . A_{cr} , $\varphi(r^+)$, r_s^+ , r_{min}^+ and r_{max}^+ defined in the text body. .	63

LISTINGS

ACRONYMS

DRY Don't Repeat Yourself

API Application Programming Interface

UML Unified Modeling Language

ORGANIZATION OF THE THESIS - TO BE FILLED

Part I

INTRODUCTION

Turbulent multiphase flows are present in numerous natural systems. They are a matter of current studies in many fields, including atmospheric physics, oceanography, astrophysics and technology. Such flows are characterized by a large complexity, due to the nonlinear nature and mutual couplings between different physical phenomena, i.e. flow dynamics, phase transitions, heat transfer, phase-to-phase interactions etc. One of such turbulent multiphase systems is an atmospheric cloud. Its complexity should encourage in-depth research, because according to latest IPCC report [22] "Clouds and aerosols continue to contribute the largest uncertainty to estimates and interpretations of the Earth's changing energy budget." However the cloud research has been progressing very slowly. One of the reasons for this is the poor understanding of the basics of turbulence phenomenon itself, including its multi-scale nature and the couplings between the many scales. Phenomena occurring in a cloud on a millimetre scale can be of great importance for a whole cloud system of hundreds of meters in size [Bodenschatz_2010]. Therefore, it is perfectly justified to study very simplistic models operating even only on a small part of the cloud. The research presented in this thesis is motivated by such simplistic approach. Methods used in the following thesis neglect many effects connected to large scale dynamics in the atmosphere, as well as thermodynamic, radiative and chemical effects. These simplifications enable us to treat the cloud as a model set of polydisperse, heavy, inertial, sedimenting particles interacting with an incompressible, turbulent air flow. The work is aimed at studying spatial patterns of cloud droplets formed due to a presence of a single vortex model - a substitute of a turbulent flow. This way one of the mechanisms of interaction between particles and turbulence, particle clustering, is examined. The problems stated in the thesis are universal and fit into the current research on the general interaction between particles and flow in multiphase turbulent flows. The following introductory chapter states the research questions and hypotheses as well as put them into the perspective of recent advances in the topics of turbulence structure, atmospheric turbulence, particle clustering and its role in cloud evolution.

1

INTRODUCTION

RESEARCH PROBLEM EXPLORATION - LITERATURE REVIEW

Turbulence

Finally, there is a physical problem that is common to many fields, that is very old, and that has not been solved. It is not the problem of finding new fundamental particles, but something left over from a long time ago—over a hundred years. Nobody in physics has really been able to analyze it mathematically satisfactorily in spite of its importance to the sister sciences. It is the analysis of circulating or turbulent fluids.

— Richard Feynmann[19]

Richard Feynmann said these words more then 50 years ago and his message seems to be still valid. Fluid turbulence has attracted the attention of physicists, mathematicians, and engineers for over one hundred years. Phenomenon of turbulence present in nature is mostly associated with the observational aspects, which play far more important role due to the unsatisfactory state of "theory": a theory based on first principles simply does not exist. There is no consensus about physical definition of "turbulent motion" or agreement on mathematical "turbulence problem" to be solved. However unlike other complicated physical phenomena it is easy to observe at least some of the numerous manifestations of turbulence. Major qualitative universal features of turbulent flow, that form the "essence" of turbulence, are listed below.

1. Spatio-temporal apparent randomness (chaoticity).
2. Extremely wide range of strongly and non-locally interacting degrees of freedom ($\sim 10^{18} - 10^{29}$ in atmospheric flows), hence its extreme complexity enforcing statistical description.
3. Chaotic nature (manifest itself by loss of predictability of turbulent flows), which at the same time posses statistically stable

properties.

4. Three dimensional and highly dissipative behaviour, thereby time irreversible and rotational. First two are probably the most specific and important attributes of turbulence.
5. Highly diffusive - turbulent flows exhibit strongly enhanced transport processes of momentum, energy and passive objects when compared to laminar flows.
6. Strongly nonlinear, non-integrable, nonlocal, non-Gaussian.

The true turbulence theory should predict and explain universal properties listed above. The best we have so far is the set of equations developed almost 200 years ago, that describe fluid motion - Navier Stokes equations (NSE). Most probably it contains all of turbulence. The problem is that we do not know global solution of these equations, and the knowledge of specific solutions does not lead to understanding the dynamics or structure of turbulent processes as a whole.

*Navier Stokes
equations*

The Navier Stokes equation is a deterministic, nonlinear partial differential field equation. It can be presented in two ways that are used to describe the fluid motion. One is called Lagrangian, where one follows all fluid particles and describes the variations around each fluid particle along its trajectory. The other is called Eulerian, where the variations are described at all fixed stations as a function of time. In Eulerian formulation the NSE are as follows:

$$\underbrace{\frac{\partial \vec{u}}{\partial t} + \vec{u} \cdot \nabla \vec{u}}_{(1)} + \underbrace{\vec{u} \cdot \nabla \vec{u}}_{(2)} = -\frac{1}{\rho} \nabla p + \underbrace{\nu \nabla^2 \vec{u}}_{(3)} + \vec{f} \quad (1)$$

where \vec{u} - fluid velocity, ρ - fluid density, p - fluid static pressure, ν - kinematic viscosity, \vec{f} - external forces.

Term (1) of NSE in this form is a standard partial time derivative. Term (2) represents advection of a fluid parcel. Those terms together create what is called the material derivative: $\frac{D}{Dt}$. Term (3) expresses pressure gradient and term (4) represents viscous forces.

Dimensionless version of the NSE brings to life dimensionless quantity that is very important in fluid mechanics - the so-called Reynolds number Re . It estimates the ratio of inertial forces (given by term (2) in 1) to viscous forces (given by term (4) in 1) within a fluid parcel. It can be presented with the use of characteristic scales of the fluid flow: U - velocity scale and L - length scale:

$$Re = \frac{UL}{\nu} \quad (2)$$

Reynolds number

The primary physical interpretation of the Reynolds number is that for small Re the flow is dominated by laminar motion and for large Re the flow is mostly turbulent. The exact transition between these two regimes (at so called critical Reynolds number Re_{cr}) is specific for a geometry of the flow and has been a subject of separate, extensive studies. A quick estimation of the Re number for a cumulus cloud, in which $L \sim 1 \text{ km}$, $U \sim 1 \text{ m/s}$, $\nu \sim 10^{-5} \text{ m}^2/\text{s}$, leads to $Re \sim 10^8$ and the conclusion that the airflow in the cloud is extremely turbulent, since typical Re_{cr} is in the range $100 - 3000$ [1].

Though NSE have a limited kinetic foundation, it is commonly believed to be *adequate* i.e. its solutions corresponds to real fluid flows at all accessible Re , including turbulent flows. Unfortunately it is impossible to solve NSE analytically subject to most realistic initial and boundary conditions. For large Re the essence of the problem lies in the nonlinearity of the viscous term (4) in Eq.1.

Phenomenology of turbulence

Because a field theoretical solution of the Navier Stokes equation is elusive, the fruitful approach comes from asking questions concerning the physics of the processes. The problem is to identify, interpret and explain major fundamental physical mechanisms that result in the universal properties of turbulence. The first such comprehensive attempt to explain these mechanisms is phenomenological theory of cascade [98] enriched and quantified by Kolmogorov hypotheses [60]. In the following, the foundations of these theories are outlined and the basic concepts commonly used in turbulence research are explained (description in this paragraph inspired by Pope [94] and Tsinober2001).

Cascade concept postulates that in the flows of large Re kinetic energy enters the turbulence through a production mechanism at the largest scales of the flow. This energy is then transferred by inviscid processes to smaller and smaller scales, until, at the smallest scales, the energy is dissipated by viscous action. This concept defines a rate of turbulent kinetic energy (TKE) dissipation ϵ . The turbulent cascade scales emerge in the form of *eddies* - moderately coherent structures of turbulent motion localized in the region of size constrained by the arbitrary scale.

Kolmogorov hypotheses state that for every turbulent flow, at sufficiently high Reynolds number, there exist scales l_0 , l_{EI} , η such that:

- small-scale turbulent motions $l \ll l_0$ are statistically isotropic
- the statistics of the small-scale motions $l \ll l_{EI}$ have a universal form that is uniquely determined by ν and ϵ
- the statistics of the motions of scale l in the range $\eta \ll l \ll l_0$ have a universal form that is uniquely determined by ϵ , independent of ν

TKE dissipation rate
eddy

local isotropy
hypothesis

1st similarity
hypothesis

2nd similarity
hypothesis

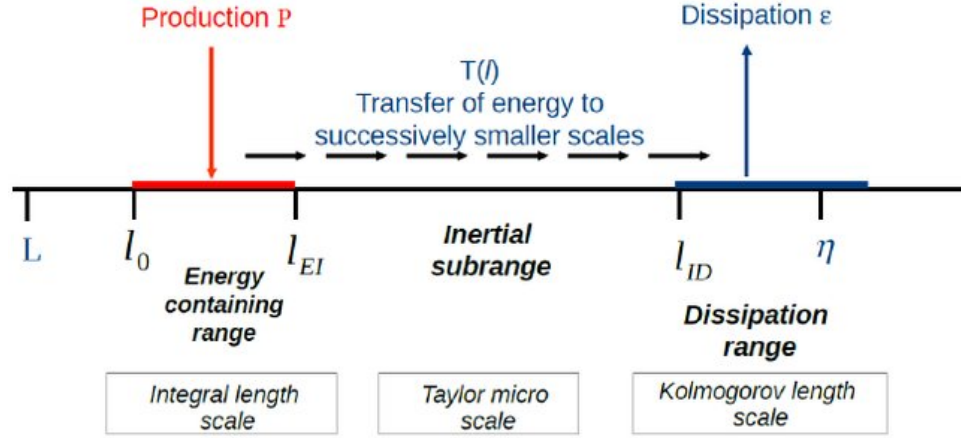


Figure 1: Turbulent eddy size ranges and transfer of energy diagram (from Saeedipour et al. [102]).

energy containing range
inertial range
dissipation range
Kolmogorov scales

Taylor microscale

Those hypotheses lead to a paradigmatic decomposition of the multiscale turbulence phenomenon to a few eddy size ranges illustrated schematically in the Fig. 1. L is the flow scale. l_0 is the scale of the smallest anisotropic eddies affected by the boundary conditions of the flow and l_0 is comparable to L . l_{EI} demarcates between anisotropic eddies and smaller isotropic eddies of universal character. The range $[l_0, l_{EI}]$ is called *energy containing range* and have bulk of the energy production. *Inertial range* $[l_{EI}, l_{ID}]$, which is the name of the subrange described by 2nd similarity hypothesis, is governed only by inertial effects, viscous effects being negligible. The smallest scales, so called *dissipation range*, are described by 1st similarity hypothesis. Based on scaling argument, out of its only parameters ϵ and ν , Kolmogorov formed unique length, velocity and time scales for this range, , which are now called Kolmogorov scales:

$$\eta \equiv (\nu^3/\epsilon)^{1/4} \sim Re^{-3/4} l_0 \quad (3)$$

$$u_\eta \equiv (\epsilon \nu)^{1/4} \sim Re^{-1/4} u_0 \quad (4)$$

$$\tau_\eta \equiv (\nu/\epsilon)^{1/2} \sim Re^{-1/2} \tau_0 \quad (5)$$

Reynolds number based on Kolmogorov scales is equal to one: $\frac{\eta u_\eta}{\nu} = 1$. It is easy to see that the larger the Re the greater is the span of scales in turbulent fluid.

A well-defined quantity that is also often used in turbulence research (especially numerical simulations) is the *Taylor microscale* λ . It does not have a clear physical interpretation, but it is the intermediate length scale at which fluid viscosity significantly affects the dynamics of turbulent eddies in the flow. In Kolmogorov turbulence:

$$\lambda = \sqrt{15\nu/\epsilon} u' \quad (6)$$

Figure 2: Some example of $4/5$ law.

where \bar{u}' is turbulence intensity - a root mean square of velocity fluctuations. Reynolds number built on this scale is called *Taylor microscale Reynolds number* Re_λ .

Probably most important and commonly used conclusions from Kolmogorov's theory concern inertial range. Firstly there is the so-called " $-5/3$ law". In the Fourier space formulation, this law concerns energy spectrum function $E(\kappa)$, which describes energy spectrum for the fluid velocity Fourier modes κ . It states that in the inertial range:

$$E(\kappa) = C\epsilon^{2/3}\kappa^{-5/3}. \quad (7)$$

The constant C is called Komogorov universal constant and experimental evidence lead to $C \approx 1.5$. Recent extensive DNS for example point to $C \approx 1.64$ [1]. Figure ?? (...). Secondly there is "Taylor hypothesis" or "frozen-flow hypothesis". It says, that in the case of statistically stationary flow with turbulence intensity small compared to mean velocity, we can approximate spatial correlations by temporal correlations. Both are commonly used to estimate ϵ from experimental data - a task, that is still a matter of vivid discussion in cloud turbulence research [117].

Kolmogorov's phenomenological theory is the only tool developed so well that it can characterize turbulent flow in many diverse applications. It even constitutes the language of many different turbulence descriptions. Despite being a good approximation of turbulence phenomenon, experimental premises indicate that a large part of its basic assumptions is flawed and many mechanisms are not captured. There is evidence that anisotropy in large scales causes anisotropy of small scales [cos] and that there is coupling between large and small scales [cos2]. The notion of "hierarchy" in turbulence is also doubted. Another important issue, not described by Kolmogorov's theory or its extensions, is the phenomenon of intermittency in small scales, inseparably connected with the notion of "structure" of turbulence. Intermittency and structure are the subject of the next paragraph.

Structure of turbulence

It is mostly agreed that turbulence posseses structure [Tsinober2001]. It is agreed as well that some aspects of this structure are intimately related to *intermittency*. Small-scale (or internal) intermittency is defined twofold: geometrically and statistically, and these aspects are not independent [Tsinober2001]. The geometric definition refers to some examined quantity x . This quantity is intermittent when for any small value x_0 , the volume of fluid in which $x > x_0$, decreases with increasing Re . In colloquial terms, when Re increases, our examined value of x is more and more "spiky" in its domain. Statistically

$-5/3$ law

intermittency

vortex tubes

a variable x with zero mean is intermittent if its probability distribution is such that extremely small and extremely large excursions are much more likely than in normally distributed variable (Gaussian). Various experiments have shown that Lagrangian statistics in turbulent flows display Gaussianly distributed velocity values and non-Gaussianly distributed velocity differences or accelerations (see for example M. and A. [67], ISHIHARA et al. [53], **cos3** and others). Measured energy dissipation rate and vorticity are intermittent as well [**cos4**]. Structures most probably responsible for the tails observed in the dissipative scales (referred to as *extreme events* too) are predominantly in the form of vortex tubes and strain sheets. Earlier studies pointed that *vortex tubes* or “*worms*”, are severely intermittent, coherent, elongated and long-lasting structures characteristic of high Reynolds number turbulent flows [82]. [77] show that these structures concentrate into clusters of the size in inertial range of scales. This implies the presence of large-scale organization of the small-scale intermittent structures. Review of the structures identification methods and the search results obtained in diverse turbulence generation setups was conducted in Wallace [118]. Some of most recent studies confirm the fact, that intense enstrophy-dominated regions are organized in small-scale vortex structures [116] and that these structures are strongly correlated with each other in space [125]. There are premises that such structures are present in inertial range as well [83]. The remaining question is if the structure changes when Re is increased. The old belief was that the only change produced by increasing the Reynolds number is extension of the inertial range, with no other structural changes. Massive computations of last decade proof otherwise and provide new data about inertial range structures’ features, in Reynolds numbers higher than ever. In Yeung P K, Zhai X M, and Sreenivasan Katepalli R [124] for example authors show that at $Re_\lambda = 1300$ (highest Re directly calculated numerically to that date) with increasing Re , the extreme events assume a form that is not characteristic of similar events at moderate Re . Events as large as 105 times the mean value were obtained, albeit rarely. They appeared chunky in character, unlike elongated vortex tubes, and generally short-lived. Extreme magnitudes of energy dissipation rate and enstrophy occurred essentially simultaneously in space and remained nearly collocated during their evolution. When imagining the structures in turbulent flow it is important to remember that “every part of the turbulent field just like the whole possesses structure.” [Tsinober2001] and the coherent structures mentioned above are not just simple object embedded in the structureless background that can be “taken out of it”. The reports mentioned above, as well as other studies, mean that we do not really know what to expect in turbulence with even higher Re . The values achieved in the laboratory and simulations, although becoming higher and higher, are still far from those found in atmo-

Figure 3: Tu bedzie rysunek takich rurek itp. z wymienionych prac.

spheric turbulence. This is one of the reasons why we are not sure whether the results of the intermittency and structure research can be applied to the atmosphere. In the next paragraph I try to elaborate on this problem.

Atmospheric turbulence

Turbulence in atmosphere, especially in clouds, influence many important processes: it governs entrainment and mixing, impacts cloud droplet evolution and interacts with large-scale cloud dynamics [20]. In-situ measurements of cloud-related turbulence are scarce and there are several reasons for that. Obviously it is not possible to have any control over the meteorological conditions. Observations made with research aircrafts are prone to aerodynamic errors and relatively low resolution due to large true airspeed. Measurements at mountain research stations are biased by orographic boundary conditions. Experimental equipment used must be resistant to hard meteorological conditions and large speeds/vibrations etc. Last but not least, field campaigns in atmospheric research are much more expensive than laboratory experiments. Despite these discouraging factors, the effort put into atmospheric turbulence measurement should pay off: after all, at our fingertips we have turbulence with the highest Re on Earth and a huge range of scales spanned between the smallest and largest eddies of turbulence, from parts of millimeters to kilometers. Little experimental evidence and complementary Direct Numerical Simulation (DNS) studies focused on atmospheric turbulence are summarised below.

Turbulence in the atmosphere is hard to analyse because of the presence of large scale anisotropies, inhomogeneity of turbulence field and nonstationary effects due to stratification, presence of liquid water and water vapor, aerosols of all kinds, sun heating, Coriolis force etc. Part of my own research concentrated on some of these factors. On the basis of relatively large data set collected in the Physics of the Stratocumulus Top (POST) campaign by in-flight measurements, we tried to characterize turbulence and passive scalars properties in marine boundary layer clouds [56, 69]. The investigation revealed complex structure of stratocumulus cloud and its surrounding, showing turbulence inhomogeneity at the range of scales reaching depth of inertial range. The transport of energy and momentum between these inhomogeneous spatial regions, called layers, is nonuniform, as well as the scaling behaviour of temperature and so called *liquid water content* (LWC, mass of the water in a cloud in a specified amount of dry air). But what is most distinctive in the results is strong anisotropy of turbulent motions at many scales [88]. Vertical fluctuations seem to be

Figure 4: Może tu jakiś wykres pomiarow epsilona z POSTu? Cos co bedzie jasne i czytelne bez wielkiego wyjajania

damped by static stability and horizontal fluctuations to be enhanced by large scale shear. This topic needs to be addressed more carefully, especially since some studies indicate that large scale anisotropy can be transmitted to small scales and be related with small-scale intermittency [120] or can totally change turbulence structure by appearing as large-scale intermittency[112]. The paradox however is that in all the turbulent studies in order to calculate turbulence properties such as TKE, ϵ , η , assumptions of isotropy, homogeneity and stationarity of small scales of turbulence are taken. What is particularly interesting, is that dissipation range is usually still not resolved in the in-situ atmospheric measurements, but ϵ estimation attracts particular attention. Its value is smaller by a few orders of magnitude than typically observed in the laboratory [Siebert2009, 56]. Some effort is put into improving ϵ estimation by accounting for low-resolution of measurements [117] or stratification and shear influence [126].

In conclusion, turbulence in the atmosphere, especially in the clouds, has properties that differ from turbulence created in the laboratory conditions. The language used to describe atmospheric turbulence is based on assumptions that are not fulfilled. Therefore, there is a need for research on its basic aspects, its structure and dynamics. This thesis by dealing with a simplistic model of cloud droplets moving in turbulence and trying to understand unique experimental evidence, offers a small contribution to the understanding of these basics. Next paragraph focuses on the great challenge which is efficient description of particle motion in the specific flow.

Single particle motion in the flow

In order to study the dynamics of particles advected by turbulent flow, one needs to have a simple formulation of the equations of motion of the advected particles. The problem is that particles of particular interest, namely cloud droplets, are finite-size, which means they are actually extended objects with their own boundaries. The rigorous way to analyse their dynamics would involve solving the Navier–Stokes equation for moving boundaries. The partial differential equations resulting from this approach are very difficult to solve and analyse. In many approximate derivations, the common concept that arises from the mathematical development is that of undisturbed fluid velocity, i.e. the velocity that the fluid would have had at the absence of the particle. In this way the flow is separated into the flow field as it would have been without particles, and the disturbance field. Widely used and very popular is the approximate differential

equation for the motion of small spherical particle in the flow that was written down by Maxey and Riley in 1983 [75]:

*Maxey-Riley
equation*

$$\vec{v} = \dot{\vec{r}}, \quad (8)$$

$$m_p \ddot{\vec{r}} = \underbrace{m_f \frac{D\vec{u}}{Dt}}_{(1)} - \underbrace{\frac{1}{2} m_f \left[\dot{\vec{v}} - \frac{D}{Dt} \left(\vec{u} + \frac{1}{10} R^2 \nabla^2 \vec{u} \right) \right]}_{(2)} - \underbrace{6\pi\mu R \vec{q}(t)}_{(3)} + \underbrace{(m_p - m_f) \vec{g}}_{(4)} - \underbrace{6\pi\mu R^2 \int_0^t d\tau \frac{d\vec{q}(\tau)}{d\tau} (\pi\nu(t-\tau))^{-\frac{1}{2}}}_{(5)} \quad (9)$$

where:

$\vec{r}(t)$ - position of the particle at time t ,

$\vec{v}(t)$ - velocity of the particle,

$\vec{u}(r(t), t)$ - undisturbed fluid velocity at the location of the particle,

$\vec{q}(t) = \vec{v}(t) - \vec{u}(\vec{r}(t), t) - R^2 \nabla^2 \vec{u}(\vec{r}(t), t)/6$ - particle-fluid velocity difference with correcting factor,

R - particle radius,

m_p - particle mass,

m_f - mass of the fluid displaced by the particle,

ρ_f - fluid density,

μ - fluid dynamic viscosity,

ν - fluid kinematic viscosity,

\vec{g} - gravitational acceleration,

and the derivatives:

$\frac{D}{Dt} = \frac{\partial}{\partial t} + \vec{u} \cdot \nabla$ - the material derivative (along fluid path),

$\frac{d}{dt} = \frac{\partial}{\partial t} + \vec{v} \cdot \nabla$ - total derivative along particle trajectory.

The *Maxey-Riley equation* (M-R) consist of a few terms which has the following physical interpretation.

- (1) - force exerted on the particle by the undisturbed fluid element in position $\vec{r}(t)$ at time t .
- (2) - *added-mass effect*, accounts for the fact that when the particle accelerates relative to the fluid, it displaces a certain amount of fluid with it.
- (3) - Stokes viscous drag.

(4) - buoyancy force.

(5) - Basset history term, arises from the fact, that the vorticity diffuses away from the particle due to viscosity.

The terms involving the factor $R^2 \nabla^2 \vec{u}$ (in (2), (3), (5)) are the *Faxén corrections*, and they account for the spatial variation of the flow field across the particle. Simulations have shown however [31] that the Faxén correction becomes significant only for particles with diameter of several times the dissipative (Kolmogorov) length scale of the flow (unlike cloud droplets). M-R equation is generally valid for small particles at low particle Reynolds numbers Re_p . This Reynolds number is calculated by using the relative velocity between particle and neighbouring fluid as the velocity scale:

$$Re_p = R|\vec{v} - \vec{u}|/\nu. \quad (10)$$

This implies that for M-R eq. to be a valid approximation, the initial velocity difference between particle and fluid must be small. Another condition is that the shear Reynolds number $Re_\zeta = R^2 \zeta / \nu \ll 1$, where Γ is the typical velocity gradient in the flow, must be small. The M-R equation can be simplified with the adoption of appropriate assumptions. We call a particle:

*small, heavy,
inertial, sedimenting
particle*

- *heavy* when its density is significantly larger than fluid density $\rho_f \ll \rho_p$,
- *small* when its radius is significantly smaller than smallest fluid spatial scale $R \ll l_f$,
- *sedimenting* when it is subject to gravity force
- *inertial* when its response time τ_p (to be defined) is larger than smallest fluid time scale $\tau_p > \tau_f$

When the particle follow these assumptions then the M-R eq. is of the form:

$$\vec{v} = \dot{\vec{r}}, \quad (11)$$

$$\dot{\vec{v}} = \tau_p^{-1} (\vec{u}(\vec{r}, t) - \vec{v}(t)) + \vec{g} - (5)/m_p \quad (12)$$

where $\tau_p = 2\rho_p R^2 / 9\mu$ is the particle inertial response time and (5) stands for the Basset history term. In this thesis droplet trajectories are calculated with the use of the approximated M-R equation- Eq.12 without history term (5):

$$\vec{v} = \dot{\vec{r}}, \quad \dot{\vec{v}} = \tau_p^{-1} (\vec{u}(\vec{r}, t) - \vec{v}(t)) + \vec{g} \quad (13)$$

The history term is omitted in this thesis due to its huge cost in numerical simulations. In the next section I discuss the applicability of certain M-R equation terms for cloud droplets in the vortex

model.(???) czy na pewno dyskutuje gdzieś ???)

The other important class of particles are so called *tracers*: their density is equal to fluid density and they follow the flow exactly, unlike the inertial particles, which detach from the flow. The main difference between dynamics of tracer and inertial particles is that volume in phase space of tracers is conserved, whereas that of inertial particles shrinks. Tracers serve as benchmark particles in clustering studies.

tracers

Particle motion research require the use of some nondimensional numbers, which describe ratio of forces working on a particle. These are Stokes number St , sedimentation parameter Sv and Froude number Fr . St characterizes the inertia of the particle, while it is the ratio of the particle response time to fluid characteristic timescale.

Stokes number

$$St \equiv \tau_p / \tau_f$$

Sv is nondimensional settling velocity (the ratio of terminal velocity v_g to the fluid characteristic velocity v_f).

sedimentaion parameter

$$Sv \equiv v_g / v_f$$

The ratio of Stokes number to the sedimentation parameter is Froude number Fr . It expresses the same time the ratio of particle response time τ_p to the residence time of the particle in a Kolmogorov eddy.

Froude number

$$Fr \equiv St / Sv$$

Fr is considered a measure of the influence of gravitational force on the droplet motion. In the limit of a large Froude number, gravity is seen as negligible.

Thus equipped with the tools of single particle motion description, one may proceed to the complex issue of particle motion in turbulent flow.

Particle motion in turbulent environment

Many efforts were made to understand the dynamics of multiphase turbulent flows. Despite that few definite conclusions can be drawn. The development of Lagrangian techniques ("following" a particle motion in the fluid) in recent years has shed some new light on the relation between particle motion and fluid motion. However we are still far from creating a thorough theory describing how (and why) particles behave in turbulent flow. The dynamics and kinematics of fluid tracers themselves are in fact the subject of current discussion [2, 16, 41, 106, 114]. In case of inertial, heavy particles there are more questions then answers. Just to start, no comprehensive investigation of the consequences of all simplifications usually made in inertial particle motion studies has been made yet [23]. Some studies try to answer what is the accuracy of Stokes drag model (term (3) in Eq. ??) when

comes to particle relative velocities (see Dou et al. [42] or Saw et al. [105] concerning water droplets in the air) or if Basset-history force, hydrodynamic interactions or turbulence small-scale anisotropy play any important role. Others consider the impact of Reynolds number as well as gravity[54, 55]. The issues raised above may substantially affect validity of the results regarding particle statistics in turbulence such as spatial distribution, collision probability, condensational growth or sedimentation velocity [32]. These statistics are especially important in cloud physics, as they determine rain formation process and cloud radiative properties. Better understanding how turbulence influences them by interaction with cloud droplets would lead to more precise characterization of cloud evolution[20]. Until now there has been a lot of theoretical and numerical research done but there is no agreement what are the key turbulent processes in this evolution (for reviews see Devenish et al. [40], Grabowski and Wang [48], Pumir and Wilkinson [95], Saito and Gotoh [103], Shaw [108], and Vaillancourt and Yau [115]). There are however some suggestions that the key processes are connected to the facts that even slight change of local droplet concentration (clustering, see next paragraph) or violent local turbulent events may influence cloud droplet growth significantly [11, 61, 70]. Experimental studies in the atmosphere [27, 46, 58, 59, 63, 73, 92, 107] and in the laboratory [Jaczewski 2005, 121] for long time have been inconclusive about the occurrence of clustering of cloud droplets on small-scales. Recently Larsen et al. [64] have finally revealed that there is statistically significant and unambiguous evidence of weak clustering on scales between about 1 and 5 mm (around 1η and 5η) for polydisperse set of cloud droplets larger than $10\mu\text{m}$ in weakly turbulent clouds. This thesis focus on the turbulence influence on droplet spatial distribution (clustering) in the context of cloud evolution. Next paragraph introduces this problem broadly.

clustering

Clustering is the central term when talking about statistical change in spatial distribution. It occurs when particle distribution deviates from random distribution, in our case due to the interaction of inertial particles with turbulent flow. There have been numerous studies on particle clustering motivated by industrial, geophysical or astrophysical applications. Most of the numerical and theoretical research focus on monodisperse and non-sedimenting particles in homogeneous, isotropic turbulence (HIT), and numerical simulations are conducted in Taylor microscale Reynolds number Re_λ which is a few order of magnitudes smaller than in the atmosphere. Thus application of such research to cloud droplet clustering is limited without further experimental investigation of polydispersity or gravity impact, matter of Re_λ increase or turbulence anisotropy/inhomogeneity influence. However, in order to properly address the complex problem, I will first review what has been achieved in a reduced problem.

Monodisperse, heavy inertial and non-sedimenting particle clustering

in HIT in theory may be divided into three regimes: small-scale clustering, preferential sampling and short-time clustering due to caustics (or sling effect) - this division and review is available in Gustavsson and Mehlig [49]. *Small-scale clustering* occurs on scales smaller than correlation length of the flow which in realistic turbulence is spatial Kolmogorov scale η representing the size of dissipative eddies. Small-scale clustering demonstrates self-similarity (clustering properties are independent of scale) and is often described with statistical and dynamical methods developed for multifractals [4, 6, 10, 24, 44]. Yet analytical calculations concerning small-scales are possible only for substantially simplified statistical models of turbulence. The hope is that the only experimental work treating about dissipation-scale clustering, that was conducted by 1D measurements on polydisperse particles in low Re , large ϵ turbulence, is in qualitative agreement with the theory [104].

small-scale clustering

Preferential sampling or preferential concentration appears at inertial scales of turbulence when particles sample only regions of the flow that posses specific features. Most frequently cited approach to preferential concentration, generated for particles in small St expansion, is a so called "Maxey centrifuge" mechanism [74]. It claims that small heavy particles gather in straining regions of the flow and are centrifuged out of vortical regions. This concept was further developed in many numerical and theoretical studies (see for example CENCINI et al. [29] and Sigurgeirsson and Stuart [110]) and confirmed experimentally (for latest see Bhatnagar et al. [15]). Alternative description formulated on the basis of DNS simulation results is *sweep-stick mechanism* [34, 47], which states that particles stick to regions of low fluid acceleration as they are swept through the flow. There were some other theoretical and numerical views using statistical methods proposed as well, see for example Bec et al. [6], Falkovich G., Fouxon A., and Stepanov M. G. [43], and Hartlep, Cuzzi, and Weston [51].

Preferential concentration/sampling

Bragg, Ireland, and Collins [25] claim that actually physical mechanisms of clustering at dissipative and inertial scales in HIT are the same and they provide the fundamental explanation for this fact. The key parameter used in their analysis is the *local Stokes number* St_l defined for an arbitrary spatial scale $\eta \ll l \ll L$. It expresses the ratio of particle response time to $\tau_l = \langle \epsilon \rangle^{-1/3} l^{2/3}$ - the eddy of size l turnover time. For any separation $l \ll L$, the clustering mechanism for $St_l \ll 1$ is related to preferential sampling of the fluid velocity gradient tensor $\nabla \vec{u}$ coarse-grained at scale $\approx l$, which is associated with centrifging out of eddies at that scale. They point as well the that this mechanism is in close relationship to sweep stick mechanism in the inertial range. For $St_l \geq O(1)$ a nonlocal mechanism contributes to the clustering process. One can take a lesson that when dealing with clustering, it is important to define the nondimensional parameters suited to the model used.

sweep-stick mechanism

local Stokes number

The other, quite new approach to clustering analysis puts in the center of attention the concept of coherent clusters of particles: their formation time, size, the local concentration in the cluster as well as their dependence on Re_λ , St , Sv , Fr . Baker et al. [5] and Momenifar and Bragg [78] on the basis of DNS analysis claim that particles in the cluster exhibit significantly higher degree of spatial organization and local accumulation, that their sedimentation velocity is higher than outside the cluster and that clusters align themselves with the local vorticity vector. Most of the experiments concerning preferential concentration focus on cluster and void analysis as well, using the technique of Voronoi triangulation [68, 79, 81, 85, 111]. Some of the research described here lead to the suggestions that turbulence intermittency and cluster/void formation are linked.

Clustering by *caustics* is the least known mechanism of the most complicated structure. The mathematical definition is that they are singularities in particle dynamics i.e. particles of totally different velocities meet in the same space point (see review in Gustavsson and Mehlig [49]). More picturesque formulation of the same mechanism is the sling effect: particle is expelled out of the vortex as if it was shot with a sling. They were observed in numerical simulations [7, 13, 45, 71]. Very recent works of Deepu, Ravichandran, and Govindarajan [38] and Ravichandran and Govindarajan [96] connect them directly to strong enhancement in particle collision probability.

Recent development in massive numerical computations made it possible to take into account other forces acting on the particle like computationally demanding Basset history force [86] or hydrodynamical interaction [80, 123] (so called "two-way coupling") and check if they impact clustering processes. The results of this work are not yet conclusive, but they lead to understanding that these forces may be of great importance. Meanwhile, sedimentation influence on clustering and vice-versa has already been explored in DNS and theory in more detail [Park2014, 3, 5, 8, 26, 39, 50, 55, 78, 100, 101, 113, 119, 122]. Nevertheless the role of gravity in clustering remains an open field. For now, it seems that gravity weakens the clustering of small particles $St < 1$ and increases of large particles $St > 1$.

The advances in studies on clustering of monodispersed particles in HIT has been summarized above. The matter is far more complicated when it comes to the collection of polydispersed particles. Recognizing the influence of polydispersity on clustering is especially important when interpreting experiments with small particles and verifying a theory on experimental basis. Natural sets of particles (like cloud droplets), but also those produced in the laboratory, usually are biased by unavoidable polydispersity. Many of the DNS and laboratory experiments cited here as monodispersed particle studies have sections dedicated to polydispersity influence. First, but still unsolved problem in dealing with polydisperse particles is choosing statisti-

cal variables that can represent the size distribution with respect to clustering processes. There were many propositions, from mean arithmetic Stokes number, to various volume, surface or particle number weighted means. Secondly, the problem is the very way of describing clustering, which would capture its complexity. Some try to define a single measure of segregation [30], other analyze collective radial distribution function (RDF) [Saw2012a, Saw2012b] as well as cluster sizes, structure and motion [65, 66]. Minier [76] reviews available statistical description methods of polydisperse, multiphase turbulent flows. Generally the scarce research agrees on a few topics: even mild polydispersity (like $\Delta St > \langle St \rangle / 5$ in Saw2012a, Saw2012b) reduces overall clustering, the lengthscale of droplet clusters falls into ranges 10-30, 20-30, 40-50 η (depends on the study), so in dissipation range, the lifetime is longer than τ_η and that more than just particle mean $\langle St \rangle$ is needed to statistically describe clustering. There is no agreement if there is dependence on Re_λ , turbulence intensity or shape of size distribution, or if cluster sizes depend on St .

From the above summary of research on clustering we can conclude that the basic mechanisms have still not been understood enough to grasp its impact on cloud evolution. *Tu jeszcze zdanie o wnioskach z powyzszego, do ktorych odwolujemy sie przy analizie dziur.* Next I follow the concept that structures connected to turbulence intermittency may play a significant role in particle spatial distribution change. However fully resolved simulations of NSE for atmospheric-like turbulence is beyond computational reach, hence the need to examine reduced models.

Vortex structures versus cloud droplet clustering

The concept of the paper by [61] is that the factor of-10 acceleration in the growth of the “lucky” droplets (the fastest one-in-a-million) combined with traditional turbulent cascade ideas is enough to explain the size-gap problem in cloud droplet growth theory. This gap, called condensation-coalescence bottleneck as well, is a lack of understanding the processes bringing in around 15 min cloud droplets, that grew by condensation to around 20 μm in radius, to 40 μm , for which size gravitational collisions become effective growth process. Although the Kostinski and Shaw [61] paper did not explain how to get such a fast growing lucky droplet, it gave the lesson that even very rare local events may have great impact on global state of a cloud. Bec et al. [11] showed in statistical analysis of DNS that there is precise connection between the intermittent nature of the carrier turbulent flow and the accelerated growth of particles by increased collisions. However one may miss important information when paying attention to global statistics only, for example where and how this collisions occur. For this reason, the researchers studying the distribution and

collisions of particles in the flow, became interested in the trend of searching for coherent structures in turbulence that can influence this processes [9, 14, 17, 36, 89].

It was mentioned before, that intense vortex structures (or vortex tubes) probably play important role in turbulence intermittency and hence may have particular impact on dynamics of heavy inertial particles. Previous efforts to study this dynamics in vortices were made by simulating droplet trajectories in a prescribed velocity field for several simple single-vortex models. Such research for the simplest model of a line vortex with stretching was conducted by Markowicz, Bajer, and Malinowski [72] with limitation to horizontally oriented vortices. Some specific features of droplet trajectories for monodisperse droplets in another model, a Burgers vortex with stretching, were examined in 2D by Marcu, Meiburg, and Newton [71] for arbitrary alignment with respect to gravity and by Hill [52] for horizontal alignment together with collisions. Ravichandran, Perlekar, and Govindarajan [97] studied the behaviour of particles near fixed points, with no gravity, between two like-signed vortices. Ravichandran and Govindarajan [96] analysed lagrangian density around the particle in 2D point vortex, gaussian vortex and collection of point vortices (no gravity), especially with respect to caustics formation. [38] used this analysis for polydisperse droplets to show growth of particles by increased collisions around single vortex. Picardo et al. [91] in the DNS of turbulent flow (without gravity) indicate the regions that are possibly responsible for enhanced collision probability - vortex-strain worm-rolls - and claim that particles in intense vortex tubes are rapidly ejected into strong straining sheets. On the whole, interest in the topic of the vortices role in particle clustering and collisions has been considerable in recent years. My research was part of this trend and surely filled in one of the gaps. Namely, in my investigation I also took into account the 3D motion of a particle under gravity force as well as described the collective motion of polydispersed particles in a vortex as a proxy of droplets in a real cloud turbulence.

RESEARCH PROBLEM STATEMENT

Generally the objective of this research is to prove that if a violent vortical structure is present in cloud turbulence, it can cause strong local clustering and segregation of cloud droplets. There are several research ideas behind it. Firstly we assume that the motion of a single sedimenting particle in the Burgers vortex model with stretching can be described by means of the formalism of dynamic systems. For some sets of vortex and particle parameters the motion of a particle in two dimensions is determined by different types of attractors. The hypothesis is that in three dimensions the situation is the same and it

leads to the clustering of particles near the vortex. What is more, such clustering in polydispersed systems leads to a strong size segregation. This work also attempts to answer the question whether the observed large heterogeneities in clouds in the form of near-circular "voids" reported in Xu2012 can be explained solely by the presence of a strong vortex in the field of cloud droplets. The studies presented in the thesis are not only unique due to the complexity of the model chosen for analysis, but first of all thanks to the fact that they are anchored to real life by in-situ, first-of-a-kind observations in atmospheric clouds. This thesis is organized as follows. Chapter ?? treats about research methods applied, both numerical and experimental. Chapter ?? contain results. Section ?? provides a detail description of single particle 3D motion in the vortex model and timescales analysis. Second section, Section ?? uses this results to characterize the collective motion of polydisperse particles. Third section, Section ?? describes experimental results. Fourth focuses on cloud "void" creation in numerical simulations. In chapter ?? the results are summarised and discussed. Chapter ?? presents final thesis conclusions and suggestions for future work.

Verification of hypothesis set in this thesis is conducted with the use of simplified model. Particles are small, sedimenting, heavy, inertial and noninteracting with each other, a vortex tube model is Burgers vortex with stretching. The only forces working on particle is Stokes drag and gravity and there is no hydrodynamical interaction between particle and the flow. On the basis of the numerous literature sources cited above I assume that a single, steady, stationary vortex is a good proxy for a rare vortical event in high Re turbulent flow as to inspect particle motion inside the structure. The Burgers vortex is a reasonable approximation of such a localised in time and space single vortex in the flow. Collisions of particles are not taken into account to extract vortex influence on spatial distribution of particles only.

As far as the observations are concerned, it is assumed that the measurement results from mountain-top observatory were not disturbed by the presence of boundaries. Further in the text there is discussion of this assumption. What is most important, however, is that I analyzed one and only case of cloud "voids" ever recorded. These observations were unique and have not been repeated to this day. During my doctoral studies I was preparing a measurement campaign to confirm these results, with the use of a newly designed device. The prepared equipment, operating well in laboratory conditions, did not comply with harsh conditions present in a cloud at the mountain observatory. The experimental difficulties accompanying the registration of a single droplet in a real cloud are described in the following chapters.

Due to numerical power limitations, the Basset history force is not included in particle motion simulations. Its role in particle motion in turbulence is a subject of most recent, separate studies. Another

consequence of these limitations is that numerical simulations do not reproduce the particle number concentrations corresponding to cloud values.

2

METHODS

This Chapter establishes research methods applied in the thesis. Section 2.1 introduces Burgers vortex analytical model and provides literature review for adjusting model parameters. Section 2.2 presents the basics of dynamical systems formalism and brings concepts used for describing the single particle motion in a model of a vortex. Section 2.3 makes a preliminary analysis of the particle equation of motion, tracks the steps to its numerical solution and sets the assumptions for the proper, multiple particle model specific for this thesis. Section 2.4 is devoted to experimental techniques and observation details. Last, but not least, Section 2.5 collects the data on the properties of cloud droplets and cloud turbulence, to establish "cloud-like" conditions that are applied in numerical simulations.

VORTEX MODEL

A model of intense vortex structure chosen for the analysis is Burgers vortex with stretching [28]. It is exact, axisymmetric, steady solution to NSE and a product of balance between stretching effect and viscous diffusion [90]. It is commonly used as an approximation of a vortex tube in DNS and laboratory experiments [12, 57, 84]. Despite its simplicity and limited connection to 3D turbulence, Burgers vortex serves as a testing ground for many physical and mathematical ideas.

Burgers vortex is a 3D steady velocity field \vec{u} determined by two parameters: *circulation* Γ and *stretching strength* γ . The irrotational motion sweeps vorticity radially inward while simultaneously straining the vortex tube in the axial direction, as presented schematically in Fig. 5. These processes exactly counterbalance the tendency for vorticity to diffuse radially outward and as a result it is constant in time. If vortex axis is aligned with z-axis in the cylindrical coordinate system (r, φ, z) , then its vorticity:

$$\vec{\omega} = \frac{\Gamma}{2\pi\delta^2} e^{-\frac{r^2}{2\delta^2}} \hat{e}_z \quad (14)$$

and velocity field:

$$\vec{u} = -\frac{\gamma}{2} r \hat{e}_r + \frac{\Gamma}{2\pi r} \left(1 - e^{-\frac{r^2}{2\delta^2}} \right) \hat{e}_\varphi + \gamma z \hat{e}_z, \quad (15)$$

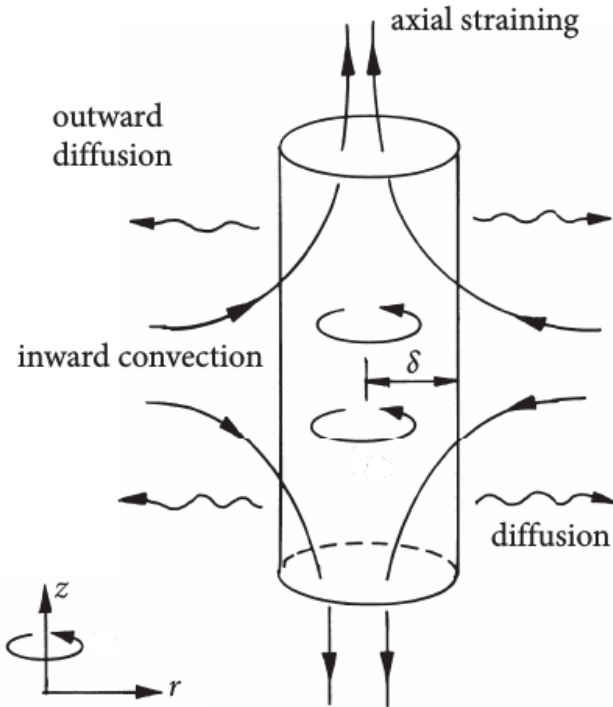


Figure 5: Straining of vorticity in Burgers vortex. δ is vortex core size (from Davidson [37]).

vortex core size
vortex turnover time

where $\delta = \sqrt{2\nu/\gamma}$ is the *vortex core size*. The characteristic timescale of the Burgers vortex flow, *vortex core turnover time*, is:

$$\tau_f = \delta^2 \Gamma^{-1} \quad (16)$$

By the definition, azimuthal velocity reaches its maximum at $r = r_s \delta$, where $r_s = \text{const}$, so the definition introduces a spatial scale r_s into the system. Precise analytical formulation is such, that $r_s = \sqrt{-2W(1, -\exp(-1/2)/2) - 1}$, where $W(k, x)$ denotes Lambert W functions' k-th branch of x. For the purposes of this thesis, only the numerical estimation is used: $r_s \approx 1.5852011$. Burgers vortex velocity components scaled with vortex spatial and time scales, δ and τ_f , are:

$$\vec{u}^+ = -A r^+ \hat{e}_r + \frac{1}{2\pi r^+} \left(1 - e^{-\frac{r^+}{2}} \right) \hat{e}_\varphi + 2A z^+ \hat{e}_z \quad (17)$$

where $A = \text{Re}_v^{-1}$ is vortex strain parameter, defined later in the text, and $+$ denotes dimensionless variables. Three dimensionless velocity components are plotted in Fig.6 for $A = 0.001$.

In order to adjust the model to atmospheric turbulence application, one needs to calibrate model parameters. Past theoretical and experimental studies lack general conclusions about vortex characteristic time and length scales, intensity and appearance in turbulence. Most of this inconclusive information that is available is summarised here. Statistical analysis of DNS data [12, 57, 77, 93] and of experimental data [82] indicate that Burgers vortex core size δ

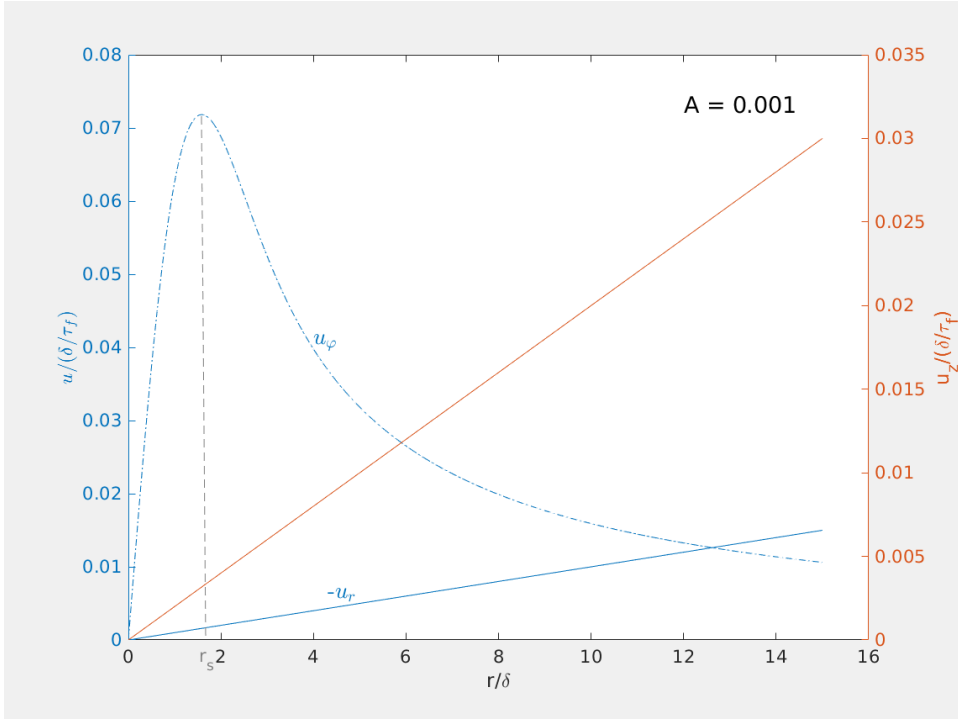


Figure 6: Burgers vortex dimensionless velocity components in cylindrical coordinates for arbitrary strain parameter $A = 0.001$. r_s is defined in the text.

has a log-normal probability distribution. It scales roughly with the Kolmogorov length scale: $\delta = m\eta$ and m range varies in different papers. Generally its minimum reaches 1 and maximum around 12–22. The mean values fall into the range $\langle m \rangle = 3 – 7$. Jimenez and Wray [57] estimates the length of a tube and claim that it scales as $\simeq Re_\lambda^{1/2}$. All these studies had relatively low Reynolds number: $Re_\lambda \simeq 100 – 1000$. Belin et al. [12] reports that the vortex Reynolds number is $Re_v = \Gamma/\nu \approx 200 – 400$. This research, among other papers, shows that azimuthal velocity decreases much faster far from the axis than in Burgers vortex model. Pirozzoli [93] investigated this issue as well, but in more detail. Moisy and Jimenez [77] analyzing DNS instant velocity fields propose that vorticity structures' geometrical aspect ratios evolve towards long tubes ($1 : 1 : 10$), while increasing vorticity threshold. In the study by Biferale, Scagliarini, and Toschi [18], statistics of vortex filament lifetime for a low Taylor microscale Reynolds number Re_λ indicate that the maximum lifetime is on the order of the integral timescale, whereas its mean lifetime scales with the Kolmogorov timescale. Many of the works cited here suggest that there is a relation between root mean square velocity fluctuations \bar{u}' and the circulation parameter Γ .

Tu dodac jeszcze jedna informacje o skalowaniu.

DYNAMICAL SYSTEMS FORMALISM

Dynamical systems theory includes an extensive body of knowledge about qualitative properties of generic smooth families of vector fields and discrete maps. The theory abandons the goal of describing the qualitative dynamics of all systems as hopeless and instead restricts its attention to phenomena that are found in selected systems. Here are presented the dynamical phenomena that are relevant to deterministic system of a single particle moving in Burgers vortex as determined by Eq.13.

Topological features of a dynamical system - singularities, periodic orbits, and the ways in which the orbits intertwine - are invariant under a general continuous change of coordinates. Equilibria and periodic orbits are flow invariant sets. Local quantities such as the eigenvalues of equilibria and periodic orbits, and global quantities such as Lyapunov exponents, metric entropy, and fractal dimensions are examples of properties of dynamical systems independent of coordinate choice. That is why these quantities are good descriptors of flow structure. The definitions of several of the above are given below.

dynamical system

A *dynamical system* is a triple $\{M, f, T\}$ consisting of manifold M called the phase (or state) space endowed with a family of smooth evolution functions f^t that for any time $t \in T$ map the manifold into itself: $f^t : M \mapsto M$. In the case of continuous-time dynamical system and real time $t \in \mathbb{R}$, the family $\{f^t\}_{t \in T}$ of evolution operators is called a *flow* (under additional conditions). A *flow map* for a given t transforms a state vector $x_0 \in M$ into another state vector $x \in M$:

$$f^t : x_0 \mapsto x(x_0, t) \quad (18)$$

trajectory and orbit

A sequence of points $x(t) = f^t(x_0)$ for t in finite range is called the *trajectory* through the point x_0 . A trajectory can be stationary, periodic or aperiodic. An *orbit* refers to totality of states that can be reached from the point x_0 .

Continuous dynamical system can be written as system of coupled ordinary differential equations. When a dynamical system is represented by a set of equations $\dot{x}(t) = v(x, t)$, then $v(x, t)$ is called a *generalized velocity field*.

equilibrium point

Equilibrium point x_k (also referred to as a stationary, fixed, critical, invariant, rest, stagnation) is a state vector for which $\forall t v(x_k, t) = 0$ (equivalently $\forall t f^t : x_k \mapsto x_k$). A *periodic orbit/cycle* p is the set of points $M_p \subset M$ swept out by a trajectory that returns to the initial point in a finite time.

periodic orbit

attractor

An *attractor* Ω is a subset of M onto which a flow is contracting i.e. there exists a connected state space volume that maps into itself under forward evolution. The attractor may be unique, or there can coexist any number of distinct attracting sets, each with its own *basin of attraction* - the set of all points that fall into the attractor under forward evolution. The attractor can be a fixed point (a sink), a periodic

orbit (a limit cycle), aperiodic, or any combination of the above. Conversely, if we can enclose a set Ω by a connected state space volume $M_0 \subset M$ and then show that almost all points within M_0 , but not in Ω , eventually exit M_0 , we refer to Ω as a *repeller*.

The state space M is stratified into a union of orbits. In order to understand the dynamics of the system it is enough to understand how M is stratified and to grasp the nature of its orbits. The central term in this process is stability. Stability matrix is a basic tool characterizing the stability of an orbit:

$$A_{ij}(x) \equiv \frac{\partial}{\partial x_j} (v_i(x)) \quad (19)$$

where $x = x(x_0, t)$ is a trajectory. It expresses the rate of the infinitesimal neighbourhood deformation along the trajectory. However to get to know finite time deformation needed for stability analysis, one needs to know the Jacobian matrix J^t . Its relations to stability matrix are provided here only for the cases of interest to this thesis: equilibrium points and periodic orbits.

For equilibrium point x_k the Jacobian matrix is:

$$J^t(x_k) = e^{A(x_k)t} \quad (20)$$

hence the stability of equilibrium point x_k is determined by eigenvalues of stability matrix $\lambda_k^{(l)} = a_k^{(l)} + i b_k^{(l)}$. Assuming that these eigenvalues are non-degenerate, $\lambda^{(l)} \neq \lambda^{(m)}$ for any pair of eigenvalues, the following claims are present.

- If all $a^{(l)} < 0$, then the equilibrium is stable - a *sink*. For $b^{(l)} = 0$, it is an *stable node*; for $b^{(l)} \neq 0$, it is an *stable spiral*.
- If some $a^{(l)} < 0$, and other $a^{(l)} > 0$, the equilibrium is hyperbolic, or a *saddle*.
- If all $a^{(l)} > 0$, then the equilibrium is repelling, or a *source*. For $b^{(l)} = 0$, it is an *unstable node*; for $b^{(l)} \neq 0$, it is an *unstable spiral*.
- If $\det A(x_k) = 0$, $\text{tr} A(x_k) \neq 0$ it is neutral, a *center* (elliptic).
- If some $a^{(l)} = 0$ there is a symmetry or a bifurcation.

Figures 7 and 8 show diagrams of number of equilibrium point examples. It is important to realise that these examples are pictured in phase space, not in real space.

A periodic orbit of a continuous-time flow can be:

- stable, a sink or a *limit cycle*, *limit cycle*
- hyperbolic or a saddle, unstable to perturbations outside its stable manifold,

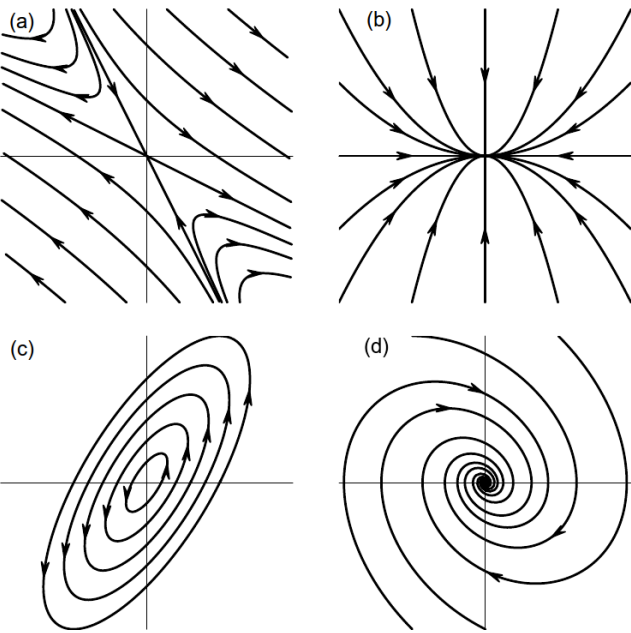


Figure 7: Trajectories in linearized neighborhoods of several 2-dimensional equilibria: (a) saddle (hyperbolic), (b) stable node (attracting), (c) center (elliptic), (d) stable spiral (from Cvitanović et al. [35]).

- elliptic, neutral or marginal,
- partially hyperbolic,
- repelling, or a source, unstable to any perturbation

The range of system parameter values for which a periodic orbit is stable is called its *the stability window*. The set of initial points that are asymptotically attracted to stable periodic orbit in infinity (for a fixed set of system parameter values) is called *the basin of attraction* of the limit cycle. For the detailed analysis of periodic orbit stability conditions see [35].

Hopf bifurcation

Bifurcation is a change of the topological type of the system as its parameters pass through a *bifurcation (critical) value*. One of the classes of bifurcations is so called *Hopf bifurcation*. Suppose α is a bifurcation parameter and $\alpha_{cr} = 0$ is the critical value. In Hopf bifurcation, for $\alpha \leq 0$ the equilibrium is a stable focus. If $\alpha > 0$ the equilibrium becomes an unstable focus and the system has a stable periodic orbit. This is presented schematically in Fig.9.

In order to use the methodology described above to analyze the motion of a particle in a vortex of axial symmetry, it is necessary to first define the state space. When choosing a cylindrical coordinates in \mathfrak{R}^3 the position vector is $\vec{r} = \vec{r}(r, \varphi, z)$, the state vector is $\mathbf{x} = (r, \varphi, z, \dot{r}, \dot{\varphi}, \dot{z})$ and generalized velocity $\mathbf{v} = (\dot{r}, \dot{\varphi}, \dot{z}, \ddot{r}, \ddot{\varphi}, \ddot{z})$.

Tutaj byc moze jeszcze cos dopisac o tym, jak sie to ma do naszej kwestii (po przepisaniu rozdzialu 3 w tym formalizmie dokladniej).

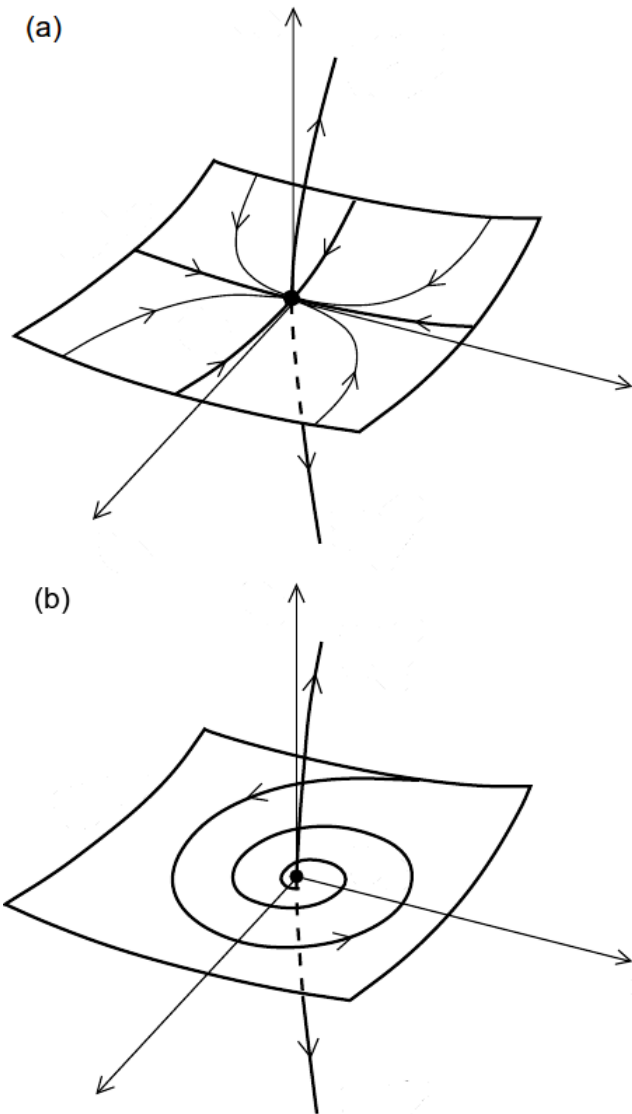


Figure 8: Trajectories in linearized neighborhoods of 3-dimensional equilibria: (a) saddle, (b) saddle-focus.

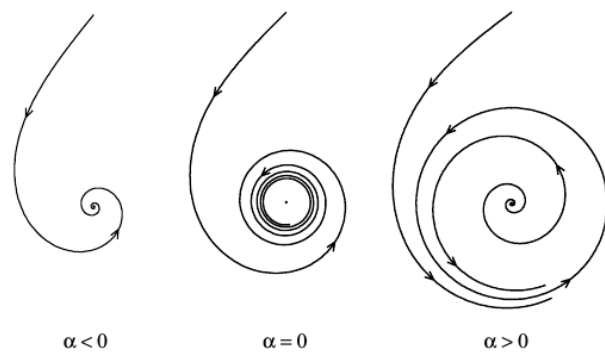


Figure 9: Hopf bifurcation depicted in a plane. α is bifurcation parameter, its critical value is $\alpha_{cr} = 0$. The figure comes from [62].

NUMERICAL SIMULATIONS

Single particle trajectory

Solving Eq.13, the equation of particle motion, for arbitrary parameters and initial conditions, even in steady vortex flow as defined in ?? requires numerical calculations. Below are described the consecutive steps needed to perform these calculations. First few steps of the procedure are also of use for analytical analysis.

In the rectangular coordinate system, in which z axis is aligned with vortex axis, gravity force vector, without loss of generality, is defined to be inclined by the arbitrary angle $\theta \in (0, 90^\circ]$ to vortex axis:

$$\vec{g} = -g (\sin \theta \hat{e}_y + \cos \theta \hat{e}_z) \quad (21)$$

where g is gravitational constant. In cylindrical coordinates:

$$\vec{g}/g = -\sin \theta \sin \varphi \hat{e}_r - \sin \theta \cos \varphi \hat{e}_\varphi - \cos \theta \hat{e}_z, \quad (22)$$

$$\ddot{\vec{r}} = (\ddot{r} - r\dot{\varphi}^2)\hat{e}_r + (2\dot{r}\dot{\varphi} + r\ddot{\varphi})\hat{e}_\varphi + \ddot{z}\hat{e}_z. \quad (23)$$

Equation 13 decomposed into components looks therefore as follows:

$$\ddot{r} - r\dot{\varphi}^2 = \tau_p^{-1} (-\gamma r/2 - \dot{r}) - g \sin \theta \sin \varphi \quad (24)$$

$$2\dot{r}\dot{\varphi} + r\ddot{\varphi} = \tau_p^{-1} \left(\frac{\Gamma}{2\pi r} (1 - \exp(-\gamma r^2/4\nu)) - r\dot{\varphi} \right) - g \sin \theta \cos \varphi \quad (25)$$

$$\ddot{z} = \tau_p^{-1} (\gamma z - \dot{z}) - g \cos \theta \quad (26)$$

The system is primarily dependend on a set of six dimensional parameters: $\{\Gamma, \gamma, \theta, \tau_p, g, \nu\}$. The non-dimensionalization however leads to Eq. ??-?? and gives a set of 4 dimensionless parameters $\{St, S_v, \theta, A\}$ to be defined below Dimensionless variables are denoted henceforth by $+$.

$$\ddot{r}^+ - r^+ \dot{\varphi}^{+2} = -St^{-1} (Ar^+ + \dot{r}^+ + S_v \sin \varphi) \quad (27)$$

$$2\dot{r}^+ \dot{\varphi}^+ + r^+ \ddot{\varphi}^+ = St^{-1} \left(\frac{1}{2\pi r^+} (1 - e^{-\frac{r^+2}{2}}) - r^+ \dot{\varphi}^+ - S_v \cos \varphi \right) \quad (28)$$

$$\ddot{z}^+ = St^{-1} (Az - \dot{z}^+ - S_v \cot \theta) \quad (29)$$

vortex strain parameter
A quantity $A = \nu \Gamma^{-1} = Re_v^{-1}$ is the dimensionless strain parameter, the inverse of vortex Reynolds number Re_v . Stokes number here is calculated with the use of vortex turnover time τ_f so $St = \nu \tau_p A^{-1} \delta^{-2}$. The sedimentation parameter is $S_v = \nu^{-1} g A \delta \tau_p \sin \theta$. It characterizes the motion in a plane perpendicular to the vortex axis (r, φ), that is called here *2D space*. As one can see the equation describing particle motion along the vortex axis (Eq. ??) are independent from the equations describing motion in 2D space (Eq.??, ??), i.e. they depend on different variables. Thus they can be solved separately. The analysis

of single droplet motion using similar formalism was conducted by Marcu, Meiburg, and Newton [71].

The set of equations 28-29 is used next to transcribe the state vector evolution:

$$\dot{\mathbf{x}}^+ = \frac{d}{dt^+} \begin{bmatrix} r^+ \\ \varphi \\ z^+ \\ \dot{r}^+ \\ \dot{\varphi}^+ \\ \dot{z}^+ \end{bmatrix} = \begin{bmatrix} \dot{r}^+ \\ \dot{\varphi}^+ \\ \dot{z}^+ \\ -M_1 r^+/2 - M_2 \dot{r}^+ - M_3 \sin \varphi^+ + r \dot{\varphi}^{+2} \\ M_2 (1 - \exp(-r^{+2}/2)) / 2\pi r^{+2} - M_3 \cos \varphi^+ / r^+ - 2\dot{r}^+ \dot{\varphi}^+ / r^+ - M_2 \dot{\varphi}^+ \\ M_1 z^+ - M_2 \dot{z}^+ - M_4 \end{bmatrix} \quad (30)$$

while for convenience, new equation parameters are defined:

$$M_1 = \frac{\tau_p}{\gamma^{-1}} St^{-2}, \quad (31)$$

$$M_2 = St^{-1}, \quad (32)$$

$$M_3 = Fr^{-2}, \quad (32)$$

$$M_4 = Fr^{-2} \cot \theta.$$

In such a form the set of dimensionless equations (Eq. 30) is solved numerically in Matlab environment by *ode45* build in solver, which is based on an explicit Runge-Kutta (4,5) formula, the Dormand-Prince pair. It is a single-step solver and it uses adaptive time steps. Relative error tolerance assumed is 10^{-3} , absolute error tolerance is 10^{-6} .

Multiple particles in vortex domain

To imitate processes occurring in clouds and examine the effect exerted on a droplet field by the presence of a vortex, a 3D vortex model was designed. Its domain is cylindrical in shape, of radius D and half-length Z (see Fig. 10). Initially the domain is filled uniformly with a given number concentration n of particles. No interaction between droplets is imposed. During the course of simulation, particles leaving the simulation domain are removed.

New particles are constantly placed in the simulation domain in the following way. Cylinder shell of constant width $\Delta r_{box} = 200\mu\text{m}$ (chosen as a compromise between largest particle size and grid accuracy) is discretized by imposing a rectangular grid on it, where one grid box has real dimensions $(\Delta r_{box}, \Delta \varphi_{box}, \Delta z_{box})$ and volume V_{box} .

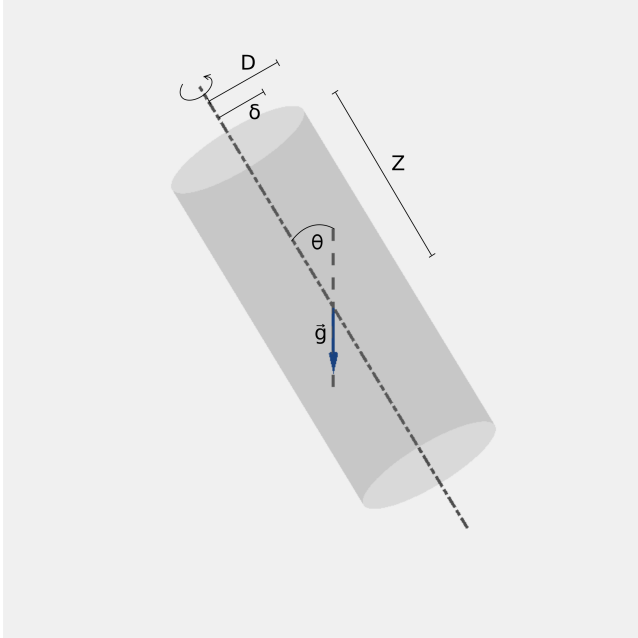


Figure 10: A scheme of numerical simulation's vortex model domain. D is cylinder radius, Z is its half-length, δ is vortex core size, θ is gravity alignment angle, \vec{g} is gravity direction.

$$\Delta r_{\text{box}} = \Delta z_{\text{box}} = 200 \mu\text{m}, \quad (33)$$

$$\Delta \varphi_{\text{box}} = \Delta r_{\text{box}}/D, \quad (34)$$

$$V_{\text{box}} = \Delta r_{\text{box}}^3, \quad (35)$$

$$\vec{v}_{\text{box}} = \vec{u}_r(r = D) = -\gamma D/2 \hat{e}_r, \quad (36)$$

$$iN_i = n * V_{\text{box}}, \quad (37)$$

$$\Delta t_{\text{box}} = \Delta r_{\text{box}}/|\vec{v}_{\text{box}}| = 2\Delta r_{\text{box}}(\gamma D)^{-1}. \quad (38)$$

Initial particle velocity \vec{v}_{box} is set to equal fluid radial stretching velocity at cylinder surface. Initial positions of the new particles are generated on the grid with number density n and randomized with homogeneous spatial distribution, so the probability of having a particle in an arbitrary i -th box is the same for all the boxes and equals N_i . New particles are placed in the shell at time intervals of equal duration Δt_{box} . The initiation of new particles is designed in such a manner to somehow connect the vortex domain with an external environment where the concentration of particles is assumed to be n as well.

Tu moze jeszcze bedzie fragment o tym jak sie zmienia liczba czastek w czasie w roznych symulacjach.

Droplet number concentration within the domain is almost constant and the pattern does not change. After a few seconds, each simulation becomes steady.

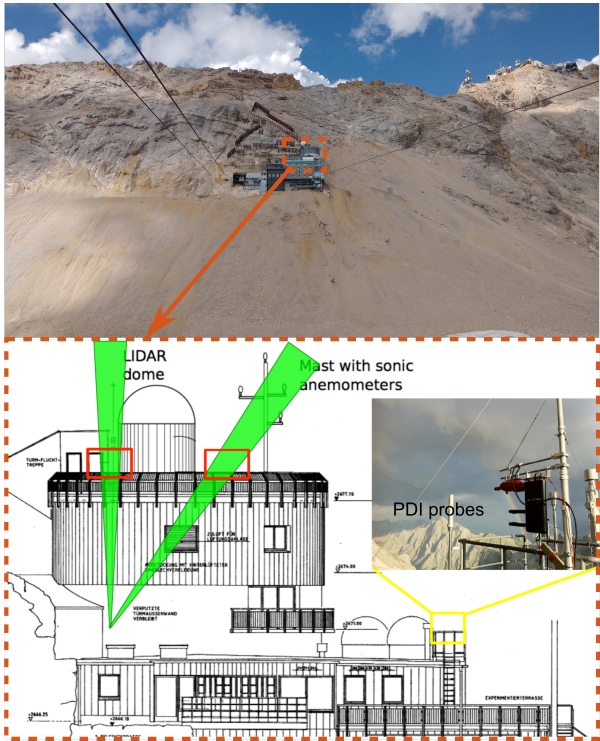


Figure 11: Upper part of the figure presents an image of UFS observatory on the slope of Zugspitze. Lower part shows the arrangement of instruments at the UFS roof.

CLOUD VOIDS OBSERVATION

Observations of the already mentioned cloud structures called cloud voids were performed with the use of lasersheet photography technique. They were accompanied by simultaneous measurement of turbulence and cloud droplet properties. The details of the lasersheet technique and turbulence methods are outlined below in subsequent subsections.

Observations were performed on 27 and 29 August 2011 at Umweltforschungsstation Schneefernerhaus (UFS) on the slopes of Zugspitze in the German Alps. Each time, the cloud event lasted for several hours. Figure 11 presents the measurement setup on UFS roof. For a detailed description of the observatory and characterization of the usual cloud and turbulence conditions on site, see Risius et al. [99] and Siebert et al. [109]. Authors of these papers showed that turbulence and cloud microphysical properties at the measurement site are quite reasonable representations of measurements made in “free” clouds away from the surface.

Atmospheric turbulence measurements

High-resolution measurements of small-scale turbulence during cloud void events were performed by 3D ultrasonic anemometers operated at 10 Hz, providing digital outputs for three components of wind velocity $\vec{u} = (u, v, w)$, where u and v are horizontal components and w is vertical velocity. Having 3D velocity, the mean wind velocity and its fluctuations are estimated in appropriately selected time intervals (also by running average). The time series is treated as spatial series on the basis of Taylor's frozen-flow hypothesis. Velocity fluctuations' 2nd order structure functions are calculated. The Kolmogorov law formulated for the structure functions analogous to $5/3$ law for energy spectrum in inertial range [7] determines mean energy dissipation rate $\langle \epsilon \rangle$ and further the Kolmogorov spatial scale $\langle \eta \rangle$.

Droplet size distribution was measured by a phase Doppler interferometer (PDI) probe mounted approximately 6 m down from the cloud voids observation point. The principle of the device is based on heterodyne detection of Doppler-shifted light from individual droplets, that results in a robust measurement of the droplet diameter and a single component of the droplet velocity vector [33].

Relative humidity and temperature measurements were conducted on-site as well. Relative humidity during cloud immersion was around 100%. More on cloud microphysical properties measurements can be found in Siebert et al. [109].

Lasersheet photography

In laserheet photography particles are illuminated by a plane of light, and a camera placed at a certain angle to this plane collects images of the light scattered on the particles. Generally particle image recorded by a camera depends on the incoming light, the mutual position of light sheet and camera sensor, sensor properties and the certain characteristics of the scattering itself. Firstly, the light incident on the particle is characterized by its spectrum and spatial structure of the incident beam, what depends on the particle position with respect to width, length and divergence of laser sheet. Secondly, the camera sensor pixel responds with a signal registration only if it receives an amount of energy exceeding a certain threshold. The amount of light received by the camera depends on aperture and exposure time. Light scattered by a particle passes through the optics and undergoes some transformations, specific to a camera. What is more, the particle image on the sensor is characterized by the internal intensity distribution (diffraction pattern). All this influences single pixel signal intensity. Image size depends on particle size, optics' magnification, position with respect to the focus and other factors[87]. Thirdly, the

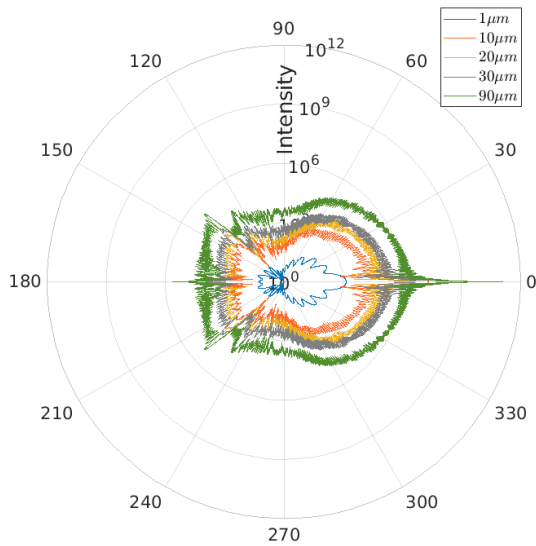


Figure 12: Relative intensity of scattered light (on radial axis, in logarithmic scale) on scattering angle and sphere radius according to Mie scattering theory.

scattered light intensity at an arbitrary angle depends nonlinearly on particle size when comes to light scattering on cloud-like particles. A larger particle can give a lower scattered intensity than a smaller one, or there may be several orders of magnitude difference in intensity between particles differing by 1 order of magnitude in size. The scattering theory applied for cloud droplets and visible light is called Mie theory and is summarised next.

The Mie scattering theory is a rigorous mathematical theory describing the problem of elastic scattering of light by a dielectric sphere of arbitrary size and homogeneous refractive index in the case in which a sphere size is similar to or larger than the wavelength of the incident light. It shows a complex angular and particle size dependency of the scattered light intensity (van de Hulst, 1957). Figure ?? presents this dependency for chosen parameter ranges. Thus, brightness of images of laser light scattered by polydisperse set of droplets is not expected to be monotonic with the particle size.

In cloud void observations in 2011 clouds were illuminated by a laser sheet created with a frequency-doubled high-power Nd:YAG laser (532 nm, 45 W). The sheet was set either vertical or oblique with respect to gravity. The angle between the laser sheet plane and camera recording plane in the oblique case was chosen to increase the scattering intensity on droplets and falls within the range of 30–40 deg. The laser sheet in the observation region was around 50 cm wide and 1 cm thick. Images covering the approximately 2 m long section of the sheet at a distance approximately 10 m from the source were taken with a Nikon D3s 12 MP DSLR camera. Aquired images were used

for size estimation of cloud voids, i.e. small (a few centimeters' scale) clear-air regions in cloud droplet field of round or elliptic shapes. Each one's size was manually determined. In the case of a round void, the diameter was taken as the size; in the case of flattened or ellipsoidal void, the maximal chord was taken. The imprecise setting of the measurement system does not allow to evaluate the influence of the lasersheet geometry on droplet imaging in and around cloud voids.

In order to compare measurements with the results of the numerical simulations, a simplified procedure of droplet size scaling and color scaling, including the effects of laser imaging technique, is proposed. For this purpose, the following assumptions are made:

- one particle image is recorded by one pixel,
- the signal received by a pixel changes linearly with incident light intensity only,
- each particle is in focus and its image size depends linearly on the particle size,
- the experiment in clouds was set up to allow best visualization of maximal number of particles possible.

Calculation of the Mie scattering intensity is performed with the help of an algorithm that was described in [21]. The scattering angle corresponds to 40 deg. In the size range of cloud particles, the light intensity has a general growing tendency, but it is still strongly non-linear. There are 3 orders of magnitude difference between particles of 1 and 30 μm radius. Relative intensity is calculated on this basis. Next, the brightness scaling is made. It assumes that experiment was set up to enable visualization of 95 % of particle size spectrum. The particle size at which the cumulant of the particle size distribution reaches 95 % was calculated. Particles larger than this size have brightness equal to 1 in the simulation visualisations. Brightness for the other particles scales linearly with relative scattered light intensity. To mimic camera sensitivity, there is a threshold below which particles get brightness equal to 0. In the plot with white background, the relation is opposite, so the brightest particles are black, and the least bright are white. This color scaling was used in Section ?? of Chapter ?? for numerical simulation plots and calculations.

Może tutaj dwa zdania o próbie z ramka światła?

CLOUD-LIKE CONDITIONS

In this section I present collection of cloud turbulence and micro-physic data from different experiments and the ones chosen for numerical simulation here.

Parameter	Col2 []	Col2[]	Col3[]
$[R_{\min}, R_{\max}] [\mu\text{m}]$ $\langle R \rangle [\mu\text{m}]$ $\langle St \rangle$ $n [\text{cm}^{-3}]$ $\epsilon [\text{m}^2\text{s}^{-3}]$ $\eta [\text{mm}]$ Re $\lambda [\text{mm}]?$ Re_λ $v [\text{m}^2\text{s}^{-1}]$ $\mu [?]$ $\rho_p [\text{kg m}^{-3}]$ $\rho_f [\text{kg m}^{-3}]$ $g [\text{ms}^{-2}]$			

Part II

RESULTS

Tu znajdzie sie kilka zdan opisu, co mozna znalezc w poszczegolnych rozdzialach wynikowych pracy.

3

CHARACTERISTICS OF SINGLE PARTICLE MOTION IN A BURGERS VORTEX

This chapter addresses the dynamics of the system which is particle motion in a Burgers vortex, defined by set of differential equations in [30](#) and its dimensional counterpart. First, with the use of dynamical system formalism, the system is stratified into its orbits and dynamics of these orbits is determined. Second, particular emphasis is placed on describing the characteristic time scales of the motion and their relations. The aim is to find a measure of spatial pattern formation effectiveness with respect to model parameters.

As was stated before, in set Eq.[30](#) equation describing particle motion along the vortex axis is independent from the Eq. [29](#) describing motion in 2D space. Thus their separate analysis is reasonable.

MOTION ALONG THE VORTEX AXIS

Physically motion along the vortex axis is determined by stretching outflow drag and gravity force only. As a consequence, the particle position along axis shows an exponential dependence on time. The dynamics is determined by one equilibrium point, in which according to definition in Sec.[2.2](#) $\dot{z} = 0$, $\ddot{z} = 0$:

$$z_b^+ = S_v A^{-1} \cot \theta \quad (39)$$

$$z_b = z_b^+ \delta = v^{-1} g \delta^2 \tau_p \cos \theta \propto R^2 \quad (40)$$

It is obvious that $z_b > 0$, because gravity force and stretching has opposite directions only when $z > 0$. Point z_b is a source, so an unstable equilibrium. Position z_b with respect to vortex core size δ and particle radius R , for cloud-like conditions, is plotted in Fig.[13](#).

Integrating Eq. ?? with arbitrary constants C_1 and C_2 leads to:

$$z^+(t) = C_1 \exp \lambda_1 t^+ + C_2 \exp \lambda_2 t^+ + z_b^+ \quad (41)$$

so indeed there is exponential dependence on time. Setting the initial conditions to $z^+(0) = z_0^+$, $\dot{z}(0) = w_0$ gives the solution as follows:

$$\frac{z^+(t^+) - z_b^+}{z_0^+ - z_b^+} = \frac{1}{\lambda_1 - \lambda_2} \left[\lambda_1 \exp \lambda_2 t^+ - \lambda_2 \exp \lambda_1 t^+ + \frac{w_0^+}{z_0^+ - z_b^+} (\exp \lambda_1 t^+ - \exp \lambda_2 t^+) \right]$$

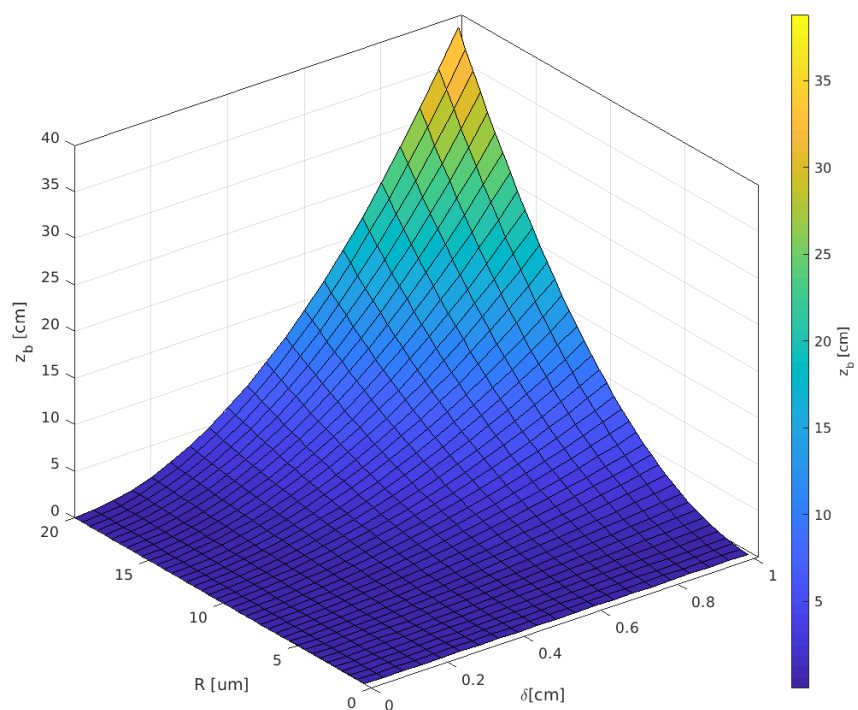


Figure 13: Equilibrium position z_b versus vortex core size δ and particle radius R . Plot variables' ranges correspond to cloud-like conditions.

(42)

where $\lambda_{1/2} = (\mp\sqrt{1+4ASt} - 1) / 2St$. For conviniently a new non-dimensional parameter is defined:

$$k = (1 + 4ASt)^{-1/2} = (1 + 2\tau_p \gamma)^{-1/2} \quad (43)$$

where $k \in (0, 1)$. Then Eq.42, but in the dimensional form, reads:

$$\frac{z(t) - z_b}{z_0 - z_b} = \left[\frac{1}{2} (1 - k) - k \frac{\tau_p w_0}{z_0 - z_b} \right] e^{\frac{-t}{2\tau_p} (k^{-1} + 1)} + \left[\frac{1}{2} (1 + k) + k \frac{\tau_p w_0}{z_0 - z_b} \right] e^{\frac{t}{2\tau_p} (k^{-1} - 1)}. \quad (44)$$

Of obvious, in turbulence the Burgers vortex is a good approximation for a real field of a long-lasting vortex only locally in space and time. Therefore, the motion of particles in a vortex with a finite size and lifetime should be considered. For this reason we discuss and estimate below what we defined as *exit time* τ_{ex} : time at which a particle starting at $z(t=0) = z_0$ with zero initial velocity $\dot{z}(t=0) = 0$, reaches an arbitrary domain border $\pm Z$.

First, the Eq. 44 for the initial velocity set to zero, $w_0 = 0$, simplifies to:

$$\frac{z(t) - z_b}{z_0 - z_b} = \frac{1}{2} (1 - k) e^{\frac{-t}{2\tau_p} (k^{-1} + 1)} + \frac{1}{2} (1 + k) e^{\frac{t}{2\tau_p} (k^{-1} - 1)} \quad (45)$$

In this thesis it is assumed that particles are significantly smaller than vortex size: $R \ll \delta$, and thus $\tau_p \gamma \ll 1$. For large times $t \gg \tau_p$ and small particles, Eq.45 is approximated to:

$$\frac{z(t) - z_b}{z_0 - z_b} = e^{\frac{t}{\tau_z}} \quad (46)$$

where τ_z stands for characteristic time of the motion along axis:

$$\tau_z = \frac{2}{k^{-1} - 1} \tau_p = \frac{2}{\sqrt{1 + 2\tau_p \gamma} - 1} \tau_p \quad (47)$$

According to small particles assumption, τ_z is approximated as well:

$$\tau_z \approx \frac{2\tau_p}{1 + 2\tau_p \gamma / 2 - 1} = 2\gamma^{-1} = v^{-1}\delta^2. \quad (48)$$

Figure 14 presents τ_z relative error (accurate value from Eq.47 minus approximated value from Eq.ch3:eq10 with respect to accurate value) with respect to δ (x-axis) and R (color) as expressed in Eq.47. We see that for cloud-like variables' ranges (which follow small particle assumption) the approximation is fully justified. What is interesting is that in approximation τ_z does not depend on particle size, so it is the same for all particles in polydisperse dispersion. It is also easy to notice that in cloud-like conditions particle response time is

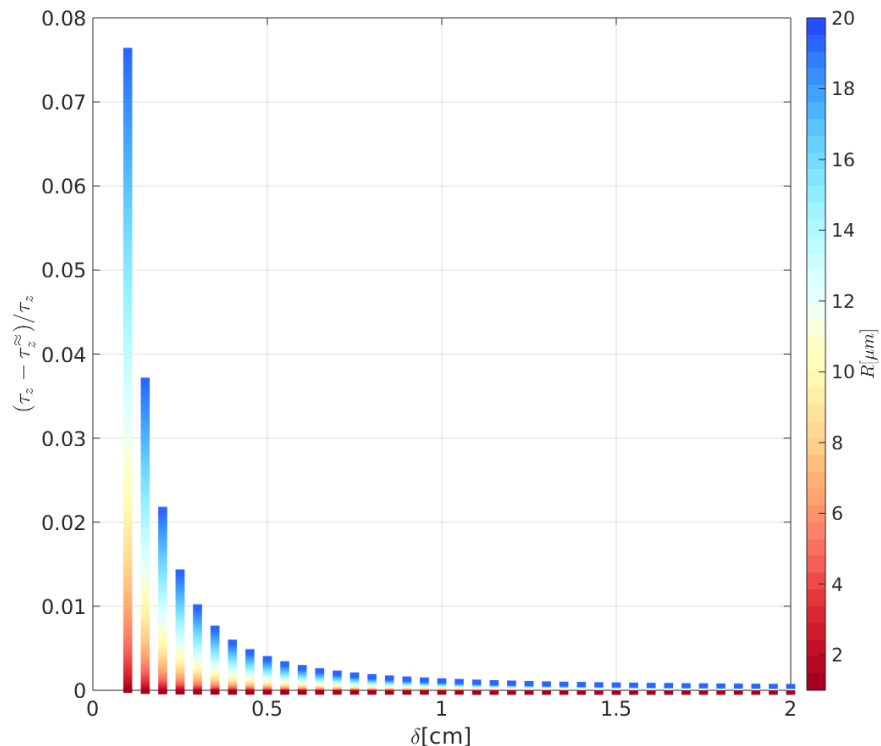


Figure 14: Characteristic time of the motion along vortex axis τ_z relative error versus vortex core size δ and particle radius R . Color indicates dependence on R . Plot variables' ranges correspond to cloud-like conditions.

always significantly smaller than characteristic time of motion along axis $\tau_z \gg \tau_p$. For example when vortex core size is 1 cm, then τ_z is approximately 6.7 s, and for 0.5cm it is 1.6 s.

Direction of motion depends on the relative position of z_0 and z_b . To find the exit time, the following equation must be solved:

$$\frac{\text{sign}(z_0 - z_b)Z - z_b}{z_0 - z_b} = e^{\frac{\tau_{ex}}{\tau_z}} \quad (49)$$

so in such approximation there is:

$$\tau_{ex} = \tau_z \log \left(\frac{\text{sign}(z_0 - z_b)Z - z_b}{z_0 - z_b} \right) \quad (50)$$

The function under the logarithm is denoted as $L(Z, z_0; z_b)$ and further:

$$L(Z, z_0; z_b) = \frac{Z - \text{sign}(z_0 - z_b)z_b}{|z_0 - z_b|} = \frac{Z/z_b - \text{sign}(z_0 - z_b)}{|z_0/z_b - 1|} = \frac{\overbrace{Z/z_b}^{Z^*} - \text{sign}(z_0/z_b - 1)}{\underbrace{|z_0/z_b - 1|}_{z_0^*}} \quad (51)$$

Then the approximated exit time:

$$\tau_{ex}(Z^*, z_0^*; \tau_z) \approx \tau_z \log(L(Z^*, z_0^*)) \quad (52)$$

$$L(Z^*, z_0^*) = \frac{Z^* - \text{sign}(z_0^* - 1)}{|z_0^* - 1|} \quad (53)$$

$$(54)$$

where $Z^* \in (1, \infty)$, $z_0^* \in [-Z^*, Z^*] \setminus \{1\}$. For $z_0^* = 1$ (when $z_0 = z_b$) we have $\tau_{ex} = \infty$, so it agrees with the fact, that z_b is an unstable equilibrium point. The logarithmic factor in τ_{ex} is depicted in Fig. 15. It depends on domain half-length Z and initial position z_0 ratio with respect to z_b .

It is hard to draw any conclusions for single particle exit time on the basis of Fig.???. However there is an interesting feature when thinking about the collection of particles in the vortex. Namely, the mean value of logarithmic factor over a_2 (over all initial positions) equals one for every a_1 (for every vortex half-length):

$$\langle \log L(a_1, a_2) \rangle_{a_2} = \frac{1}{2a_1} \int_{-a_1}^{a_1} \log L(a_1, a_2) da_2 = 1 \quad (55)$$

This means that independently of vortex length, when dealing with uniformly distributed set of particles, the logarithmic factor does not have influence on exit time mean.

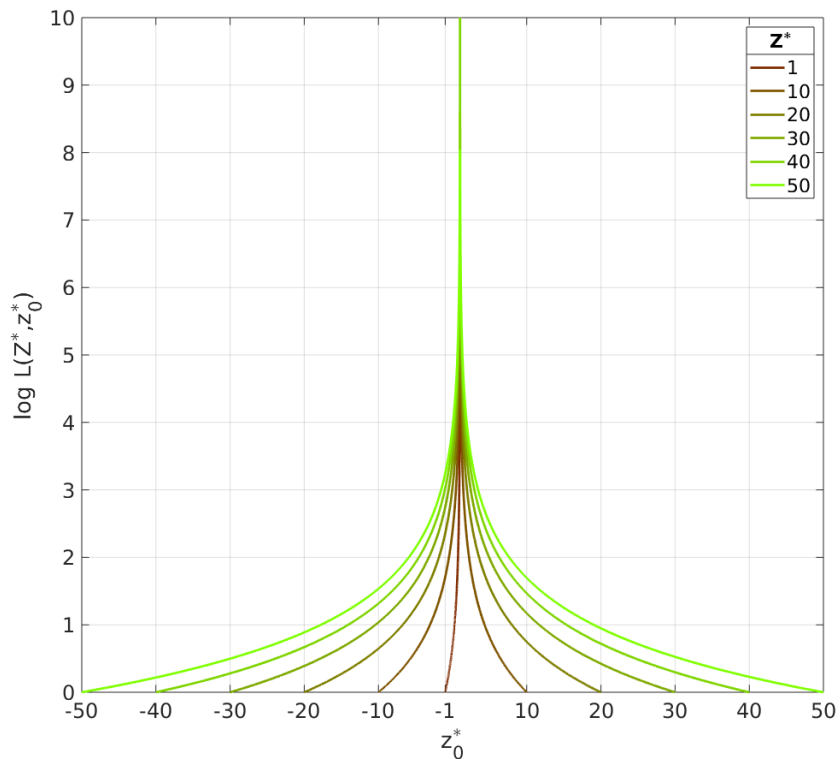


Figure 15: Logarithmic factor in τ_{ex} vs. ratio of initial position and equilibrium position a_2 . Line colors present cases of different ratios of vortex half-length and equilibrium position, a_1 .

MOTION IN THE PLANE PERPENDICULAR TO VORTEX AXIS

The solutions of Eq.?? in 2D space have several different attractors. It is helpful to distinguish two cases: with gravity and without gravity (valid as well when gravity is parallel to the vortex axis). The analysis of single droplet motion in projection on a plane (r, φ) perpendicular to the vortex axis was conducted by Marcu, Meiburg, and Newton [71] and is summarized below.

Without gravity (vertical vortex)

Since $Sv = 0$ in this case the nondimensional equations of motion are:

$$\begin{cases} \ddot{r^+} - r^+ \dot{\varphi}^+{}^2 = -St^{-1} (Ar^+ + \dot{r}^+) \\ 2\dot{r}^+ \dot{\varphi}^+ + r^+ \ddot{\varphi}^+ = St^{-1} \left(\frac{1}{2\pi r^+} (1 - e^{-\frac{r^+}{2}}) - r^+ \dot{\varphi}^+ \right) \end{cases} . \quad (56)$$

and the system is axially symmetric. This set of equations depends on two parameters only: St/A and St . Every particle trajectory is determined by its "radial destiny": either it is attracted by its stable point at vortex axis $r^+ = 0$ or by its stable orbit of radius r_{orb}^+ .

For every particle of a given St in a vortex of arbitrary strain A a stable, circular periodic orbit exists if:

$$St < St_{cr}(A) = 16\pi^2 A \quad (57)$$

For $St > St_{cr}$, there exists a stable equilibrium point positioned on the vortex axis. These cases are analyzed separately below.

At the outset, we address the easiest case of motion: the particle already in orbit. Solving periodic orbit set of equations leads to two results. Firstly, radius of the periodic orbit r_{orb}^+ satisfies the equation:

$$[1 - \exp(-r^+{}^2/2)] / 2\pi r^+{}^2 = \sqrt{A/St}. \quad (58)$$

Equation 58 can be solved numerically. The resulting r_{orb}^+ estimation are presented in Fig. 16 for some arbitrary parameter ranges.

This plot suggest that at least for some intermediate St/A values the r_{orb}^+ dependence can be close to logarithmic. Secondly every particle moving on periodic orbit has the same angular velocity (nondimensional): $\omega_{orb}^+ = \sqrt{A/St}$, or in other words, particle rotation time $\tau_{orb}^+ = \sqrt{St/A}$.

A cloud-like view at the periodic orbit issue is considered below. Periodic orbit existence condition 57 is reformulated:

$$R > R_{cr} = 12\pi \sqrt{\rho_a/2\rho_p} A \delta \quad (59)$$

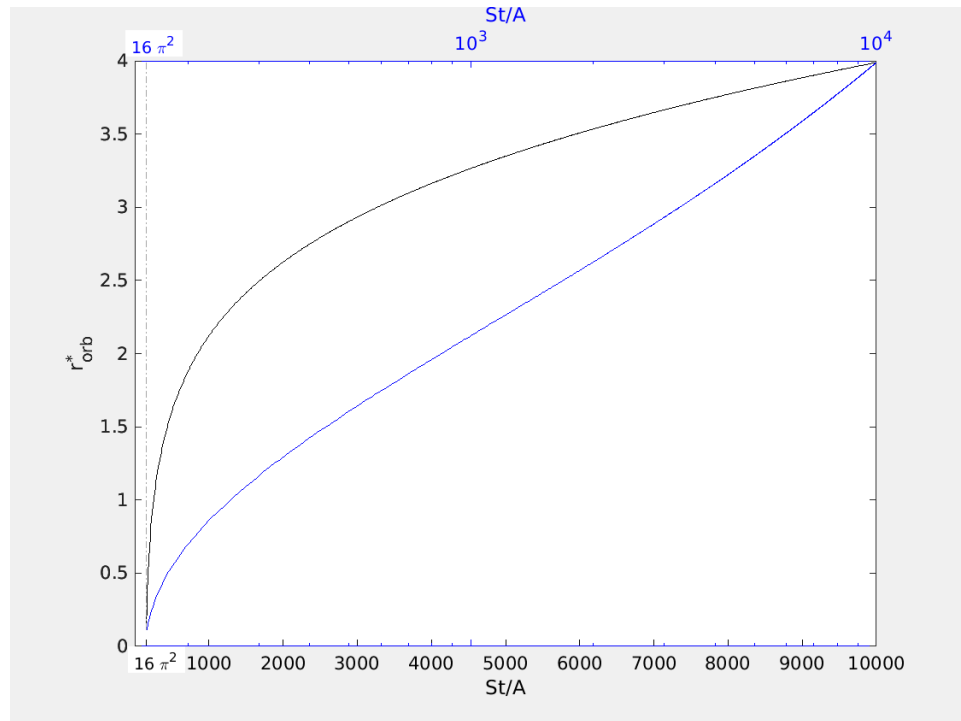


Figure 16: Particle stable orbit radius r_{orb}^+ dependence on parameter St/A .

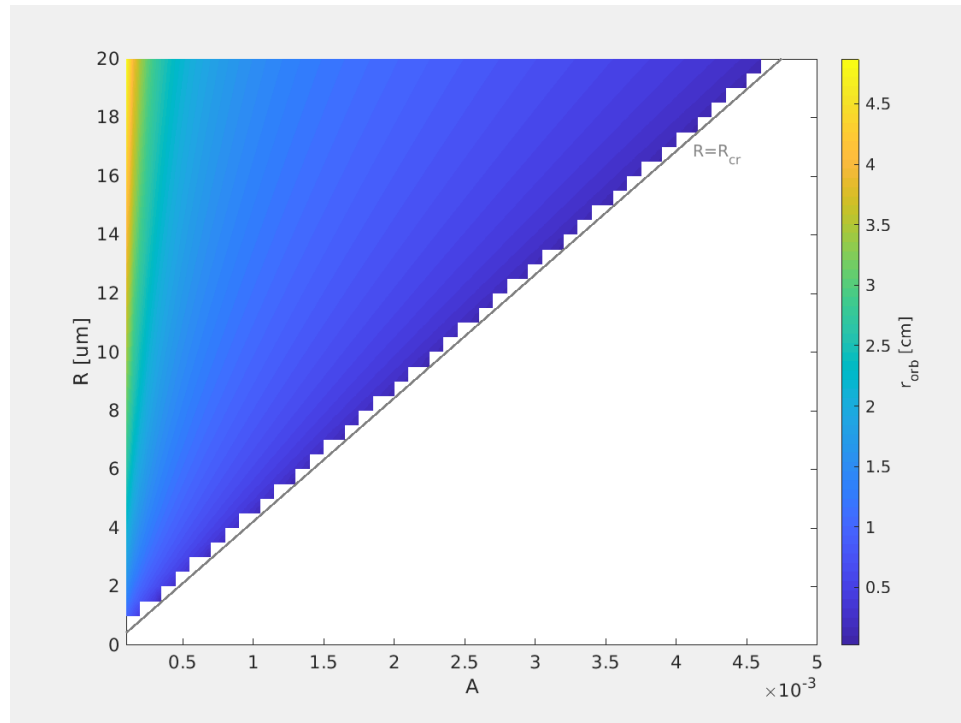


Figure 17: Particle stable orbit radius r_{orb} dependence on particle radius R and vortex strain parameter A for cloud-like parameter ranges and vortex core size $\delta = 0.5$ cm. Black line represents stable orbit existence condition.

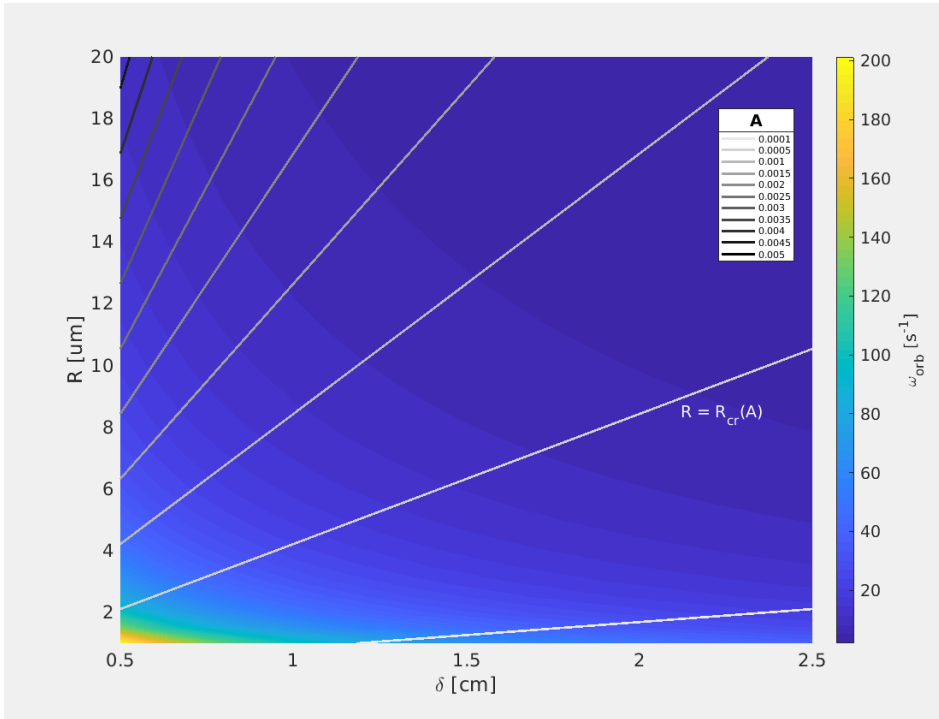


Figure 18: Particle stable orbit angular velocity ω_{orb} dependence on particle radius R and vortex core radius δ for cloud-like parameter ranges.

The r_{orb} (note: dimensional) calculation results presented in Fig. 16 are now shown in the Fig. 17, where vortex core size is chosen arbitrarily: $\delta = 0.5 \text{ cm}$. We can see that to some extent orbit radius is of vortex core radius order.

It is worth to notice that the dimensional angular velocity ω_{orb} is independent of A . It is in fact inversely proportional to particle radius R and vortex core size δ :

$$\omega_{\text{orb}} = \sqrt{A/\text{St}}\tau_f^{-1} = \delta^{-1}\sqrt{\nu\tau_p^{-1}} = \sqrt{\gamma(2\tau_p)^{-1}} = 3\nu\sqrt{\rho_a/2\rho_p}(R\delta)^{-1} \propto (R\delta)^{-1}. \quad (60)$$

Fig. 18 presents cloud-like values of angular velocity ω_{orb} . It is itself independent of A , but it is the periodic orbit existence condition that depends on A . The existence condition is presented in Fig. 18 by $R = R_{\text{cr}}(A)$ plots. For a given A periodic orbits exist in $R > R_{\text{cr}}(A)$ area.

Particle rotation time being an inverse of angular velocity is proportional to vortex core radius and particle radius:

$$\tau_{\text{orb}} = \sqrt{2\tau_p/\gamma} \propto R\delta. \quad (61)$$

The previously established assumption of small particles i.e. $\tau_p \ll \gamma^{-1}$ leads to the conclusion that $\tau_{\text{orb}} \ll \gamma^{-1}$ as well. More on timescales of motion can be found in the next section.

As we argued before Burgers vortex can be a good approximation for a real turbulent field only locally in space. The same applies to time. Therefore, it seems worthwhile to investigate the motion of a particle not only already in its orbit, but rather starting at arbitrary position and approaching its destined radial position ($r^+ = 0$ or $r^+ = r_{\text{orb}}^+$). For the sake of simplicity we should select as starting radial positions only the ones distinguished in the model and that are $r^+(0) = 0$ and $r^+(0) = r_s$. The motion of a particle defined in this way is called here a "docking process". Time at which the docking process occurs is called docking time and noted t_{doc}^+ . In short, for the purposes of further analysis, we distinguish two types of process:

- in-orbit docking: $r^+(0) = 0$, $\dot{r}^+(0) = u_r^+(0)$, particle is attracted by its periodic orbit r_{orb}^+
- axis docking: $r^+(0) = r_s$, $\dot{r}^+(0) = u_r^+(r_s)$ particle is attracted by a point on vortex axis $r^+ = 0$.

Due to the facts that the particle approach its destined radial position asymptotically, the docking process in numerical simulations was calculated between following points in the phase space:

- $r^+(0) = \epsilon$, $\dot{r}^+(0) = u_r^+(\epsilon)$ and $r^+(t_{\text{doc}}^+) = r_{\text{orb}}^+ - \epsilon$,
- $r^+(0) = r_s - \epsilon$, $\dot{r}^+(0) = u_r^+(r_s - \epsilon)$ and $r^+(t_{\text{doc}}^+) = \epsilon$.

The choice of ϵ will be elaborated on later.

Figure 19 and Fig. 21 show the process of docking particles in orbit and in axis respectively, differing in parameters St and A (for $\epsilon = 10^{-4}$). Line color corresponds to the value of parameter St/A . Fig.20 and Fig.22 represent the same data, but with the selected axis scalings:

- nondimensional time is scaled for each particle separately by its t_{doc}^+ .
- Values of radial velocity \dot{r}^+ are scaled by the fluid velocity u_r at the starting point
- The φ^+ values are scaled by rotational fluid velocity $u_\varphi^+(\epsilon)/\epsilon$ (axis docking) or particle orbit speed ω_{orb} .

Figures 19 and 20 reveal that the orbit docking particle first moves around the axis of the vortex together with the fluid, but with zero radial velocity. Then the centrifugal force acting on it causes a rapid increase in radial speed in the direction away from the vortex axis, and the distancing from the axis in turn results in a decrease in rotational velocity. This velocity after the first steep drop slowly tends to the particle velocity in the periodical orbit ω_{orb} , in accordance with the theory. At the same time the radial velocity rapidly drops

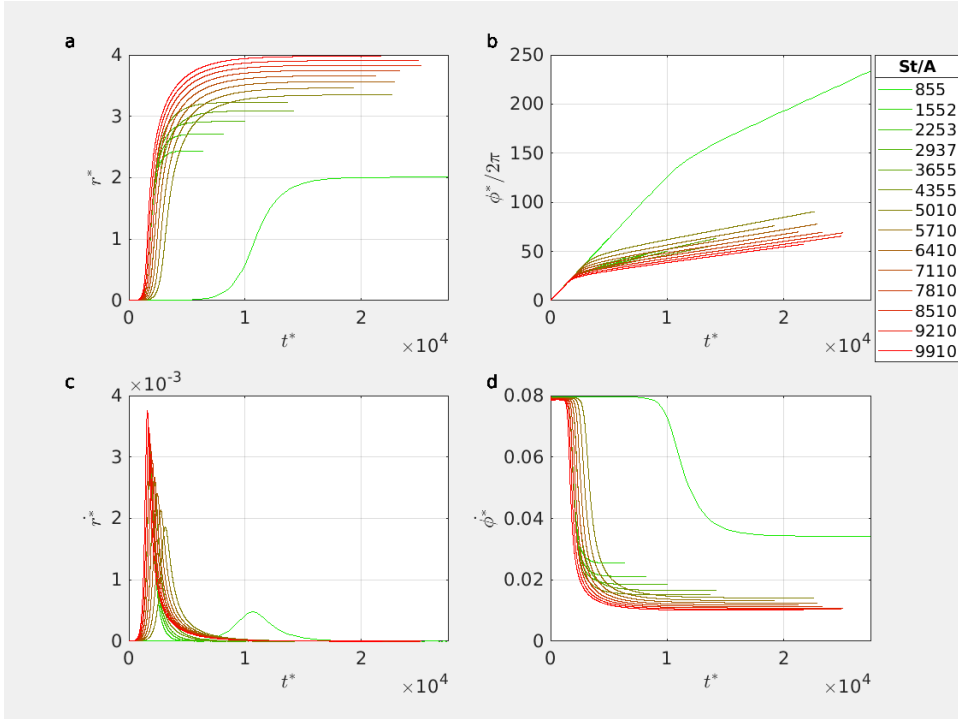


Figure 19: Particle docking in orbit for different parameters St and A , $\epsilon = 10^{-4}$. Line color corresponds to the value of parameter St/A . Panel **a** - radial coordinate, **b** - polar angle, **c** - radial velocity, **d** - angular velocity.

to reach zero. The rate of these changes depends on the parameters of the model in a complex way. After scaling the time by t_{doc}^+ it can be noticed that the docking process depends mainly monotonically on the parameter St/A . When its value decreases towards $16\pi^2$ the docking time t_{doc}^+ tends to infinity.

Jakies pomysły, jak można opisać ten ruch kropli? Chodzi przecież tylko o znalezienie skal czasowych ruchu, a nie o dokładne oszacowanie t_{doc} , który może bardzo zależeć od warunków początkowych i brzegowych.

Figures 21 and 22 show that in the point docking process a particle firstly move with radial fluid velocity $(v_r^+(r_s - \epsilon))$, which decreases almost exponentially in time with the rate depending on St/A parameter only, when the time is scaled respectively t^+/t_{doc}^+ . Angular velocity increases towards fluid velocity $v_\phi^+(\epsilon)/\epsilon$. When St/A increases towards $16\pi^2$ the docking time t_{doc}^+ tends to infinity.

The first glance at 21 and 22 leads to the observation that the radial motion (as for $r(t)$ and $\dot{r}(t)$) of the particle docking on the axis is close to exponential. Therefore, a simplified model of this process is proposed below and an attempt is made to estimate its timescale

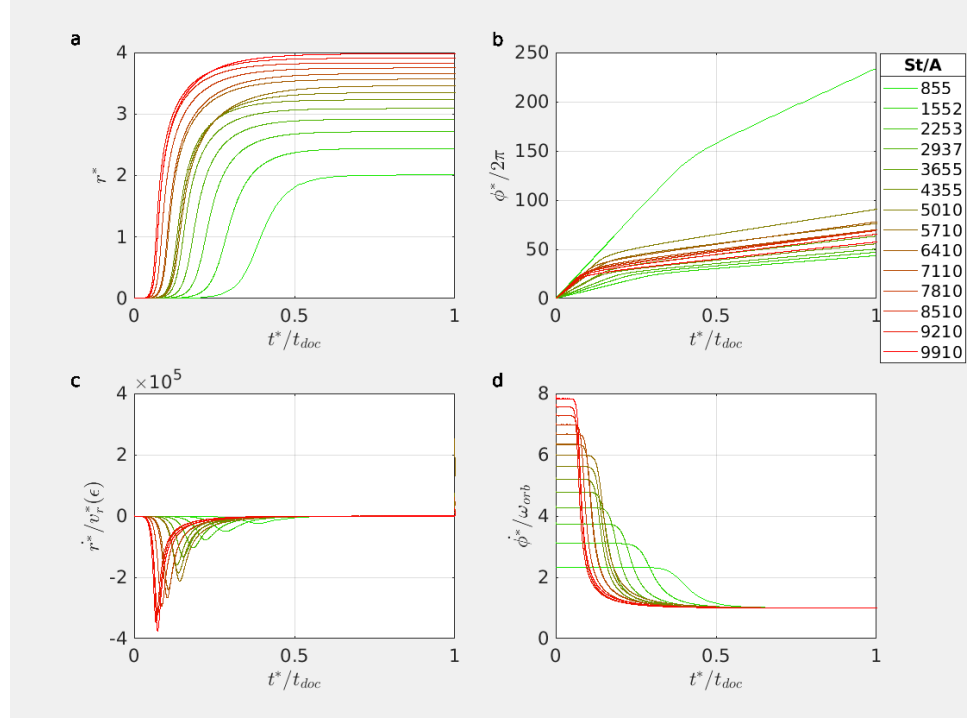


Figure 20: Same as in Fig. 19, but time is scaled by each particles docking time, **c** - radial velocity is scaled by the fluid velocity at the starting point $u_r(\epsilon)$, **d** - angular velocity is scaled by the particle orbit angular velocity ω_{orb} .

$\tau_{\text{doc}1}^+$.

Lets assume that in the axis docking process we have:

$$\begin{cases} \dot{r}^+(t) = u_r^+(r_s - \epsilon) \exp(-t/\tau_{\text{doc}1}^+), \\ r^+(0) = r_s - \epsilon, \\ r^+(t_{\text{doc}}) = \epsilon \end{cases} . \quad (62)$$

Then:

$$r^+(t^+) = r_s - \epsilon + (r_s - \epsilon) A \tau_{\text{doc}1}^+ (\exp(-t^+/\tau_{\text{doc}1}^+) - 1). \quad (63)$$

The numerical simulations results presented in Fig. 22 suggest that it is reasonable to assume: $\tau_{\text{doc}1}^+ = t_{\text{doc}}^+ g^{-1}(St/A)$ where $g(St/A)$ is an arbitrary function. This assumption used in the relation for t_{doc}^+ based on Eq.63 gives:

$$r^+(t_{\text{doc}}^+) = \epsilon = r_s - \epsilon + (r_s - \epsilon) A \tau_{\text{doc}1}^+ (\exp(-g(St/A)) - 1) \quad (64)$$

and finally:

$$\tau_{\text{doc}1}^+ = \frac{r_s - 2\epsilon}{r_s - \epsilon} \frac{1}{A} [1 - \exp(-g(St/A))]^{-1} \quad (65)$$

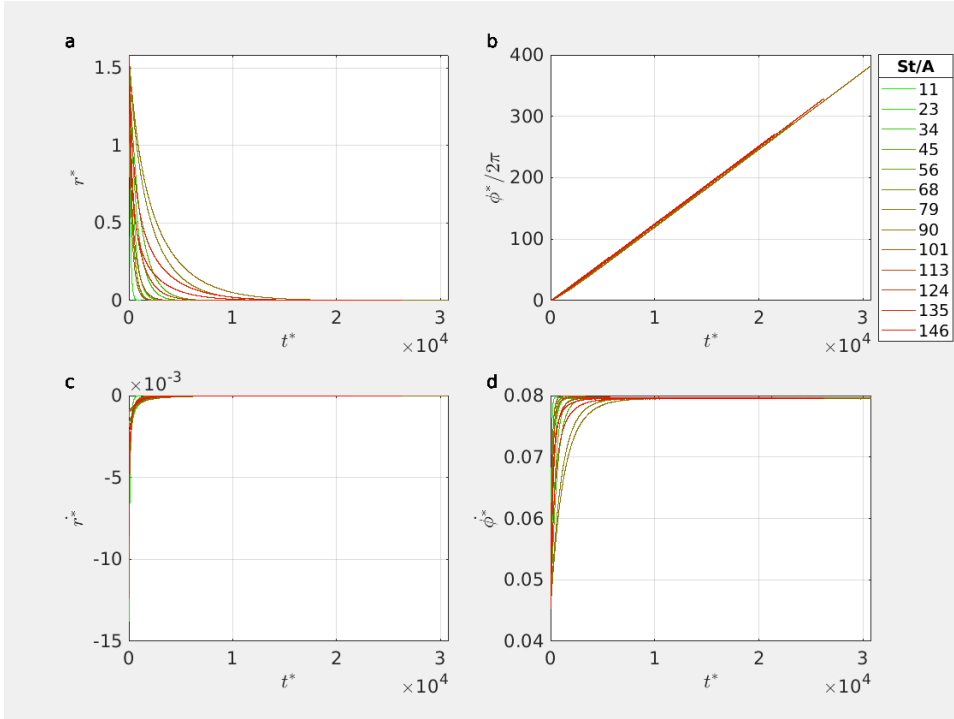


Figure 21: Particle docking on axis for different parameters St and A , $\epsilon = 10^{-4}$. Line color corresponds to the value of parameter St/A . Panel **a** - radial coordinate, **b** - polar angle, **c** - radial velocity, **d** - angular velocity.

This could suggest that $\tau_{\text{doc}1}^+ \simeq A^{-1}$. In order to validate this hypothesis we fitted the relation proposed in Eq. 62 to particle trajectories where $\tau_{\text{doc}1}$ was the fitting parameter. Fig. 23 presents the scatter plot of the results times A . Point color represents Stokes number.

This plot leads to the conclusion that axis docking timescale can be approximated by A^{-1} . Dimensional axis docking timescale is then:

$$\tau_{\text{doc}1} \simeq \frac{\tau_f}{A} = 2\gamma^{-1} \quad (66)$$

We see that $\tau_{\text{doc}1}$ depends primarily on γ^{-1} , exactly as in the case of motion along vortex axis (see Eq. 48).

Further the analysis of t_{doc}^+ for arbitrary parameter ranges was conducted. Figure 24 and 25 present the results of t_{doc}^+ numerical calculation, with respect to St and A in 3D and 2D plots respectively. Blank spaces in the figures represent sets of parameters for which calculation was numerically expensive and hence the result was not included. Vertical axis in 24 and colorscale in both figures are logarithmic. Black line in Fig. 25 represents the $St = St_{\text{cr}}(A)$.

Fig. 24 and 25 suggest some preliminary thoughts. First, defined in a twofold way the time t_{doc} seems to have a physical sense: the values

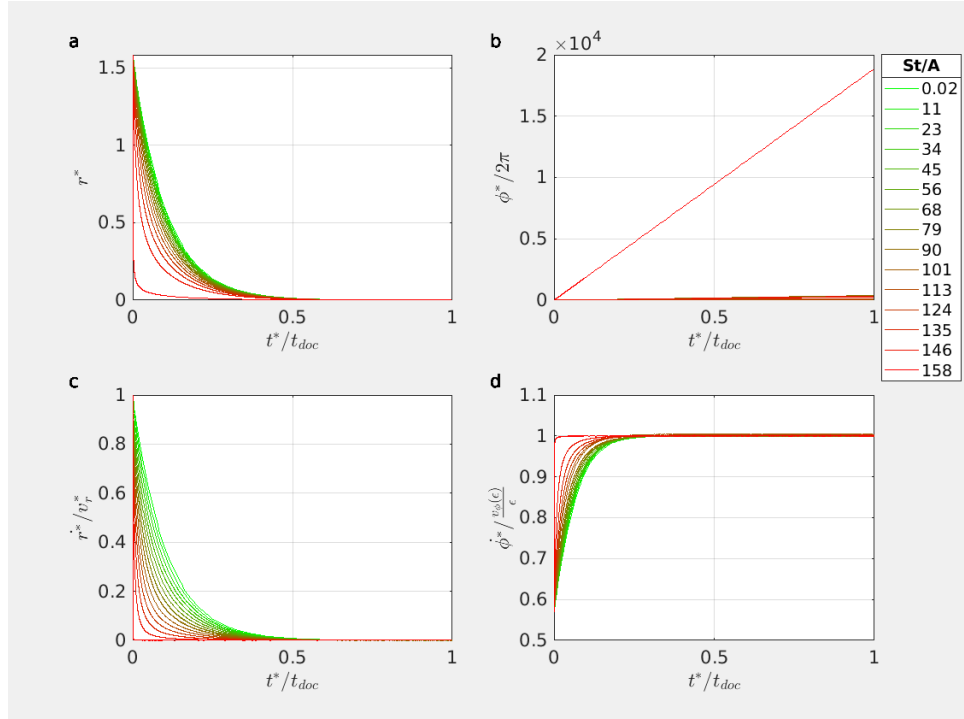


Figure 22: Same as in Fig. 21, but time is scaled by each particles docking time, **c** - radial velocity is scaled by the fluid velocity at the starting point $u_r(r_s)$, **d** - angular velocity is scaled by the fluid angular velocity $u_\varphi(\epsilon)/\epsilon$.

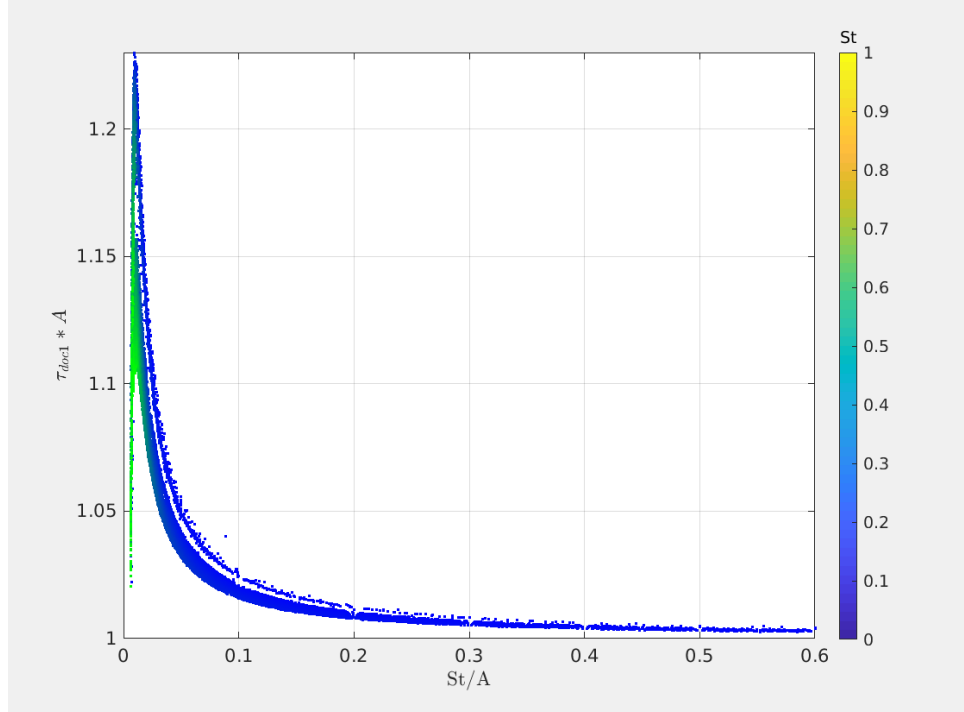


Figure 23: Results of fitting the relation proposed in Eq. 62 to particle trajectories with the fitting parameter τ_{doc1} . For transparency Y axis shows fitting parameter times A.

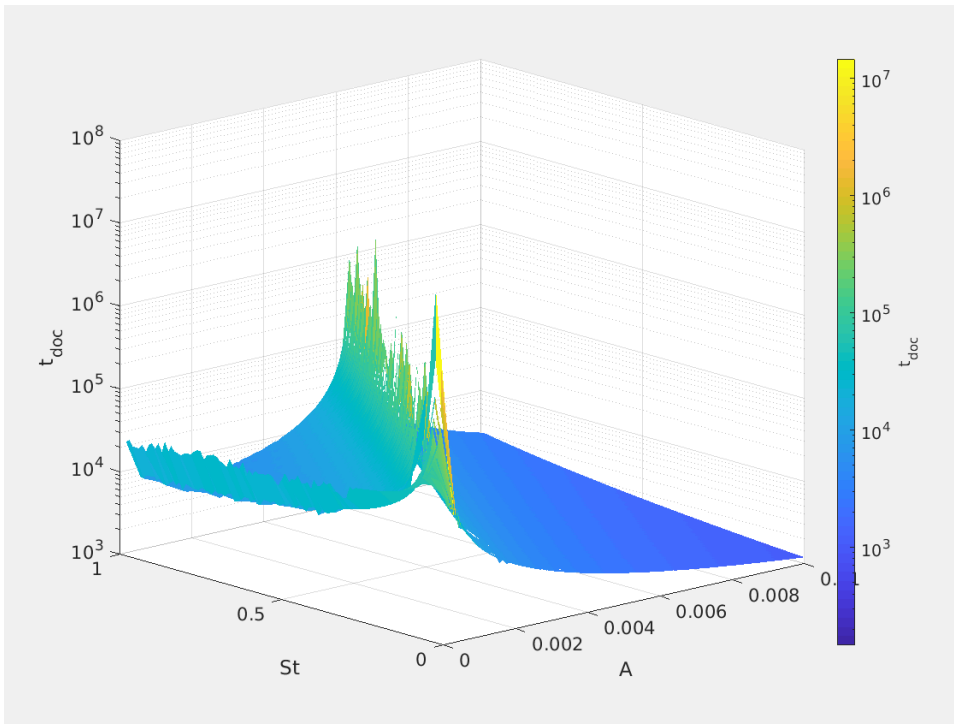


Figure 24: Docking time calculated numerically with respect to St and A for arbitrary variable ranges with $\epsilon = 10^{-5}$. Blank spaces represent lack of data, numerically too expensive.

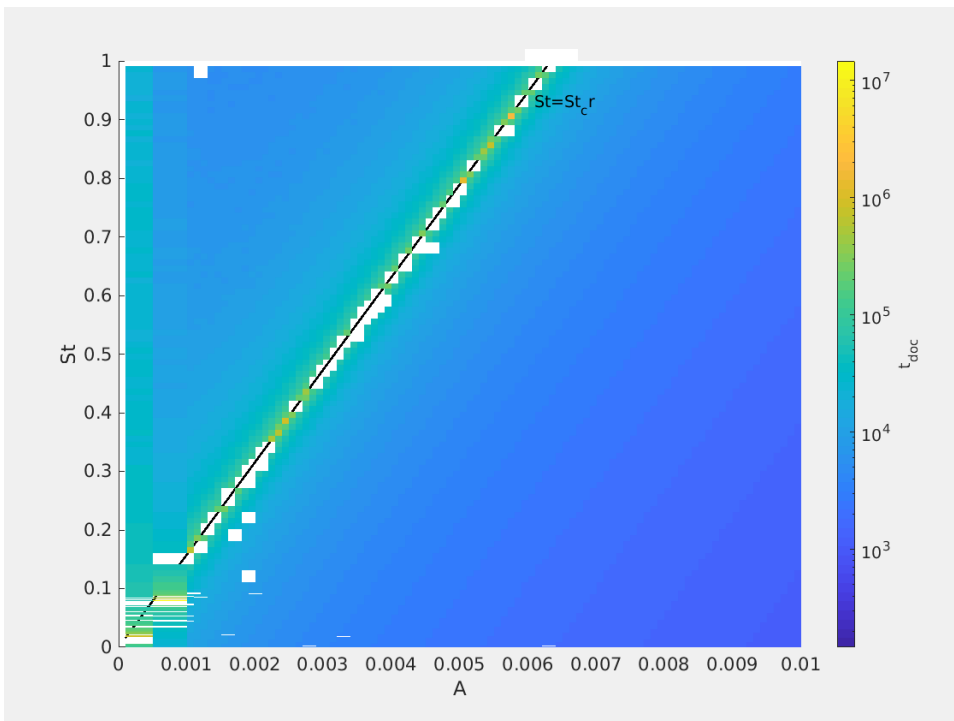


Figure 25: The same as in Fig. 24, projection. Black line $St = St_{\text{cr}}(A)$ shows the stability border: particles to the left are attracted by periodic orbits, particles to the right by stable points on vortex axis.

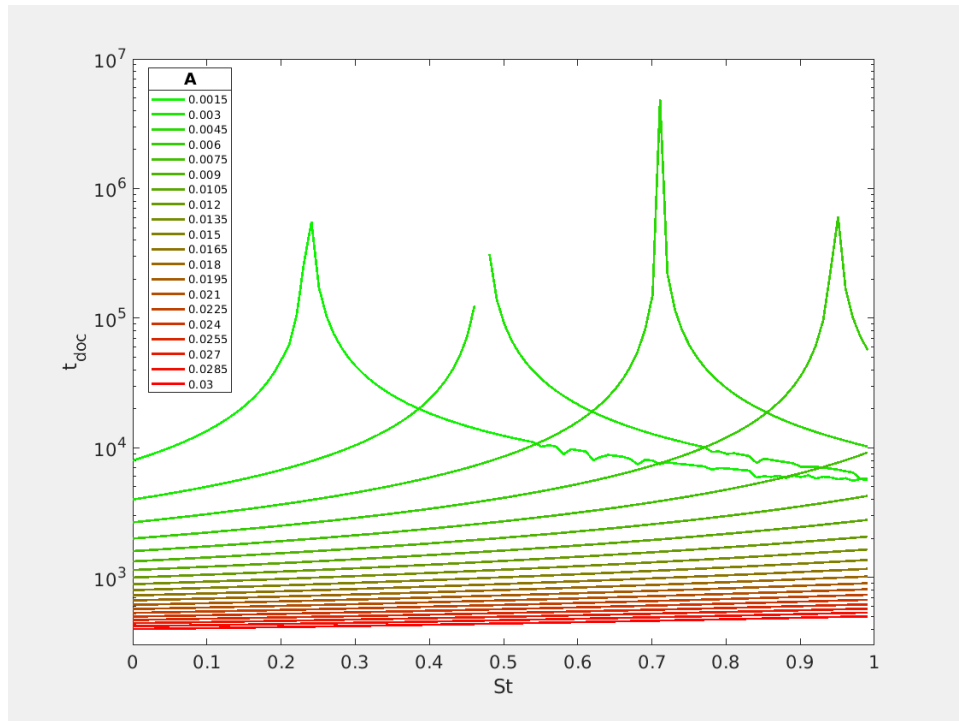


Figure 26: Docking time calculated numerically with respect to St for a few chosen A values, $\epsilon = 10^{-5}$.

are of a similar order, and around the sharp boundary of two regimes: $St = St_{\text{cr}}(A)$, they seem to tend towards infinity, what agrees with theroretical prediction. Secondly,

Tutaj jeszcze pozostały ewentualnie do wrzucenia jakieś wnioski z rysunków?

- wyrazne szalone (log!) maksimum wokol $St = St_{\text{cr}}$, poniewaz sila dzialajaca na czastke jest malutka
- Dla $St < St_{\text{cr}}$ glownym parametrem wydaje sie byc St/A razy cos tam, bo linie sa prawie rownolegle dla malych A wzrost czasu prawie wylacznie ze zmniejszajacym sie A - orbity sa tak daleko?

Since ϵ in theory is infinitesimally small but the numerical calculation demands finite value, the sensitivity analysis was conducted below for $\epsilon = 10^{-n}$, $n = 1, 2, 3, 4, 5$.

Dopisac, gdy juz cos wiecej bedzie wiadomo o samym czasie dokowania.

With gravity (inclined vortex)

Nonparallel alignment of the gravity vector and vortex axis ($\theta \neq 0$) destroys the axial symmetry of the system and introduces the presence of other attractors, such as limit cycles and multiple equilibrium

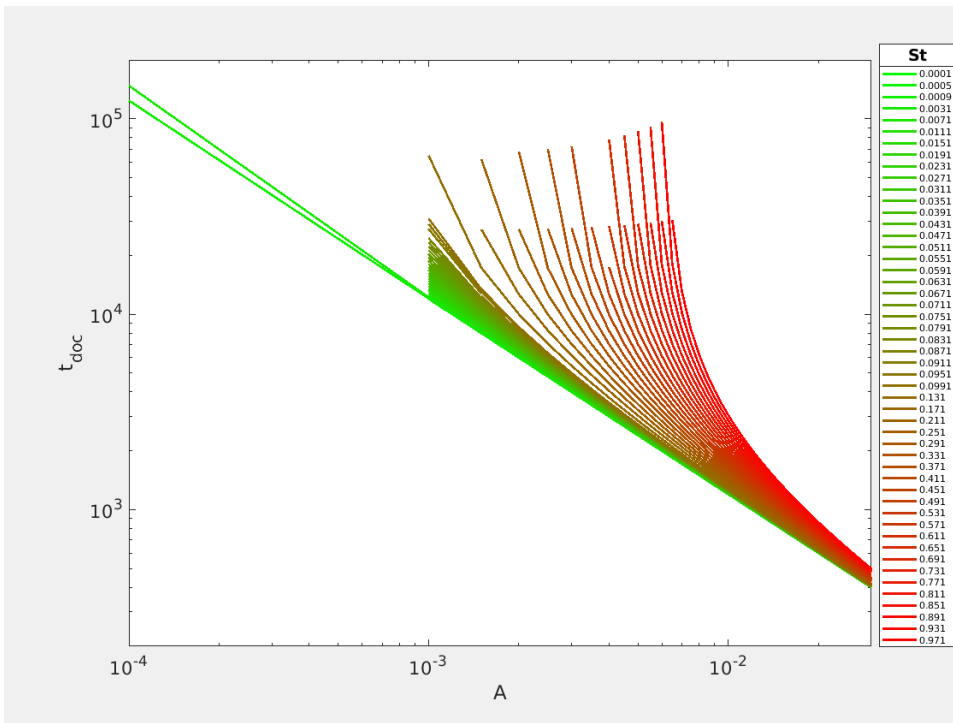


Figure 27: Docking time calculated numerically with respect to A for a few chosen St values, for $A > \text{St}/16\pi i^2$, $\epsilon = 10^{-5}$.

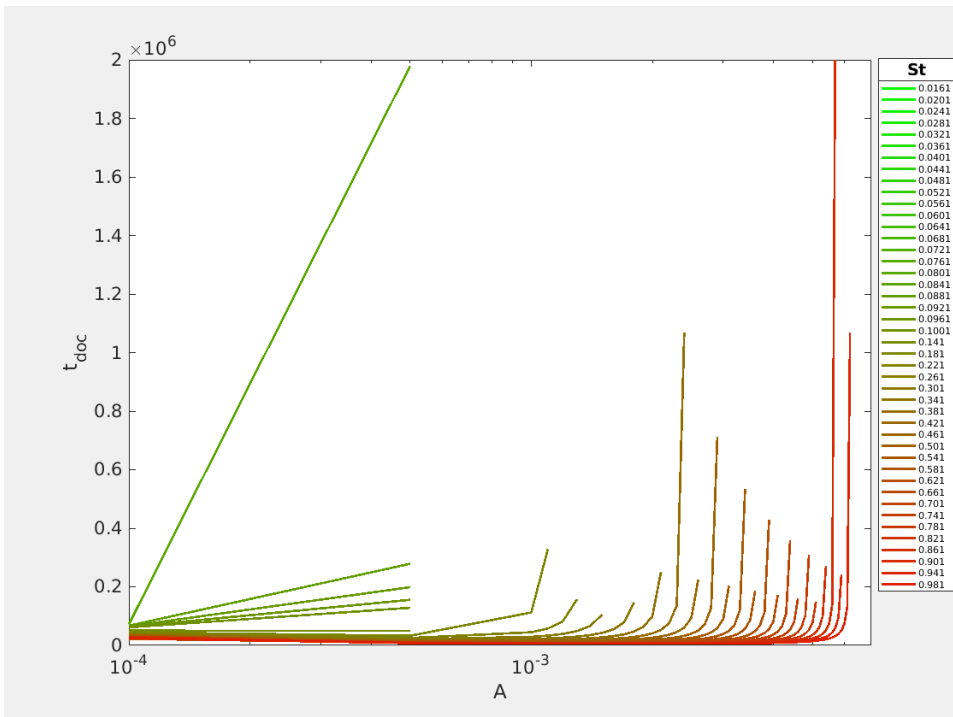


Figure 28: Docking time calculated numerically with respect to A for a few chosen St values, for $A < \text{St}/16\pi i^2$, $\epsilon = 10^{-5}$.

Table 1: Existence of equilibrium points with respect to A and S_v parameters.
 $A_{cr}, r_s^+, r_{min}^+, S_v \text{ min}, S_v \text{ max}$ defined in the text body.

$A \geq A_{cr}$	S_v - arbitrary	1 eq. point
$A < A_{cr}$	$< S_v \text{ min}$	1 eq. point at $r^+ < r_s$
	$[S_v \text{ min}, S_v \text{ max}]$	2 or 3 eq. points
	$> S_v \text{ max}$	1 eq. point at $r^+ > r_{\max}$

Table 2: Burgers vortex non-dimensional numbers

A_{cr}	0.02176
r_i^+	2.1866
r_s^+	1.585201

points outside the axis.

For a nonzero θ , every particle always has equilibrium points in 2D space. Positions of these points are determined by S_v and A . They can be uniquely determined by solving the equation for the radial component r^+ only:

$$f_A(r^+) = S_v, \quad (67)$$

where function $f_A(r^+)$ is defined for each A :

$$f_A(r^+) = r^+ A \sqrt{1 + \left(\frac{1 - \exp\left(\frac{-r^2}{2}\right)}{2\pi A r^2} \right)^2} \quad (68)$$

and is called an equilibrium curve (see Fig.2 in Marcu, Meiburg, and Newton [71]). Detailed analysis of equilibrium point equation is performed below and leads to the conclusions summarised in Table 1.

Equilibrium curves for a dozen of A values are shown in Fig. 29. It is easy to find that $f_A(0) = 0$ and $\lim_{r^+ \rightarrow \infty} f_A(r^+) = \infty$. Moreover, there exists a critical value A_{cr} for which bifurcation from one unique solution (for $A \geq A_{cr}$) to maximally three solutions (for $A < A_{cr}$) occurs. A_{cr} corresponds to the equilibrium curve that has a horizontal slope at the inflection point. A_{cr} value was estimated numerically (see the Table 2). It is also easy to prove that the equilibrium curves asymptotically tend to the function $f_{A \rightarrow 0+}(r) = (1 - \exp(-r^2/2)) / 2\pi r$. This function, unlike equilibrium curves for $A \in (0, A_{cr})$ does not have a minimum.

For $A \geq A_{cr}$ the equilibrium curve is a monotonically increasing function of r^+ so there exists exactly one solution for every S_v value. For $A < A_{cr}$ the equilibrium curve always has one maximum at r_{\max}^+

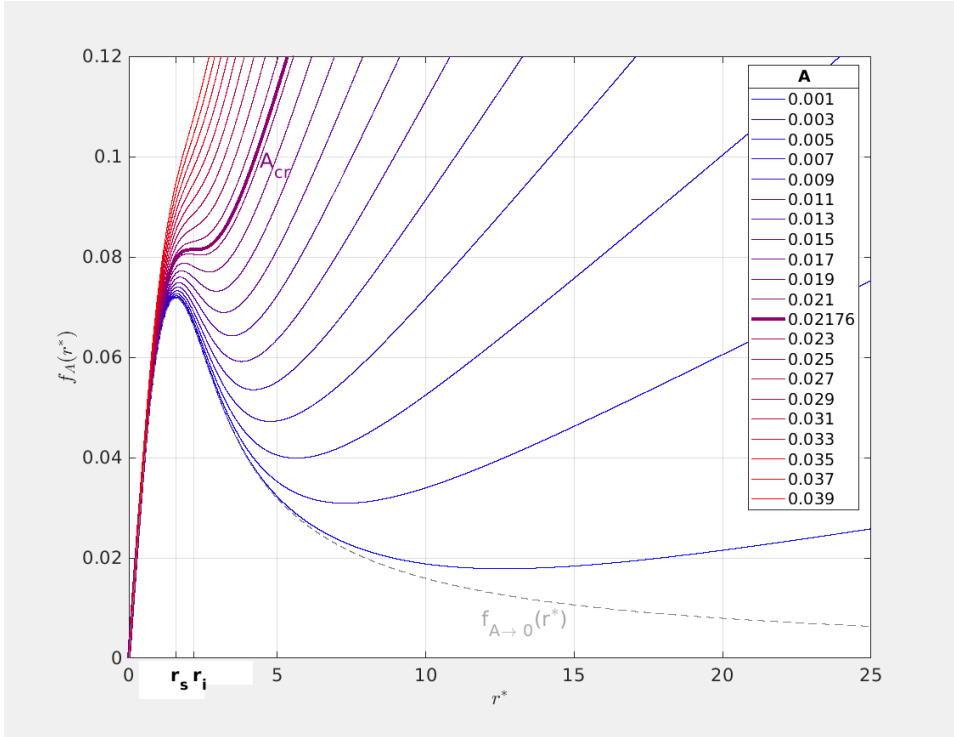


Figure 29: Equilibrium curve plots for different A values. A_{cr} , r_s , r_i defined in the text body. Gray dashed line shows an equilibrium curve which is an asymptotic limit when $A \rightarrow 0+$

and one minimum at r_{\min}^+ . The inflection point at $A = A_{cr}$ on the equilibrium curve lies at r_i^+ (see the Table 2). It restricts values of r_{\max}^+ from above and values of r_{\min}^+ from below.

Consequently, for $S_v < f_A(r_{\min}^+)$ and for $S_v > f_A(r_{\max}^+)$, there is only one solution. For $S_v \text{ min} = f_A(r_{\min}^+)$ and for $S_v \text{ max} = f_A(r_{\max}^+)$, there are two solutions. For $f_A(r_{\min}^+) < S_v < f_A(r_{\max}^+)$, there are three solutions. From a different perspective: the conditions necessary, but not sufficient, to obtain the three solutions, are $A < A_{cr}$ and $S_v < f_{A_{cr}}(r_i) = 0.0815$.

Not only is the existence of the solutions important but their stability as well. Let r_0 denote an arbitrary solution of Eq. 67. The exact form of the stability condition of the solution r_0^+ is governed by the function $\phi(r_0^+)$ (as defined in Marcu, Meiburg, and Newton [71]). The condition can take two different forms depending on the sign of this function

$$\phi(r_0^+) = \frac{1}{(2\pi)^2} \left[\frac{1 - \exp(-r_0^{+2}/2)}{r_0^{+2}} \right] \left[\frac{1 - \exp(-r_0^{+2}/2)}{r_0^{+2}} - \exp(-r_0^{+2}/2) \right]. \quad (69)$$

which plot is shown in Fig.30, panel a).

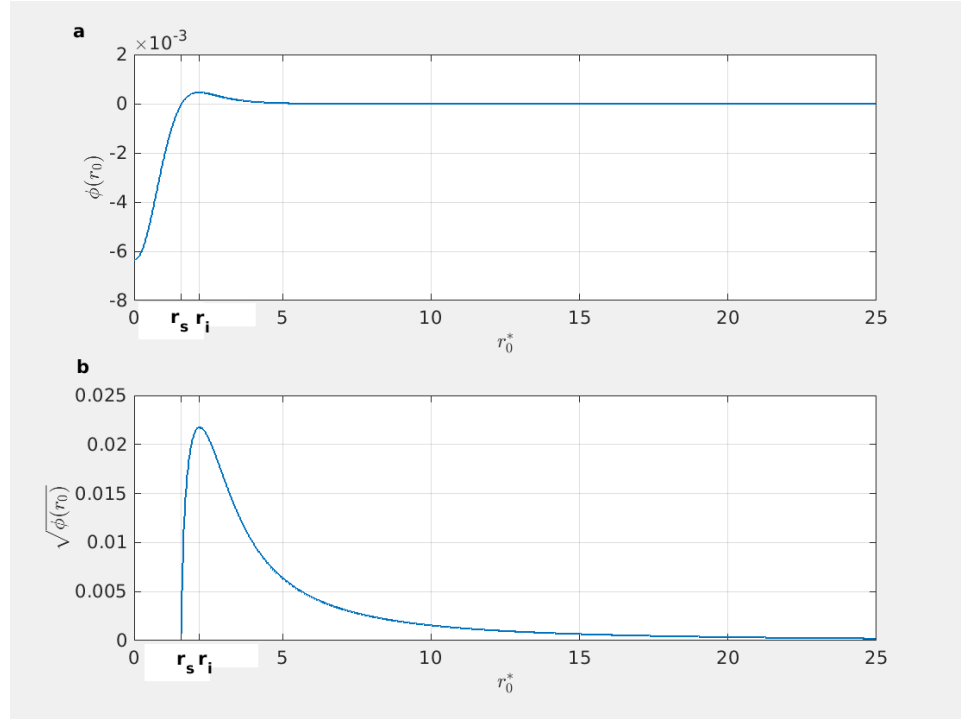


Figure 30: Plot of the function $\phi(r_0^+)$ determining equilibrium point stability (a) and its square radius $\sqrt{\phi(r_0^+)}$ (b) with respect to equilibrium point radial position.

The function has only one zero at r_s^+ (see Table 2). For small radii ($r_0^+ < r_s^+$), the equilibrium is stable if:

$$\frac{St}{A} \leq \frac{1}{|\phi(r_0^+)|}. \quad (70)$$

For greater radii ($r_0^+ > r_s^+$), the condition for stability depends explicitly only on A :

$$A \geq \sqrt{\phi(r_0^+)}. \quad (71)$$

The equilibrium point satisfying the first type of the condition was shown to be a focus, the second type to be a node.

Analysis of the equilibrium point stability conditions by Marcu, Meiburg, and Newton [71] is expanded here with emphasis on the dependence on strain parameter A . The results are described in detail below and summarised in Table 3.

Generally, stability conditions are different for A ranges separated by $\max_{r_0^+} (\sqrt{\phi(r_0^+)}) = A_{cr}$. $A > A_{cr}$ always satisfies then the condition expressed by 71. The term "partly unstable" in the table refers to the following: In the range of $r_{max}^+ \leq r_0^+ < r_{min}^+$, for a given A , only a small fraction of the total range (near points r_{max}^+ and r_{min}^+) is

Table 3: Stability conditions of particle equilibrium points present in the Burgers vortex with respect to vortex strain parameter A and dimensionless distance from the vortex axis r^+ . A_{cr} , $\varphi(r^+)$, r_s^+ , r_{min}^+ and r_{max}^+ defined in the text body.

	$\leq r_s^+$	(r_s^+, r_{max}^+)	$[r_{max}^+, r_{min}^+]$	$\geq r_{min}^+$
$A < A_{cr}$	unstable for $St > A/ \varphi(r_0^+) $	stable	partly unstable	stable
$A \geq A_{cr}$			stable	

stable. This range grows with increasing A . Numerical experiments show, however, that their domain of attraction in the presence of other stable points (at least one exists always) is relatively small.

The combination of multiple existence conditions with stability conditions creates a variety of single particle motion scenarios. Some of them are shown in Fig.4-9 in Marcu, Meiburg, and Newton [71]. These scenarios are used in the next section to carry out a search for vortex model parameter values that produce a void. Fig. ?? here illustrates one of these scenarios in which there are three equilibrium points: I - unstable point near the axis, II - unstable middle distance point, III - stable point far from the axis. A particle, depending on initial position and velocity, rotates around point I or is weakly attracted by unstable point II or is strongly attracted by stable point III.

Dodac cos tutaj o tej publikacji Sapsin And Haler 2010 o przyciąganiu cząstek inercyjnych przez powolne rozmaitscī.

TIME SCALES OF SINGLE PARTICLE MOTION

We were able to find approximate relations of a few timescales for single particle motion in Burgers vortex: exit time τ_{ex} , connected to timescale of motion along the axis τ_z , no-gravity orbit rotation time τ_{orb} and no-gravity axis docking time τ_{doc1} . For ease of reference, these approximations are summarised in Table ???. Several conclusions about three dimensional particle motion can be drawn from the comparison of the separately derived time scales:

1. τ_{doc1} and τ_z are approximately independent of particle radius R and vortex strain A .
2. $\tau_{orb} \ll \tau_z$ for small particles (like cloud droplets).
3. $\tau_{orb} \ll \tau_{ex}$ for small particles as long as the logarithmic part in Eq.54 is not significantly smaller than 1. It means that particle starting far from vortex "lids" is able to swirl around the vortex axis for significant amount of time before being expelled by motion along vortex axis.

4. $\frac{\tau_{ex}}{\tau_{dock}} = 4 \log L(a_1, a_2)$, which implies that axis docking time and exit time are of the same order as long as $\log L(a_1, a_2)$ is close to 1/4. It means that particle starting position and vortex length determines the fact if particle is able to approach its stable point on vortex axis before being expelled.

Tu nastapi jakies podsumowanie rozdzialu.

4

CLOUD VOIDS - INTERPRETATION AND EXPLANATION

CLOUD VOIDS EXPERIMENT DESCRIPTION

and recorded size spectra of droplets. Droplet and turbulence measurements are summarized in Table 1. The mean values refer to 30 min long record corresponding to the camera acquisition series.

POLYDISPERSE PARTICLE MOTION ANALYSIS

Content

CLOUD VOIDS CREATION MECHANISM

Content

CLOUD VOIDS SIMULATION

5

POLYDISPERSE PARTICLE MOTION - STATISTICAL ANALYSIS

SECTION TITLE

Content

Subsection Title

Content

Subsection Title

Content

SECTION TITLE

Content

Part III
APPENDIX

BIBLIOGRAPHY

- [1] In: ().
- [2] A. Arnèodo et al. "Universal Intermittent Properties of Particle Trajectories in Highly Turbulent Flows." In: *Phys. Rev. Lett.* 100 (25 2008), p. 254504. DOI: [10.1103/PhysRevLett.100.254504](https://doi.org/10.1103/PhysRevLett.100.254504). URL: <https://link.aps.org/doi/10.1103/PhysRevLett.100.254504>.
- [3] Orlando Ayala, Bogdan Rosa, Lian-Ping Wang, and Wojciech W Grabowski. "Effects of turbulence on the geometric collision rate of sedimenting droplets. Part 1. Results from direct numerical simulation." In: *New Journal of Physics* 10.7 (2008), p. 075015. DOI: [10.1088/1367-2630/10/7/075015](https://doi.org/10.1088/1367-2630/10/7/075015). URL: <https://doi.org/10.1088%2F1367-2630%2F10%2F7%2F075015>.
- [4] JÉRÉMIE BEC. "Multifractal concentrations of inertial particles in smooth random flows." In: *Journal of Fluid Mechanics* 528 (2005), pp. 255–277. DOI: [10.1017/S0022112005003368](https://doi.org/10.1017/S0022112005003368).
- [5] Lucia Baker, Ari Frankel, Ali Mani, and Filippo Coletti. "Coherent clusters of inertial particles in homogeneous turbulence." In: *Journal of Fluid Mechanics* 833 (2017), pp. 364–398. DOI: [10.1017/jfm.2017.700](https://doi.org/10.1017/jfm.2017.700).
- [6] J. Bec, L. Biferale, M. Cencini, A. Lanotte, S. Musacchio, and F. Toschi. "Heavy Particle Concentration in Turbulence at Dissipative and Inertial Scales." In: *Phys. Rev. Lett.* 98 (8 2007), p. 084502. DOI: [10.1103/PhysRevLett.98.084502](https://doi.org/10.1103/PhysRevLett.98.084502). URL: <https://link.aps.org/doi/10.1103/PhysRevLett.98.084502>.
- [7] J Bec, L Biferale, M Cencini, A S Lanotte, and F Toschi. "Spatial and velocity statistics of inertial particles in turbulent flows." In: *Journal of Physics: Conference Series* 333 (2011), p. 012003. DOI: [10.1088/1742-6596/333/1/012003](https://doi.org/10.1088/1742-6596/333/1/012003). URL: <https://doi.org/10.1088%2F1742-6596%2F333%2F1%2F012003>.
- [8] Jérémie Bec, Holger Homann, and Samriddhi Sankar Ray. "Gravity-Driven Enhancement of Heavy Particle Clustering in Turbulent Flow." In: *Phys. Rev. Lett.* 112 (18 2014), p. 184501. DOI: [10.1103/PhysRevLett.112.184501](https://doi.org/10.1103/PhysRevLett.112.184501). URL: <https://link.aps.org/doi/10.1103/PhysRevLett.112.184501>.
- [9] Jérémie Bec, Luca Biferale, Massimo Cencini, Alessandra S. Lanotte, and Federico Toschi. "Effects of vortex filaments on the velocity of tracers and heavy particles in turbulence." In: *Physics of Fluids* 18.8 (2006), p. 081702. DOI: [10.1063/1.2338598](https://doi.org/10.1063/1.2338598).

- eprint: <https://doi.org/10.1063/1.2338598>. URL: <https://doi.org/10.1063/1.2338598>.
- [10] Jérémie Bec, Luca Biferale, Guido Boffetta, Massimo Cencini, Stefano Musacchio, and Federico Toschi. “Lyapunov exponents of heavy particles in turbulence.” In: *Physics of Fluids* 18.9 (2006), p. 091702. DOI: [10.1063/1.2349587](https://doi.org/10.1063/1.2349587). eprint: <https://doi.org/10.1063/1.2349587>. URL: <https://doi.org/10.1063/1.2349587>.
 - [11] Jérémie Bec, Samriddhi Sankar Ray, Ewe Wei Saw, and Holger Homann. “Abrupt growth of large aggregates by correlated coalescences in turbulent flow.” In: *Phys. Rev. E* 93 (3 2016), p. 031102. DOI: [10.1103/PhysRevE.93.031102](https://doi.org/10.1103/PhysRevE.93.031102). URL: <https://link.aps.org/doi/10.1103/PhysRevE.93.031102>.
 - [12] F. Belin, F. Moisy, P. Tabeling, and H. Willaime. “Worms in a turbulence experiment, from hot wire time series.” In: *Fundamental Problematic Issues in Turbulence. Trends in Mathematics.* Springer Basel A.G., 1999, pp. 129–140. DOI: [10.1007/978-3-0348-8689-5_14](https://doi.org/10.1007/978-3-0348-8689-5_14).
 - [13] Gregory P Bewley, Ewe-Wei Saw, and Eberhard Bodenschatz. “Observation of the sling effect.” In: *New Journal of Physics* 15.8 (2013), p. 083051. DOI: [10.1088/1367-2630/15/8/083051](https://doi.org/10.1088/1367-2630/15/8/083051). URL: <https://doi.org/10.1088%2F1367-2630%2F15%2F8%2F083051>.
 - [14] Akshay Bhatnagar, Anupam Gupta, Dhrubaditya Mitra, Rahul Pandit, and Prasad Perlekar. “How long do particles spend in vortical regions in turbulent flows?” In: *Phys. Rev. E* 94 (5 2016), p. 053119. DOI: [10.1103/PhysRevE.94.053119](https://doi.org/10.1103/PhysRevE.94.053119). URL: <https://link.aps.org/doi/10.1103/PhysRevE.94.053119>.
 - [15] Akshay Bhatnagar, Anupam Gupta, Dhrubaditya Mitra, and Rahul Pandit. “Heavy inertial particles in turbulent flows gain energy slowly but lose it rapidly.” In: *Phys. Rev. E* 97 (3 2018), p. 033102. DOI: [10.1103/PhysRevE.97.033102](https://doi.org/10.1103/PhysRevE.97.033102). URL: <https://link.aps.org/doi/10.1103/PhysRevE.97.033102>.
 - [16] L. Biferale, G. Boffetta, A. Celani, B. J. Devenish, A. Lanotte, and F. Toschi. “Lagrangian statistics of particle pairs in homogeneous isotropic turbulence.” In: *Physics of Fluids* 17.11 (2005), p. 115101. DOI: [10.1063/1.2130742](https://doi.org/10.1063/1.2130742). eprint: <https://doi.org/10.1063/1.2130742>. URL: <https://doi.org/10.1063/1.2130742>.
 - [17] L. Biferale, F. Bonaccorso, I. M. Mazzitelli, M. A. T. van Hinsberg, A. S. Lanotte, S. Musacchio, P. Perlekar, and F. Toschi. “Coherent Structures and Extreme Events in Rotating Multi-phase Turbulent Flows.” In: *Phys. Rev. X* 6 (4 2016), p. 041036. DOI: [10.1103/PhysRevX.6.041036](https://doi.org/10.1103/PhysRevX.6.041036). URL: <https://link.aps.org/doi/10.1103/PhysRevX.6.041036>.

- [18] Luca Biferale, Andrea Scagliarini, and Federico Toschi. "On the measurement of vortex filament lifetime statistics in turbulence." In: *Physics of Fluids* 22.6 (2010), p. 065101. DOI: [10.1063/1.3431660](https://doi.org/10.1063/1.3431660). eprint: <https://doi.org/10.1063/1.3431660>. URL: <https://doi.org/10.1063/1.3431660>.
- [19] R. B. Bird. In: *AICHE Journal* 10.6 (1964), pp. 794–794.
- [20] E. Bodenschatz, S. P. Malinowski, R. A. Shaw, and F. Stratmann. "Can We Understand Clouds Without Turbulence?" In: *Science* 327.5968 (2010), pp. 970–971. ISSN: 0036-8075. DOI: [10.1126/science.1185138](https://doi.org/10.1126/science.1185138). eprint: <http://science.sciencemag.org/content/327/5968/970.full.pdf>. URL: <http://science.sciencemag.org/content/327/5968/970>.
- [21] Craig F. Bohren and Donald R. Huffman. "Absorption and Scattering of Light by Small Particles." In: (1998). DOI: [10.1002/9783527618156](https://doi.org/10.1002/9783527618156).
- [22] O. Boucher et al. "Climate Change 2013: The Physical Science Basis. Contribution of Working Group I to the Fifth Assessment Report of the Intergovernmental Panel on Climate Change." In: Cambridge, United Kingdom and New York, NY, USA, 2013, p. 1535.
- [23] Mickaël Bourgoin and Haitao Xu. "Focus on dynamics of particles in turbulence." In: *New Journal of Physics* 16.8 (2014), p. 085010. DOI: [10.1088/1367-2630/16/8/085010](https://doi.org/10.1088/1367-2630/16/8/085010). URL: <https://doi.org/10.1088%2F1367-2630%2F16%2F8%2F085010>.
- [24] Andrew D Bragg and Lance R Collins. "New insights from comparing statistical theories for inertial particles in turbulence: II. Relative velocities." In: *New Journal of Physics* 16.5 (2014), p. 055014. DOI: [10.1088/1367-2630/16/5/055014](https://doi.org/10.1088/1367-2630/16/5/055014). URL: <https://doi.org/10.1088%2F1367-2630%2F16%2F5%2F055014>.
- [25] Andrew D. Bragg, Peter J. Ireland, and Lance R. Collins. "Mechanisms for the clustering of inertial particles in the inertial range of isotropic turbulence." In: *Phys. Rev. E* 92 (2 2015), p. 023029. DOI: [10.1103/PhysRevE.92.023029](https://doi.org/10.1103/PhysRevE.92.023029). URL: <https://link.aps.org/doi/10.1103/PhysRevE.92.023029>.
- [26] Andrew D. Bragg, Peter J. Ireland, and Lance R. Collins. "On the relationship between the non-local clustering mechanism and preferential concentration." In: *Journal of Fluid Mechanics* 780 (2015), pp. 327–343. DOI: [10.1017/jfm.2015.474](https://doi.org/10.1017/jfm.2015.474).
- [27] Jean-Louis Brenguier and Laure Chaumat. "Droplet Spectra Broadening in Cumulus Clouds. Part I: Broadening in Adiabatic Cores." In: *Journal of the Atmospheric Sciences* 58.6 (2001), pp. 628–641. DOI: [10.1175/1520-0469\(2001\)058<0628:DSBICC>2.0.CO;2](https://doi.org/10.1175/1520-0469(2001)058<0628:DSBICC>2.0.CO;2). eprint: [https://doi.org/10.1175/1520-0469\(2001\)058<0628:DSBICC>2.0.CO;2](https://doi.org/10.1175/1520-0469(2001)058<0628:DSBICC>2.0.CO;2)

- 058<0628:DSBICC>2.0.CO;2. URL: [https://doi.org/10.1175/1520-0469\(2001\)058<0628:DSBICC>2.0.CO](https://doi.org/10.1175/1520-0469(2001)058<0628:DSBICC>2.0.CO).
- [28] J.M. Burgers. “A Mathematical Model Illustrating the Theory of Turbulence.” In: ed. by Richard Von Mises and Theodore Von Kármán. Vol. 1. Advances in Applied Mechanics. Elsevier, 1948, pp. 171–199. DOI: [10.1016/S0065-2156\(08\)70100-5](https://doi.org/10.1016/S0065-2156(08)70100-5). URL: <http://www.sciencedirect.com/science/article/pii/S0065215608701005>.
- [29] M. CENCINI, J. BEC, L. BIFERALE, G. BOFFETTA, A. CELANI, A. S. LANOTTE, S. MUSACCHIO, and F. TOSCHI. “Dynamics and statistics of heavy particles in turbulent flows.” In: *Journal of Turbulence* 7 (2006), N36. DOI: [10.1080/14685240600675727](https://doi.org/10.1080/14685240600675727). eprint: <https://doi.org/10.1080/14685240600675727>. URL: <https://doi.org/10.1080/14685240600675727>.
- [30] Enrico Calzavarini, Massimo Cencini, Detlef Lohse, and Federico Toschi. “Quantifying Turbulence-Induced Segregation of Inertial Particles.” In: *Phys. Rev. Lett.* 101 (8 2008), p. 084504. DOI: [10.1103/PhysRevLett.101.084504](https://doi.org/10.1103/PhysRevLett.101.084504). URL: <https://link.aps.org/doi/10.1103/PhysRevLett.101.084504>.
- [31] Enrico Calzavarini, Romain Volk, Emmanuel Lévéque, Jean-François Pinton, and Federico Toschi. “Impact of trailing wake drag on the statistical properties and dynamics of finite-sized particle in turbulence.” In: *Physica D: Nonlinear Phenomena* 241.3 (2012). Special Issue on Small Scale Turbulence, pp. 237–244. ISSN: 0167-2789. DOI: [10.1016/j.physd.2011.06.004](https://doi.org/10.1016/j.physd.2011.06.004). URL: <http://www.sciencedirect.com/science/article/pii/S0167278911001448>.
- [32] S. Chen, M.-K. Yau, P. Bartello, and L. Xue. “Bridging the condensation–collision size gap: a direct numerical simulation of continuous droplet growth in turbulent clouds.” In: *Atmospheric Chemistry and Physics* 18.10 (2018), pp. 7251–7262. DOI: [10.5194/acp-18-7251-2018](https://doi.org/10.5194/acp-18-7251-2018). URL: <https://www.atmos-chem-phys.net/18/7251/2018>.
- [33] P. Y. Chuang, E. W. Saw, J. D. Small, R. A. Shaw, C. M. Sipperley, G. A. Payne, and W. D. Bachalo. “Airborne Phase Doppler Interferometry for Cloud Microphysical Measurements.” In: *Aerosol Sci. Tech.* 42.8 (2008), pp. 685–703. DOI: [10.1080/02786820802232956](https://doi.org/10.1080/02786820802232956). eprint: [http://dx.doi.org/10.1080/02786820802232956](https://dx.doi.org/10.1080/02786820802232956).
- [34] S. W. Coleman and J. C. Vassilicos. “A unified sweep-stick mechanism to explain particle clustering in two- and three-dimensional homogeneous, isotropic turbulence.” In: *Phys. Fluids* 21.11 (2009), p. 113301. DOI: [10.1063/1.3257638](https://doi.org/10.1063/1.3257638). eprint: <https://doi.org/10.1063/1.3257638>.

- [35] P. Cvitanović, R. Artuso, R. Mainieri, G. Tanner, and G. Vattay. *Chaos: Classical and Quantum*. Copenhagen: Niels Bohr Inst., 2016.
- [36] J. DÁVILA and J. C. R. HUNT. “Settling of small particles near vortices and in turbulence.” In: *Journal of Fluid Mechanics* 440 (2001), pp. 117–145. DOI: [10.1017/S0022112001004694](https://doi.org/10.1017/S0022112001004694).
- [37] P. A. Davidson. “Turbulence: An introduction for scientists and engineers.” In: (2004).
- [38] P. Deepu, S. Ravichandran, and Rama Govindarajan. “Caustics-induced coalescence of small droplets near a vortex.” In: *Phys. Rev. Fluids* 2 (2 2017), p. 024305. DOI: [10.1103/PhysRevFluids.2.024305](https://doi.org/10.1103/PhysRevFluids.2.024305). URL: <https://link.aps.org/doi/10.1103/PhysRevFluids.2.024305>.
- [39] A. Dejoan and R. Monchaux. “Preferential concentration and settling of heavy particles in homogeneous turbulence.” In: *Physics of Fluids* 25.1 (2013), p. 013301. DOI: [10.1063/1.4774339](https://doi.org/10.1063/1.4774339). eprint: <https://doi.org/10.1063/1.4774339>. URL: <https://doi.org/10.1063/1.4774339>.
- [40] B. Devenish et al. “Droplet growth in warm turbulent clouds.” In: *Q. J. Royal Meteorol. Soc.* 138 (2012), pp. 1401–1429. DOI: [10.1002/qj.1897](https://doi.org/10.1002/qj.1897).
- [41] Rohit Dhariwal and Andrew D. Bragg. “Fluid particles only separate exponentially in the dissipation range of turbulence after extremely long times.” In: *Phys. Rev. Fluids* 3 (3 2018), p. 034604. DOI: [10.1103/PhysRevFluids.3.034604](https://doi.org/10.1103/PhysRevFluids.3.034604). URL: <https://link.aps.org/doi/10.1103/PhysRevFluids.3.034604>.
- [42] Zhongwang Dou, Peter J. Ireland, Andrew D. Bragg, Zach Liang, Lance R. Collins, and Hui Hui Meng. “Particle-pair relative velocity measurement in high-Reynolds-number homogeneous and isotropic turbulence using 4-frame particle tracking velocimetry.” In: *Experiments in Fluids* 59 (2018), pp. 1–17.
- [43] Falkovich G., Fouxon A., and Stepanov M. G. “Acceleration of rain initiation by cloud turbulence.” In: *Nature* 419.6903 (2002), pp. 151–154. ISSN: 1476-4687. DOI: [10.1038/nature00983](https://doi.org/10.1038/nature00983).
- [44] G. Falkovich, A. Fouxon, and M. Stepanov. “Statistics of Turbulence-Induced Fluctuations of Particle Concentration.” In: *Sedimentation and Sediment Transport*. Ed. by A. Gyr and W. Kinzelbach. Dordrecht: Springer Netherlands, 2003, pp. 155–158. ISBN: 978-94-017-0347-5.
- [45] Gregory Falkovich and Alain Pumir. “Sling Effect in Collisions of Water Droplets in Turbulent Clouds.” In: *J. Atmos. Sci.* 64.12 (2007), pp. 4497–4505. DOI: [10.1175/2007JAS2371.1](https://doi.org/10.1175/2007JAS2371.1).

- [46] S. Glienke, A. Kostinski, J. Fugal, R. A. Shaw, S. Borrmann, and J. Stith. "Cloud droplets to drizzle: Contribution of transition drops to microphysical and optical properties of marine stratocumulus clouds." In: *Geophysical Research Letters* 44.15 (2017), pp. 8002–8010. DOI: [10.1002/2017GL074430](https://doi.org/10.1002/2017GL074430). eprint: [https://agupubs.onlinelibrary.wiley.com/doi/abs/10.1002/2017GL074430](https://agupubs.onlinelibrary.wiley.com/doi/pdf/10.1002/2017GL074430).
- [47] Susumu Goto and J. C. Vassilicos. "Sweep-Stick Mechanism of Heavy Particle Clustering in Fluid Turbulence." In: *Phys. Rev. Lett.* 100 (5 2008), p. 054503. DOI: [10.1103/PhysRevLett.100.054503](https://doi.org/10.1103/PhysRevLett.100.054503). URL: <https://link.aps.org/doi/10.1103/PhysRevLett.100.054503>.
- [48] Wojciech W. Grabowski and Lian-Ping Wang. "Growth of Cloud Droplets in a Turbulent Environment." In: *Ann. Rev. Fluid Mech.* 45.1 (2013), pp. 293–324. DOI: [10.1146/annurev-fluid-011212-140750](https://doi.org/10.1146/annurev-fluid-011212-140750). eprint: <https://doi.org/10.1146/annurev-fluid-011212-140750>.
- [49] K. Gustavsson and B. Mehlig. "Statistical models for spatial patterns of heavy particles in turbulence." In: *Adv. Phys.* 65.1 (2016), pp. 1–57. DOI: [10.1080/00018732.2016.1164490](https://doi.org/10.1080/00018732.2016.1164490).
- [50] K. Gustavsson, S. Vajedi, and B. Mehlig. "Clustering of Particles Falling in a Turbulent Flow." In: *Phys. Rev. Lett.* 112 (21 2014), p. 214501. DOI: [10.1103/PhysRevLett.112.214501](https://doi.org/10.1103/PhysRevLett.112.214501). URL: <https://link.aps.org/doi/10.1103/PhysRevLett.112.214501>.
- [51] Thomas Hartlep, Jeffrey N. Cuzzi, and Brian Weston. "Scale dependence of multiplier distributions for particle concentration, enstrophy, and dissipation in the inertial range of homogeneous turbulence." In: *Phys. Rev. E* 95 (3 2017), p. 033115. DOI: [10.1103/PhysRevE.95.033115](https://doi.org/10.1103/PhysRevE.95.033115). URL: <https://link.aps.org/doi/10.1103/PhysRevE.95.033115>.
- [52] Reginald Janusz Hill. "Geometric collision rates and trajectories of cloud droplets falling into a Burgers vortex." In: *Phys. Fluids* 17 (2005), p. 037103. DOI: [10.1063/1.1858191](https://doi.org/10.1063/1.1858191).
- [53] T. ISHIHARA, Y. KANEDA, M. YOKOKAWA, K. ITAKURA, and A. UNO. "Small-scale statistics in high-resolution direct numerical simulation of turbulence: Reynolds number dependence of one-point velocity gradient statistics." In: *Journal of Fluid Mechanics* 592 (2007), pp. 335–366. DOI: [10.1017/S0022112007008531](https://doi.org/10.1017/S0022112007008531).
- [54] Peter J. Ireland, Andrew D. Bragg, and Lance R. Collins. "The effect of Reynolds number on inertial particle dynamics in isotropic turbulence. Part 1. Simulations without gravitational

- effects." In: *Journal of Fluid Mechanics* 796 (2016), pp. 617–658. doi: [10.1017/jfm.2016.238](https://doi.org/10.1017/jfm.2016.238).
- [55] Peter J. Ireland, Andrew D. Bragg, and Lance R. Collins. "The effect of Reynolds number on inertial particle dynamics in isotropic turbulence. Part 2. Simulations with gravitational effects." In: *Journal of Fluid Mechanics* 796 (2016), pp. 659–711. doi: [10.1017/jfm.2016.227](https://doi.org/10.1017/jfm.2016.227).
- [56] I. Jen-La Plante, Y. Ma, K. Nurowska, H. Gerber, D. Khelif, K. Karpinska, M. K. Kopec, W. Kumala, and S. P. Malinowski. "Physics of Stratocumulus Top (POST): turbulence characteristics." In: *Atmospheric Chemistry and Physics* 16.15 (2016), pp. 9711–9725.
- [57] J. Jimenez and A. Wray. "On the characteristics of vortex filaments in isotropic turbulence." In: *J. Fluid Mech.* 373 (1998), pp. 255–285. doi: [10.1017/S0022112098002341](https://doi.org/10.1017/S0022112098002341).
- [58] A. B. KOSTINSKI and R. A. SHAW. "Scale-dependent droplet clustering in turbulent clouds." In: *Journal of Fluid Mechanics* 434 (2001), pp. 389–398. doi: [10.1017/S0022112001004001](https://doi.org/10.1017/S0022112001004001).
- [59] Y. Knyazikhin, R. B. Myneni, A. Marshak, W. J. Wiscombe, M. L. Larsen, and J. V. Martonchik. "Small-Scale Drop Size Variability: Impact on Estimation of Cloud Optical Properties." In: *Journal of the Atmospheric Sciences* 62.7 (2005), pp. 2555–2567. doi: [10.1175/JAS3488.1](https://doi.org/10.1175/JAS3488.1). eprint: <https://doi.org/10.1175/JAS3488.1>. URL: <https://doi.org/10.1175/JAS3488.1>.
- [60] A. N. Kolmogorov. "Energy dissipation in locally isotropic turbulence." In: *Doklady AN SSSR*. Vol. 32. 1. 1941, pp. 19–21.
- [61] Alexander B. Kostinski and Raymond A. Shaw. "Fluctuations and Luck in Droplet Growth by Coalescence." In: *Bulletin of the American Meteorological Society* 86.2 (2005), pp. 235–244. doi: [10.1175/BAMS-86-2-235](https://doi.org/10.1175/BAMS-86-2-235). eprint: <https://doi.org/10.1175/BAMS-86-2-235>. URL: <https://doi.org/10.1175/BAMS-86-2-235>.
- [62] Y. Kuznetsov. 3rd ed. Vol. 112. Applied Mathematical Sciences. Springer-Verlag New York, 2004. ISBN: 978-1-4757-3978-7.
- [63] KATRIN LEHMANN, HOLGER SIEBERT, MANFRED WENDISCH, and RAYMOND A. SHAW. "Evidence for inertial droplet clustering in weakly turbulent clouds." In: *Tellus B* 59.1 (2007), pp. 57–65. doi: [10.1111/j.1600-0889.2006.00230.x](https://doi.org/10.1111/j.1600-0889.2006.00230.x). eprint: <https://onlinelibrary.wiley.com/doi/pdf/10.1111/j.1600-0889.2006.00230.x>. URL: <https://onlinelibrary.wiley.com/doi/abs/10.1111/j.1600-0889.2006.00230.x>.

- [64] Michael L. Larsen, Raymond A. Shaw, Alexander B. Kostinski, and Susanne Glienke. "Fine-Scale Droplet Clustering in Atmospheric Clouds: 3D Radial Distribution Function from Airborne Digital Holography." In: *Phys. Rev. Lett.* 121 (20 2018), p. 204501. DOI: [10.1103/PhysRevLett.121.204501](https://doi.org/10.1103/PhysRevLett.121.204501). URL: <https://link.aps.org/doi/10.1103/PhysRevLett.121.204501>.
- [65] H. Lian, X. Y. Chang, and Y. Hardalupas. "Time resolved measurements of droplet preferential concentration in homogeneous isotropic turbulence without mean flow." In: *Physics of Fluids* 31.2 (2019), p. 025103. DOI: [10.1063/1.5063673](https://doi.org/10.1063/1.5063673). eprint: <https://doi.org/10.1063/1.5063673>. URL: <https://doi.org/10.1063/1.5063673>.
- [66] Huan Lian, Georgios Charalampous, and Yannis Hardalupas. "Preferential concentration of poly-dispersed droplets in stationary isotropic turbulence." In: *Experiments in Fluids* 54.5 (2013), p. 1525. ISSN: 1432-1114. DOI: [10.1007/s00348-013-1525-3](https://doi.org/10.1007/s00348-013-1525-3). URL: <https://doi.org/10.1007/s00348-013-1525-3>.
- [67] Kholmyansky M. and Tsinober A. "On the origins of intermittency in real turbulent flows." In: *Intermittency in Turbulent Flows*. Ed. by Vassilicos J.C. Cambridge University Press, 2001, pp. 183–192.
- [68] Manish M and Srikrishna Sahu. "Analysis of droplet clustering in air-assist sprays using Voronoi tessellations." In: *Physics of Fluids* 30.12 (2018), p. 123305. DOI: [10.1063/1.5053473](https://doi.org/10.1063/1.5053473). eprint: <https://doi.org/10.1063/1.5053473>. URL: <https://doi.org/10.1063/1.5053473>.
- [69] Yong-Feng Ma, Szymon P. Malinowski, Katarzyna Karpińska, Hermann E. Gerber, and Wojciech Kumala. "Scaling Analysis of Temperature and Liquid Water Content in the Marine Boundary Layer Clouds during POST." In: *Journal of the Atmospheric Sciences* 74.12 (2017), pp. 4075–4092.
- [70] Deepak G. Madival. "A model study of the effect of clustering on the last stage of drizzle formation." In: *Quarterly Journal of the Royal Meteorological Society* (2019). DOI: [10.1002/qj.3659](https://doi.org/10.1002/qj.3659). eprint: <https://rmets.onlinelibrary.wiley.com/doi/pdf/10.1002/qj.3659>. URL: <https://rmets.onlinelibrary.wiley.com/doi/abs/10.1002/qj.3659>.
- [71] B. Marcu, E. Meiburg, and P. K. Newton. "Dynamics of heavy particles in a burgers vortex." In: *Phys. Fluids* 7 (1995), pp. 400–410. DOI: [10.1063/1.868778](https://doi.org/10.1063/1.868778).
- [72] Krzysztof Markowicz, Konrad Bajer, and Szymon P. Malinowski. "Influence of small-scale turbulence structures on the concentration of cloud droplets." In: *13th Conference on Clouds and*

- Precipitation*. Vol. 1. ICCP-IAMAS. Desert Research Institute, 2000, pp. 159–162.
- [73] Alexander Marshak, Yuri Knyazikhin, Michael L. Larsen, and Warren J. Wiscombe. “Small-Scale Drop-Size Variability: Empirical Models for Drop-Size-Dependent Clustering in Clouds.” In: *Journal of the Atmospheric Sciences* 62.2 (2005), pp. 551–558. DOI: [10.1175/JAS-3371.1](https://doi.org/10.1175/JAS-3371.1). eprint: <https://doi.org/10.1175/JAS-3371.1>. URL: <https://doi.org/10.1175/JAS-3371.1>.
 - [74] M. R. Maxey. “The gravitational settling of aerosol particles in homogeneous turbulence and random flow fields.” In: *J. Fluid Mech.* 174 (1987), pp. 441–465. DOI: [10.1017/S0022112087000193](https://doi.org/10.1017/S0022112087000193).
 - [75] Martin R. Maxey and James J. Riley. “Equation of motion for a small rigid sphere in a nonuniform flow.” In: *The Physics of Fluids* 26.4 (1983), pp. 883–889.
 - [76] Jean-Pierre Minier. “Statistical descriptions of polydisperse turbulent two-phase flows.” In: *Physics Reports* 665 (2016). Statistical descriptions of polydisperse turbulent two-phase flows, pp. 1–122. ISSN: 0370-1573. DOI: [10.1016/j.physrep.2016.10.007](https://doi.org/10.1016/j.physrep.2016.10.007). URL: <http://www.sciencedirect.com/science/article/pii/S0370157316303350>.
 - [77] F. Moisy and J. Jimenez. “Geometry and clustering of intense structures in isotropic turbulence.” In: *J. Fluid Mech.* 513 (2004), pp. 111–133. DOI: [10.1017/S0022112004009802](https://doi.org/10.1017/S0022112004009802).
 - [78] Mohammadreza Momenifar and Andrew D. Bragg. “Local analysis of the clustering, velocities and accelerations of particles settling in turbulence.” In: *arXiv e-prints*, arXiv:1908.00341 (2019), arXiv:1908.00341. arXiv: [1908.00341 \[physics.flu-dyn\]](https://arxiv.org/abs/1908.00341).
 - [79] R. Monchaux, M. Bourgoin, and A. Cartellier. “Preferential concentration of heavy particles: A Voronoï analysis.” In: *Physics of Fluids* 22.10 (2010), p. 103304. DOI: [10.1063/1.3489987](https://doi.org/10.1063/1.3489987). eprint: <https://doi.org/10.1063/1.3489987>. URL: <https://doi.org/10.1063/1.3489987>.
 - [80] R. Monchaux and A. Dejoan. “Settling velocity and preferential concentration of heavy particles under two-way coupling effects in homogeneous turbulence.” In: *Phys. Rev. Fluids* 2 (10 2017), p. 104302. DOI: [10.1103/PhysRevFluids.2.104302](https://doi.org/10.1103/PhysRevFluids.2.104302). URL: <https://link.aps.org/doi/10.1103/PhysRevFluids.2.104302>.
 - [81] Romain Monchaux, Mickael Bourgoin, and Alain Cartellier. “Analyzing preferential concentration and clustering of inertial particles in turbulence.” In: *International Journal of Multiphase Flow* 40 (2012), pp. 1–18. ISSN: 0301-9322. DOI: [10.1016/j.ijmultiphaseflow.2011.12.001](https://doi.org/10.1016/j.ijmultiphaseflow.2011.12.001). URL: <http://www.sciencedirect.com/science/article/pii/S030193221100245X>.

- [82] H. Mouri, A. Hori, and Y. Kawashima. "Vortex tubes in velocity fields of laboratory isotropic turbulence." In: *Phys. Lett. A* 276 (2003), pp. 115–121. DOI: [10.1103/PhysRevE.67.016305](https://doi.org/10.1103/PhysRevE.67.016305).
- [83] "Multiscale analysis of the invariants of the velocity gradient tensor in isotropic turbulence." In: (2018).
- [84] John C. Neu. "The dynamics of stretched vortices." In: *J. Fluid Mech.* 143 (June 1984), pp. 253–276. DOI: [10.1017/S0022112084001348](https://doi.org/10.1017/S0022112084001348). URL: <https://www.cambridge.org/core/article/dynamics-of-stretched-vortices/1783CBAF5D397FD30CD90BB137533477>.
- [85] Martín Obligado, Tomás Teitelbaum, Alain Cartellier, Pablo Mininni, and Mickaël Bourgoin. "Preferential concentration of heavy particles in turbulence." In: *Journal of Turbulence* 15.5 (2014), pp. 293–310. DOI: [10.1080/14685248.2014.897710](https://doi.org/10.1080/14685248.2014.897710). eprint: <https://doi.org/10.1080/14685248.2014.897710>. URL: <https://doi.org/10.1080/14685248.2014.897710>.
- [86] S. Olivieri, F. Picano, G. Sardina, D. Iudicone, and L. Brandt. "The effect of the Basset history force on particle clustering in homogeneous and isotropic turbulence." In: *Physics of Fluids* 26.4 (2014), p. 041704. DOI: [10.1063/1.4871480](https://doi.org/10.1063/1.4871480). eprint: <https://doi.org/10.1063/1.4871480>. URL: <https://doi.org/10.1063/1.4871480>.
- [87] M. G. Olsen and R. J. Adrian. "Out-of-focus effects on particle image visibility and correlation in microscopic particle image velocimetry." In: *Exp. Fluids* 29.1 (2000), S166–S174. ISSN: 1432-1114. DOI: [10.1007/s003480070018](https://doi.org/10.1007/s003480070018).
- [88] J. G. Pedersen, Y.-F. Ma, W. W. Grabowski, and S. P. Malinowski. "Anisotropy of Observed and Simulated Turbulence in Marine Stratocumulus." In: *Journal of Advances in Modeling Earth Systems* 10.2 (2018), pp. 500–515.
- [89] Vincent E. Perrin and Harmen J. J. Jonker. "Effect of the eigenvalues of the velocity gradient tensor on particle collisions." In: *Journal of Fluid Mechanics* 792 (2016), pp. 36–49. DOI: [10.1017/jfm.2016.70](https://doi.org/10.1017/jfm.2016.70).
- [90] A E Perry and M S Chong. "A Description of Eddying Motions and Flow Patterns Using Critical-Point Concepts." In: *Annual Review of Fluid Mechanics* 19.1 (1987), pp. 125–155. DOI: [10.1146/annurev.fl.19.010187.001013](https://doi.org/10.1146/annurev.fl.19.010187.001013). eprint: <https://doi.org/10.1146/annurev.fl.19.010187.001013>. URL: <https://doi.org/10.1146/annurev.fl.19.010187.001013>.
- [91] Jason R. Picardo, Lokahith Agasthya, Rama Govindarajan, and Samriddhi Sankar Ray. "Flow structures govern particle collisions in turbulence." In: *Phys. Rev. Fluids* 4 (3 2019), p. 032601. DOI: [10.1103/PhysRevFluids.4.032601](https://doi.org/10.1103/PhysRevFluids.4.032601). URL: <https://link.aps.org/doi/10.1103/PhysRevFluids.4.032601>.

- [92] M. Pinsky and A. P. Khain. "Fine Structure of Cloud Droplet Concentration as Seen from the Fast-FSSP Measurements. Part I: Method of Analysis and Preliminary Results." In: *Journal of Applied Meteorology* 40.8 (2001), pp. 1515–1537. DOI: [10.1175/1520-0450\(2001\)040<1515:FSOCDC>2.0.CO;2](https://doi.org/10.1175/1520-0450(2001)040<1515:FSOCDC>2.0.CO;2). eprint: [https://doi.org/10.1175/1520-0450\(2001\)040<1515:FSOCDC>2.0.CO](https://doi.org/10.1175/1520-0450(2001)040<1515:FSOCDC>2.0.CO); URL: [https://doi.org/10.1175/1520-0450\(2001\)040<1515:FSOCDC>2.0.CO](https://doi.org/10.1175/1520-0450(2001)040<1515:FSOCDC>2.0.CO).
- [93] S. Pirozzoli. "On the velocity and dissipation signature of vortex tubes in isotropic turbulence." In: *Physica D* 241 (2012), pp. 202–207. DOI: [10.1016/j.physd.2011.03.005](https://doi.org/10.1016/j.physd.2011.03.005).
- [94] Stephen B Pope. *Turbulent flows*. Cambridge: Cambridge Univ. Press, 2011.
- [95] Alain Pumir and Michael Wilkinson. "Collisional Aggregation Due to Turbulence." In: *Annual Review of Condensed Matter Physics* 7.1 (2016), pp. 141–170. DOI: [10.1146/annurev-conmatphys-031115-011538](https://doi.org/10.1146/annurev-conmatphys-031115-011538). eprint: <https://doi.org/10.1146/annurev-conmatphys-031115-011538>. URL: <https://doi.org/10.1146/annurev-conmatphys-031115-011538>.
- [96] S. Ravichandran and Rama Govindarajan. "Caustics and clustering in the vicinity of a vortex." In: *Phys. Fluids* 27.3 (2015), p. 033305. DOI: [10.1063/1.4916583](https://doi.org/10.1063/1.4916583). eprint: <https://doi.org/10.1063/1.4916583>.
- [97] S. Ravichandran, Prasad Perlekar, and Rama Govindarajan. "Attracting fixed points for heavy particles in the vicinity of a vortex pair." In: *Phys. Fluids* 26.1 (2014), p. 013303. DOI: [10.1063/1.4861395](https://doi.org/10.1063/1.4861395). eprint: <https://doi.org/10.1063/1.4861395>.
- [98] Lewis F. Richardson. *Weather prediction by numerical process*. Cambridge University Press, 1922. URL: <https://archive.org/details/weatherpredictio00richrich>.
- [99] S. Risius, H. Xu, F. Di Lorenzo, H. Xi, H. Siebert, R. A. Shaw, and E. Bodenschatz. "Schneefernerhaus as a mountain research station for clouds and turbulence." In: *Atmos. Meas. Tech.* 8.8 (2015), pp. 3209–3218. DOI: [10.5194/amt-8-3209-2015](https://doi.org/10.5194/amt-8-3209-2015). URL: <http://www.atmos-meas-tech.net/8/3209/2015>.
- [100] Bogdan Rosa and Jacek Pozorski. "Impact of subgrid fluid turbulence on inertial particles subject to gravity." In: *Journal of Turbulence* 18.7 (2017), pp. 634–652. DOI: [10.1080/14685248.2017.1317099](https://doi.org/10.1080/14685248.2017.1317099). eprint: <https://doi.org/10.1080/14685248.2017.1317099>. URL: <https://doi.org/10.1080/14685248.2017.1317099>.

- [101] Bogdan Rosa, Hossein Parishani, Orlando Ayala, and Lian-Ping Wang. "Settling velocity of small inertial particles in homogeneous isotropic turbulence from high-resolution DNS." In: *International Journal of Multiphase Flow* 83 (2016), pp. 217–231. ISSN: 0301-9322. DOI: [10.1016/j.ijmultiphaseflow.2016.04.005](https://doi.org/10.1016/j.ijmultiphaseflow.2016.04.005). URL: <http://www.sciencedirect.com/science/article/pii/S0301932215301543>.
- [102] Mahdi Saeedipour, Simon Schneiderbauer, Stefan Pirker, and Salar Bozorgi. "Numerical simulation of turbulent liquid jet breakup using a sub-grid criterion with industrial application." In: Sept. 2014.
- [103] Izumi Saito and Toshiyuki Gotoh. "Turbulence and cloud droplets in cumulus clouds." In: *New Journal of Physics* 20.2 (2018), p. 023001. DOI: [10.1088/1367-2630/aaa229](https://doi.org/10.1088/1367-2630/aaa229). URL: <https://doi.org/10.1088%2F1367-2630%2Faaa229>.
- [104] Ewe Wei Saw, Raymond A. Shaw, Sathyanarayana Ayyalaso-mayajula, Patrick Y. Chuang, and Ármann Gylfason. "Inertial Clustering of Particles in High-Reynolds-Number Turbulence." In: *Phys. Rev. Lett.* 100 (21 2008), p. 214501. DOI: [10.1103/PhysRevLett.100.214501](https://doi.org/10.1103/PhysRevLett.100.214501). URL: <https://link.aps.org/doi/10.1103/PhysRevLett.100.214501>.
- [105] Ewe-Wei Saw, Gregory P. Bewley, Eberhard Bodenschatz, Samriddhi Sankar Ray, and Jérémie Bec. "Extreme fluctuations of the relative velocities between droplets in turbulent airflow." In: *Physics of Fluids* 26.11 (2014), p. 111702. DOI: [10.1063/1.4900848](https://doi.org/10.1063/1.4900848). eprint: <https://doi.org/10.1063/1.4900848>. URL: <https://doi.org/10.1063/1.4900848>.
- [106] R. Scatamacchia, L. Biferale, and F. Toschi. "Extreme Events in the Dispersions of Two Neighboring Particles Under the Influence of Fluid Turbulence." In: *Phys. Rev. Lett.* 109 (14 2012), p. 144501. DOI: [10.1103/PhysRevLett.109.144501](https://doi.org/10.1103/PhysRevLett.109.144501). URL: <https://link.aps.org/doi/10.1103/PhysRevLett.109.144501>.
- [107] R. A. Shaw, A. B. Kostinski, and M. L. Larsen. "Towards quantifying droplet clustering in clouds." In: *Quarterly Journal of the Royal Meteorological Society* 128.582 (2002), pp. 1043–1057. DOI: [10.1256/003590002320373193](https://doi.org/10.1256/003590002320373193). eprint: <https://onlinelibrary.wiley.com/doi/pdf/10.1256/003590002320373193>. URL: <https://onlinelibrary.wiley.com/doi/abs/10.1256/003590002320373193>.
- [108] Raymond A. Shaw. "Particle-turbulence interactions in atmospheric clouds." In: *Annual Review of Fluid Mechanics* 35.1 (2003), pp. 183–227. DOI: [10.1146/annurev.fluid.35.101101.161125](https://doi.org/10.1146/annurev.fluid.35.101101.161125). eprint: <https://doi.org/10.1146/annurev.fluid.35.101101.161125>. URL: <https://doi.org/10.1146/annurev.fluid.35.101101.161125>.

- [109] H. Siebert, R. A. Shaw, J. Ditas, T. Schmeissner, S. P. Malinowski, E. Bodenschatz, and H. Xu. "High-resolution measurement of cloud microphysics and turbulence at a mountaintop station." In: *Atmos. Meas. Tech.* 8.8 (2015), pp. 3219–3228. DOI: [10.5194/amt-8-3219-2015](https://doi.org/10.5194/amt-8-3219-2015). URL: <http://www.atmos-meas-tech.net/8/3219/2015>.
- [110] H. Sigurgeirsson and A. M. Stuart. "A model for preferential concentration." In: *Physics of Fluids* 14.12 (2002), pp. 4352–4361. DOI: [10.1063/1.1517603](https://doi.org/10.1063/1.1517603). eprint: <https://doi.org/10.1063/1.1517603>. URL: <https://doi.org/10.1063/1.1517603>.
- [111] Sholpan Sumbekova, Alain Cartellier, Alberto Aliseda, and Mickael Bourgoin. "Preferential concentration of inertial sub-Kolmogorov particles: The roles of mass loading of particles, Stokes numbers, and Reynolds numbers." In: *Phys. Rev. Fluids* 2 (2 2017), p. 024302. DOI: [10.1103/PhysRevFluids.2.024302](https://doi.org/10.1103/PhysRevFluids.2.024302). URL: <https://link.aps.org/doi/10.1103/PhysRevFluids.2.024302>.
- [112] Keiko Takahashi, Koji Goto, Ryo Onishi, and Masatoshi Imada. "Large-scale intermittency and rare events boosted at dimensional crossover in anisotropic turbulence." In: *Phys. Rev. Fluids* 3 (2018), p. 124607.
- [113] Josin Tom and Andrew D. Bragg. "Multiscale preferential sweeping of particles settling in turbulence." In: *Journal of Fluid Mechanics* 871 (2019), pp. 244–270. DOI: [10.1017/jfm.2019.337](https://doi.org/10.1017/jfm.2019.337).
- [114] Federico Toschi and Eberhard Bodenschatz. "Lagrangian Properties of Particles in Turbulence." In: *Annual Review of Fluid Mechanics* 41.1 (2009), pp. 375–404. DOI: [10.1146/annurev.fluid.010908.165210](https://doi.org/10.1146/annurev.fluid.010908.165210). eprint: <https://doi.org/10.1146/annurev.fluid.010908.165210>. URL: <https://doi.org/10.1146/annurev.fluid.010908.165210>.
- [115] Paul A. Vaillancourt and M. K. Yau. "Review of Particle-Turbulence Interactions and Consequences for Cloud Physics." In: *Bulletin of the American Meteorological Society* 81.2 (2000), pp. 285–298. DOI: [10.1175/1520-0477\(2000\)081<0285:ROPIAC>2.3.C0;2](https://doi.org/10.1175/1520-0477(2000)081<0285:ROPIAC>2.3.C0;2). eprint: [https://doi.org/10.1175/1520-0477\(2000\)081<0285:ROPIAC>2.3.C0;2](https://doi.org/10.1175/1520-0477(2000)081<0285:ROPIAC>2.3.C0;2). URL: [https://doi.org/10.1175/1520-0477\(2000\)081<0285:ROPIAC>2.3.C0](https://doi.org/10.1175/1520-0477(2000)081<0285:ROPIAC>2.3.C0).
- [116] Dimitar G. Vlaykov and Michael Wilczek. "On the small-scale structure of turbulence and its impact on the pressure field." In: *Journal of Fluid Mechanics* 861 (2019), pp. 422–446. DOI: [10.1017/jfm.2018.857](https://doi.org/10.1017/jfm.2018.857).
- [117] M. Wacławczyk, Y.-F. Ma, J. M. Kopeć, and S. P. Malinowski. "Novel approaches to estimating the turbulent kinetic energy dissipation rate from low- and moderate-resolution velocity

- fluctuation time series." In: *Atmospheric Measurement Techniques* 10.12 (2017), pp. 4573–4585. DOI: [10.5194/amt-10-4573-2017](https://doi.org/10.5194/amt-10-4573-2017). URL: <https://www.atmos-meas-tech.net/10/4573/2017>.
- [118] James M. Wallace. "Twenty years of experimental and direct numerical simulation access to the velocity gradient tensor: What have we learned about turbulence?" In: *Physics of Fluids* 21.2 (2009), p. 021301.
- [119] Lian-Ping Wang, Orlando Ayala, Yan Xue, and Wojciech W. Grabowski. "Comments on "Droplets to Drops by Turbulent Coagulation"." In: *Journal of the Atmospheric Sciences* 63.9 (2006), pp. 2397–2401. DOI: [10.1175/JAS3750.1](https://doi.org/10.1175/JAS3750.1). eprint: <https://doi.org/10.1175/JAS3750.1>. URL: <https://doi.org/10.1175/JAS3750.1>.
- [120] Z. Warhaft. "Turbulence in nature and in the laboratory." In: *Proceedings of the National Academy of Sciences* 99.suppl 1 (2002), pp. 2481–2486. ISSN: 0027-8424. DOI: [10.1073/pnas.012580299](https://doi.org/10.1073/pnas.012580299). eprint: https://www.pnas.org/content/99/suppl_1/2481.full.pdf. URL: https://www.pnas.org/content/99/suppl_1/2481.
- [121] Z Warhaft. "Laboratory studies of droplets in turbulence: towards understanding the formation of clouds." In: *Fluid Dynamics Research* 41.1 (2008), p. 011201. DOI: [10.1088/0169-5983/41/1/011201](https://doi.org/10.1088/0169-5983/41/1/011201). URL: <https://doi.org/10.1088%2F0169-5983%2F41%2F1%2F011201>.
- [122] Eric J. P. Woittiez, Harm J. J. Jonker, and Luís M. Portela. "On the Combined Effects of Turbulence and Gravity on Droplet Collisions in Clouds: A Numerical Study." In: *Journal of the Atmospheric Sciences* 66.7 (2009), pp. 1926–1943. DOI: [10.1175/2005JAS2669.1](https://doi.org/10.1175/2005JAS2669.1). eprint: <https://doi.org/10.1175/2005JAS2669.1>. URL: <https://doi.org/10.1175/2005JAS2669.1>.
- [123] M. A. Yavuz, R. P. J. Kunnen, G. J. F. van Heijst, and H. J. H. Clercx. "Extreme Small-Scale Clustering of Droplets in Turbulence Driven by Hydrodynamic Interactions." In: *Phys. Rev. Lett.* 120 (24 2018), p. 244504. DOI: [10.1103/PhysRevLett.120.244504](https://doi.org/10.1103/PhysRevLett.120.244504). URL: <https://link.aps.org/doi/10.1103/PhysRevLett.120.244504>.
- [124] Yeung P K, Zhai X M, and Sreenivasan Katepalli R. "Extreme events in computational turbulence." In: *Proceedings of the National Academy of Sciences of the United States of America* 112.41 (2015), pp. 12633–12638. ISSN: 1091-6490 0027-8424. URL: <https://www.ncbi.nlm.nih.gov/pubmed/26424452>.

- [125] P. K. Yeung, D. A. Donzis, and K. R. Sreenivasan. "Dissipation, enstrophy and pressure statistics in turbulence simulations at high Reynolds numbers." In: *Journal of Fluid Mechanics* 700 (2012), pp. 5–15.
- [126] S. Zilitinkevich, O. Druzhinin, A. Glazunov, E. Kadantsev, E. Mortikov, I. Repina, and Y. Troitskaya. "Dissipation rate of turbulent kinetic energy in stably stratified sheared flows." In: *Atmospheric Chemistry and Physics* 19.4 (2019), pp. 2489–2496. DOI: [10.5194/acp-19-2489-2019](https://doi.org/10.5194/acp-19-2489-2019). URL: <https://www.atmos-chem-phys.net/19/2489/2019>.

DECLARATION

Put your declaration here.

Warszawa, 2018

Katarzyna Karpińska

COLOPHON

This document was typeset using the typographical look-and-feel `classicthesis` developed by André Miede. The style was inspired by Robert Bringhurst's seminal book on typography "*The Elements of Typographic Style*". `classicthesis` is available for both L^AT_EX and LyX:

<https://bitbucket.org/amiede/classicthesis/>

Happy users of `classicthesis` usually send a real postcard to the author, a collection of postcards received so far is featured here:

<http://postcards.miede.de/>